UNIVERSITY OF EAST ANGLIA

JOHN INNES CENTRE

Role of heterotrimeric G protein β subunit during root endosymbioses

PIERRE DANGEVILLE

Thesis submitted to the University of East Anglia

for the degree of Doctor of Philosophy

2022

Abstract

Root endosymbiosis is formed with nitrogen-fixing bacteria and phosphate-delivering arbuscular mycorrhizal fungi. These endosymbionts colonize the root cell intracellular space of their host to trade nutrients in exchange for photosynthetic-derived carbon source. Prior to root colonization, specific chemical communication between the two partners is required to establish a root endosymbiotic interaction. Recognition by the host of bacterial or fungal symbiotic elicitors results similarly in induction of nuclear calcium oscillations essential for transcriptional reprograming and induction of symbiotic genes. But the transducing signal that activates nuclear calcium signalling in this pathway is unknown. Heterotrimeric G protein β subunit (Gβ) has been previously shown to positively regulate root endosymbiosis with nitrogen-fixing bacteria in three legumes. We hypothesised that Gβ functions in transducing signal during root endosymbioses. Loss-of-function of *Medicago truncatula Gβ* confirmed its positive role during association with symbiotic bacteria. Characterization of several *MtGβ* mutants with missense mutations allowed us to identify several amino acid residues critical for its function. Live-cell imaging following application of symbiotic elicitors enabled us to determine its role during activation of nuclear calcium signalling. Furthermore, we identified a protein target of *Mt*Gβ that together may control root endosymbioses. This study investigates the role of the *Mt*Gβ in transducing signals during root endosymbiosis, confirming its positive regulatory function and identifying critical amino acid residues and a potential protein target involved in this process.

Keywords: Root legume symbioses, nuclear calcium signalling, heterotrimeric G protein β subunit.

Acknowledgements

To Myriam, thank you for your immense support, for letting me joining your lab, and giving me the opportunity to achieve my goals. You are an amazing supervisor. I am deeply grateful for all the help and teaching you gave me and for sharing your passion of science.

To my primary external supervisor, Janneke Balk, thank you for your great support, the discussions, and your sharp eye.

To my secondary external supervisor, Nick Talbot, thank you for your support and interest you had on this project.

To Allan Downie, thank you for being always positive, your kind attention towards me and keeping pushing me up.

To the UK Research and Innovation department, for funding the NRP DTP PhD programme, which gave me the opportunity to participate in science research as a PhD student. To the John Innes Centre, for providing this excellent work environment.

To the Graduate School Office staff, thank you all for providing one the best support and assistance that any PhD student may obtain.

To the laboratory support staff and to Eleanor Rickaby, to the media kitchen and to Sarah Barber, to the horticultural service staff and to Timothy Wells, thank you so much for your amazing work and support that have helped us every day. To Grant Calder and Sergio Lopez, thank you for training me and giving me so much support.

To Caroline Stone, for providing us with insect cell strain and sharing your great expertise.

To Rik Huisman, for teaching me everything about cloning.

To Baptiste Castel, for helping me design the CRISPR-CAS9 experiments.

To the current and former members of the Charpentier lab: Nuno, Aisling, Fran, Neftali, Pilar, Lauren, Anson, Emily, Edmund, Giulia, Nicola, Catherine, Clemence, and Janni, for a truly great work environment, interesting discussions, friendship, and so much delicious cakes.

To Pablo, I'm so glad that science gave us the opportunity to meet each other. Thank you for your great support and your invaluable friendship.

To Thorsten, Antoine, Clemence, and Jérôme, thank you for being the persons you are and your friendship.

À tous mes amis d'enfance qui m'ont soutenu tout au long de cette thèse, merci d'avoir participé à faire la personne que je suis aujourd'hui.

À toute ma famille, merci infiniment de votre soutien et amour inconditionnels.

Table of contents

List of Figures

List of Tables

List of Abbreviations

AM	arbuscular mycorrhiza
AD	activation domain of GAL4
Arb	arbuscule
BD	DNA-binding domain of GAL4
Ca^{2+}	calcium
CaM	calmodulin
Cas9	nuclease 9
cDNA	complementary DNA
cds	coding sequence
CFP	cyan fluorescent protein
CO	short-chain chitooligosaccharide
CRISPR	clustered regularly interspaced short palindromic repeats
DEX	dexamethasone
dH2O	distilled water
DNA	Deoxyribonucleic Acid
EDTA	Ethylenediaminetetraacetic acid
EMS	ethyl-methane-sulfonate
FRET	Förster Resonance Energy Transfer
G proteins	heterotrimeric G proteins
Gα	heterotrimeric G protein α subunit
Gβ	heterotrimeric G protein β subunit
Gγ	heterotrimeric G protein γ subunit
GAP	GTPase-accelerating protein
GECOs	Genetically Encoded Ca2+ indicators for Optical imaging
GFP	green fluorescent protein
GlcNAc	N-Acetylglucosamine
HA	Human influenza hemagglutinin
HEPES	4-(2-hydroxyethyl)-1-piperazineethanesulfonic acid
IP	infection pocket
IPTG	β-D-1-thiogalactopyranoside
IRH	intra-radical hyphae
IT	infection thread
KASP	Kompetitive Allele Specific PCR

LCO	lipochitooligosaccharide
LysM	lysine motif
M13	myosin-light chain kinase
MBP	maltose binding protein
MVA	mevalonate
Myc-factors	Mycorrhization factors
NaCl	sodium chloride
NCBI	National Center for Biotechnology Information
NES	nuclear export signal
NLS	nuclear localization signal
Nod-factors	Nodulation factors
PCR	Polymerase Chain Reaction
PIT	pre-infection thread
PPA	prepenetration apparatus
RLK	receptor-like kinase
RNA	Ribonucleic acid
SDS-PAGE	sodium dodecyl sulfate–polyacrylamide gel electrophoresis
sgRNA	single guide RNA
SL	strigolactone
Sm2011:*LacZ*	Sinorhizobium meliloti strain 2011 expressing LacZ gene
T-DNA	transfer DNA
TILLING	targeting-induced-local-lesions-in-genomes
Tris-HCl	2-amino-2-(hydroxymethyl)propane-1,3-diol;hydrochloride
Ves	vesicule
X-gal	5-bromo-4-chloro-3-indolyl-β-D-galactopyranoside
XLG	extra-large G protein
Y2H	yeast-two-hybrid
YC3.6	Yellow Cameleon 3.6
YFP	yellow fluorescent protein

Chapter I

Thesis Introduction

1.1 General introduction

Land plants are constantly interacting with a diverse range of microorganisms resulting in either beneficial or detrimental outcomes. Two well-studied mutualistic associations are those between plants and phosphate-delivering arbuscular mycorrhizal (AM) fungi and between legumes and nitrogen-fixing rhizobial bacteria. AM fungi and rhizobial bacteria are soil microsymbionts capable of colonizing the intracellular root tissues of their hosts to deliver nutrients in exchange for photosynthetic-derived carbon source.

In the last decades, understanding the establishment and the molecular mechanisms supporting these two root endosymbiotic associations has been an intensive research effort. Most discoveries have been predominantly made through the use of the model legumes *Medicago truncatula* and *Lotus japonicus* which offer great genetic resources and the advantage to establish endosymbiosis with both AM fungi and nitrogen-fixing rhizobia. Nonetheless, many observations and insights have also been brought up and confirmed through the use of other plant species.

The success of these endosymbiotic associations requires successful recognition of the symbiont by the plant host. Interestingly, the molecular mechanisms that follow recognition of either AM fungi or rhizobia involve a common genetic pathway resulting in generation of calcium (Ca^{2+}) oscillations within the nucleus of root cells essential for the establishment root endosymbiosis.

The secondary messenger that links recognition of the endosymbionts and activation of nuclear Ca^{2+} signalling has not yet been identified. Heterotrimeric G proteins have been shown to mediate the establishment of root endosymbiosis with rhizobial bacteria. On the basis of this discovery, I investigated whether heterotrimeric G protein signalling is implicated in the regulation of nuclear Ca^{2+} signalling during endosymbiosis for both AM- and rhizobia-plant interactions.

In this introduction, I will present the biological and molecular features of AM-plant and rhizobia-legume symbioses as well as the plant signalling pathway leading to activation

of nuclear Ca^{2+} signalling. Eventually, I will present the general aspects of heterotrimeric G protein signalling and the studies that lead me to investigate further the role of heterotrimeric G proteins in root endosymbiosis.

1.2 Physiology and signalling of endosymbiosis

1.2.1 Arbuscular mycorrhizal symbiosis

AM symbiosis forms between members of the fungal phylum Glomeromycota and more than 80% of terrestrial plant species, which include most agriculturally important crops (Harrison, 1997; Schwarzott and Walker, 2001; Lee et al., 2013). In terms of geographical distribution and phylogenetic coverage in the plant kingdom, AM is probably one of the most widespread symbioses on earth (Gutjahr and Parniske, 2013). One speculates that AM fungi have been instrumental for the transition of plants from water to land (Pirozynski and Malloch, 1975; Choi et al., 2018), as the oldest AM-like fungi fossils coincide with the emergence of early diverging land plants 400-450 million years ago (Remy et al., 1994; Redecker et al., 2000; Bidartondo et al., 2011). However, evidences pointed out that several species representing the earliest groups of land plants are predominantly symbiotic with fungi of the Mucoromycotina phylum, rather than Glomeromycota (Bidartondo et al., 2011). This suggests the coexistence of two fungal clades during land colonization and a transition in fungal dominance towards Glomeromycota during vascular plant diversification (Choi et al., 2018). Glomeromycota phylum shows surprisingly low diversity comprising approximately 240 known species despite their abundance and wide range of relationship with plant species (Lee et al., 2013). It is nonetheless predicted that the diversity of these fungi may be much greater on the basis of molecular studies (Lee et al., 2013).

AM fungi are obligate biotrophs which depend on a living photoautotrophic partner to complete their life cycle, although spores can germinate in the absence of host plants (Parniske, 2008). The AM symbiotic structure is characterised by the development of a highly branched hyphal network referred to as “arbuscule” that develops within root cortical cells (Oldroyd, 2013). The arbuscules act as the point of nutrient exchange (Oldroyd, 2013). The host provides the fungus with carbon, and receives in exchange a significant amount of additional mineral nutrients such as phosphate or ammonium extracted by the AM fungus through its soil hyphae (Harrison, 1997; Yang et al., 2012; Berruti et al., 2016; Nakmee et al.,

2016; Ingraffia et al., 2019). Some plant transporters that ensure acquisition of AM-delivered nutrients, are exclusively expressed during AM symbiosis and contribute to sustain AM colonization. In *Medicago truncatula* and *Oryzae sativa*, such transporters are the phosphate transporter *MtPT4* and *OsPT11*, respectively (Harrison, 2002; Javot et al., 2007; Yang et al., 2012). In addition to improving nutrient acquisition, AM interactions are known to enhance plant resistance towards biotic and abiotic stresses via multiple mechanisms (Cordier et al., 1998; Berruti et al., 2016).

The progression of AM colonization can be separated into successive steps that characterize the level of progression of the fungal hyphae within root cells (Figure 1.1; Gutjahr and Parniske, 2013). Prior to physical contact, the first stage known as precontact or presymbiotic stage, is characterised by an extensive branching of AM hyphae in the vicinity of roots in response to plant-derived strigolactones (SLs) (Akiyama et al., 2005; Akiyama et al., 2010). Mutation in genes encoding SL-precursor-biosynthesis enzymes results in a significant loss of AM symbiosis, highlighting the role of SL as a rhizosphere plant-signal mediating interaction with AM (Gomez-Roldan et al., 2008). Likewise, the gene *PhPDR1* in *Petunia hybrida* encodes an ATP-binding cassette (ABC) transporter responsible for SL export as root exudates and mediates AM root colonization (Kretzschmar et al., 2012).

The first physical contact is associated with the formation at the root surface of an AM hyphopodium which is analogous to an appressorium during infection by pathogenic fungi or oomycetes (Wang et al., 2012). This induces nuclear movement in the epidermal cells towards the hyphopodium surface (Genre et al., 2005). Before fungal invasion, the epidermal cell underneath the hyphopodium contact point assembles an intracellular structure known as prepenetration apparatus (PPA) that is associated with cytoskeletal reorganization (Genre et al., 2005). This paves the way for fungal hyphae to progress towards the root cortex (Genre et al., 2008). Once in cortical cells, fungal hyphae growth longitudinally through the apoplast –or symplast depending on the plant species– and form branches to initiate arbuscule formation in inner cortical cells (Genre et al., 2008). Intracellular fungal organs take place within a specialised interface compartment surrounded by the so-called perifungal membrane, an inward extension of plant plasma membrane supported by an intensive exocytotic machinery (Genre et al., 2012). Between arbuscular membrane and perifungal membrane, the so-called periarbuscular interface serves as an intracellular area allowing for the exchange of nutrients or signals between the two organisms (Choi et al., 2018).

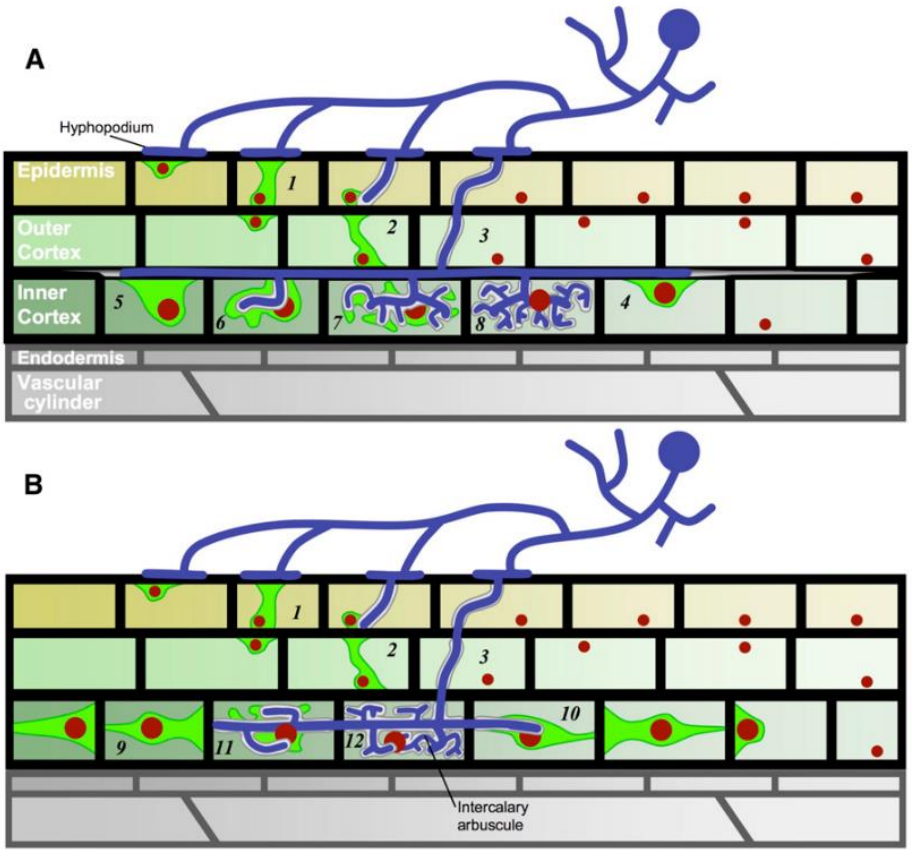

Figure 1.1 | Schematic representation of the different AM colonization patterns and associated cellular dynamics in *Medicago truncatula* and *Daucus carota*.
In *Medicago truncatula* and *Daucus carota*, the adhesion of a fungal hyphopodium to the root surface triggers the assembly of a prepenetration apparatus (PPA) in the contacted epidermal cell (1). This, in turn, initiates PPA formation in the underlying outer cortical cell (2). After radially oriented fungal crossing of the outer root layers (3), the subsequent longitudinal colonization patterns and associated inner cortical cell responses differ between the two plants. In *M. truncatula* **(A)**, intercellular hyphae grow along and between the cells. Upon direct hyphal contact, these cells respond with nuclear repositioning and localised cytoplasmic aggregations (4). Inner cortical cell penetration is preceded by the assembly of large PPAs (5 and 6). Prebranching cytoplasmic aggregations organize at sites along the intracellular trunk hyphae (6 and 7), preceding the development of the arbuscular fine branches (8). In *D. carota* **(B)**, inner cortical cell files are progressively colonised by individual intracellular hyphae that move from one cell to the next. A number of adjacent cells ahead of the hyphal tip respond concomitantly by organizing polarised funnel-shaped PPAs that predict the direction of fungal colonization (9 and 10). As for *M. truncatula*, prebranching cytoplasmic aggregations (11) precede the formation of arbuscular side branches (12). Structures are represented with the following color code: red, nucleus; green, cytoplasmic aggregation; white, perifungal interface; blue, fungus. Modified from Genre et al., 2008 with permission of Oxford University Press.

1.2.2 Symbiosis with nitrogen-fixing rhizobial bacteria

During evolution, a fraction of angiospermal plant species comprising legumes and non-legume *Parasponia* spp. have acquired the ability to establish root nodule symbiosis with a certain type of soil bacteria collectively called rhizobia (Oldroyd and Downie, 2008). Rhizobia are nitrogen-fixing bacteria which are distributed in hundreds of species in fourteen

genera of two bacterial classes, the Alphaproteobacteria and the Betaproteobacteria (Remigi et al., 2016). Besides, legumes form a wide family named *Fabaceae* –or *Leguminosae*– comprising about 20 000 species that most engage a endosymbiotic interaction with rhizobia (Peix et al., 2015). *Parasponia* comprises several tropical tree species and belongs to *Celtidaceae* (Sytsma et al., 2002). Phylogenomic analyses revealed it is likely that root nodule symbiosis originated from a common ancestor and multiple losses have occurred during evolution (Griesmann et al., 2018; van Velzen et al., 2018; van Velzen et al., 2019). The symbiotic interaction between legumes or nonlegume plants with rhizobia leads to the formation of a new root organ referred to as nodule or root nodule. This symbiosis-activated root organogenesis is referred to as nodulation.

To initiate nodulation, the perception of plant-derived flavonoids by the rhizobia activate the production of bacterial signalling molecules known as nodulation (Nod) factors (Dénarié et al., 1996; Subramanian et al., 2006). Plant recognition of Nod-factors triggers rhizobial infection and nodule organogenesis synchronously (Gage, 2004). Rhizobial infection usually occurs via root hairs (Figure 1.2) but it can also occur via cracks in epidermis or via interstitial infections between epidermal cells, depending on the plant species (Dazzo and Alfayate, 2001; González-Sama et al., 2004; Oldroyd et al., 2011).

In *Medicago truncatula* –the model used in this work– rhizobia entry is via root hairs. Rhizobial perception elicits swelling of the root hair tips characterised by multiple growth axis reorientations of the tips leading to root hair curling (Esseling et al., 2003). Rhizobia become entrapped between compressed cell walls forming a so-called infection pocket where they continue to grow and divide (Gage, 2004; Geurts et al., 2005). Next to the infection pocket, a tubular structure referred to as infection thread (IT) forms within root hair allowing for intracellular colonization. IT formation depends on prior cytoplasmic and cytoskeleton rearrangement of microtubules and actin, giving rise to columns of cytoplasmic bridges called pre-infection threads (PITs) through which the inwardly growing IT propagates (van Brussel et al., 1992; Gage, 2004; Miyahara et al., 2010). Localised plant cell wall degradation initiates IT progression within root hair without causing cell rupture (Ridge and Rolfe, 1985). IT formation and progression also depends on nuclear movement and repositioning (Newman-Griffis et al., 2019). The nucleus is connected to the IT by dense microtubules (Gage, 2004). IT progression follows the path of the moving nucleus regardless of its direction and it is ultimately oriented towards the underneath cell (Nutman, 1959; Newman-Griffis et al., 2019). Once the IT reaches the inner base of the root hair cell, nucleus of the underlying cell

repositions itself, resulting in formation of a new PIT and localised degradation of plant cell walls, allowing the IT to progress into the next cell layer. This process is repeated at each cell junction, until rhizobia ultimately reach the forming nodule (Sieberer et al., 2012). Nodules result from mitotic activation of pericycle, endodermal, and inner-cortical cells (Xiao et al., 2014). The root middle cortex becomes the nodule meristem, which shapes a newly formed organ that ultimately expands from the root to form a cylindrical structure (Timmers et al., 1999; Xiao et al., 2014). Once rhizobia enter a root nodule, they differentiate into bacteroids that can perform nitrogen fixation (Peix et al., 2015). Nitrogen-fixing bacteroids synthesise a nitrogenase enzyme complex that catalyses the reduction of atmospheric dinitrogen gas into ammonium (Lodwig and Poole, 2003). Because this reaction is oxygen-sensitive, root nodules guarantee a near-anoxic condition by synthesising leghaemoglobin, which protects the nitrogenase enzyme complex from dioxygen and maintains a sufficient oxygen supply to the nitrogen-fixing bacteroids (Ott et al., 2005). Within this protected niche and in exchange of photosynthetic-derived nutrients, rhizobia provide the host with ammonium and/or amino acids conferring important nitrogen supply when the plant is upon starving condition (Lodwig and Poole, 2003; Clarke et al., 2014).

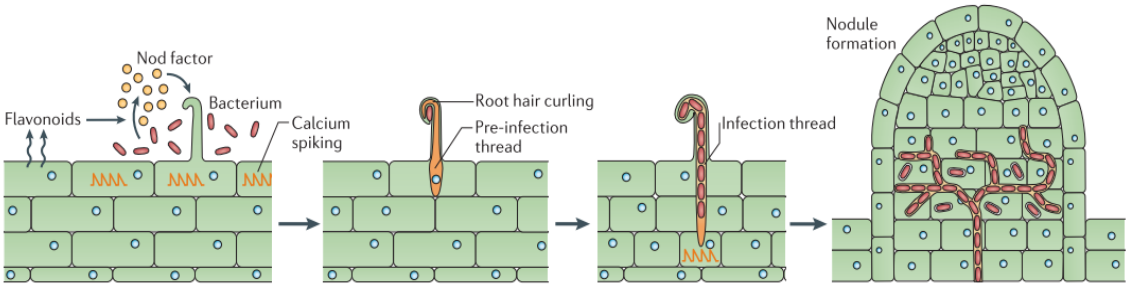

Figure 1.2 | Schematic representation of nodulation.
Flavonoids released by the plant signal to rhizobia in the rhizosphere, which in turn produce nodulation factors (Nod-factors) that are recognised by the host. Nod-factor perception activates the symbiosis signalling pathway, leading to calcium oscillations, initially in epidermal cells but later also in cortical cells preceding their colonization. Rhizobia gain entry into the plant root by root hair cells that grow around the bacteria attached at the root surface, trapping the bacteria inside a root hair curl. Infection threads are invasive invaginations of the plant cell that are initiated at the site of root hair curls and allow invasion of the rhizobia into the root tissue. The nucleus relocates to the site of infection and an alignment of endoplasmic reticulum and cytoskeleton, known as the pre-infection thread, predicts the path of the infection thread. Nodules initiate below the site of bacterial infection and form by *de novo* initiation of a nodule meristem in the root cortex. The infection threads grow towards the emergent nodules and ramify within the nodule tissue. In some cases, the rhizobia remain inside the infection threads, but more often, the bacteria are released into membrane-bound compartments inside the cells of the nodule, where the bacteria can differentiate into a nitrogen-fixing state. Modified from Oldroyd, 2013 with permission of Springer Nature.

1.2.3 Symbiont-derived elicitors promoting endosymbiotic associations

AM fungi and rhizobia both release symbiotic elicitors, commonly known as mycorrhization (Myc) and nodulation (Nod)-factors, respectively. Their recognition by the host results in transcriptional reprogramming and induction of symbiotic genes. This early signalling is the first step that paves the way for intracellular colonization of the endosymbiotic microorganisms.

Myc-factors can be grouped into at least two different molecular signals including mycorrhizal-lipochitooligosaccharides (Myc-LCOs) and short-chain chitooligosaccharides (COs), namely chitotetraose (CO4) and chitopentaose (CO5) (Maillet et al., 2011; Genre et al., 2013). Latter studies also suggested that chitooctaose (CO8) can induce symbiosis signalling in *Medicago truncatula* despite its involvement in innate immunity (Feng et al., 2019). Myc-LCOs and COs consist of several residues of β-1-4-linked *N*-acetylglucosamine (GlcNAc). Myc-LCOs are made of four GlcNAc residues and are N-acylated at the first non-reducing sugar terminal with either oleic or palmitic acid and can be either sulphated or nonsulphated at the reducing end of the last GlcNAc residue (Maillet et al., 2011). On the other hand, Nod-factors only consist of LCO molecules with tetrameric and/or pentameric β-1-4-linked GlcNAc backbones (Dénarié et al., 1996). The length and degree of saturation of the *N*-acyl group at the non-reducing sugar terminal vary widely between Nod-factors. The reducing terminal can also be conjugated with a variety of substituents such as methyl, fucosyl, acetyl and sulphate groups (Roche et al., 1991; Dénarié et al., 1996). Nod-factors are specific to each rhizobia strain and thus confer recognition specificity by the plant hosts (Oldroyd and Downie, 2008).

1.2.4 Detection of symbiotic elicitors by plant receptors

Myc and Nod-factors are perceived at the root surface by plant epidermal receptor-like kinases (RLKs) possessing extracellular Lysine Motif (LysM) domains known to bind to *N*-acetylglucosamine polymers such as LCOs and COs (Buist et al., 2008). Recognition of Myc-factors in *M. truncatula* involves amongst others two LysM-RLKs: the Chitin Elicitor Receptor Kinase1 (CERK1) and the LysM Receptor 4 (LYR4) (Feng et al., 2019). *Mt*CERK1 and *Mt*LYR4 bind to mycorrhizal COs, while the mycorrhizal LCO receptors in plants remain elusive (Feng et al., 2019). Colonization of AM fungi is partially dependant on *MtCERK1* and *MtLYK4* (Feng et al., 2019), suggesting the presence of multiple Myc-factor receptors.

The role of *CERK1* homologs for AM symbiosis in the plant kingdom is presumably conserved as a rice knock-out mutant of *OsCERK1* results in the abolishment of AM colonization (Miyata et al., 2014). On the other hand, Nod-factor perception in *M. truncatula* requires two LysM-RLKs referred to as *Mt*LYK3 (LysM-containing RLK3) and *Mt*NFP (Nod-factor perception), orthologs of the *Lotus japonicus* Nod-factor receptors *Lj*NFR1 and *Lj*NFR5, respectively (Limpens et al., 2003; Madsen et al., 2003; Radutoiu et al., 2003; Arrighi et al., 2006). Each of these LysM-RLKs form together a heterodimer complex at the plasma membrane in their respective plant species (Madsen et al., 2011; Moling et al., 2014). *Lj*NFR1 and *Lj*NFR5 perceive rhizobial LCOs by direct binding (Broghammer et al., 2012), and so was predicted *Mt*NFP via modelling (Mulder et al., 2006). Deletion of any of these LysM-RLKs results in full abolishment of epidermal colonization and root nodule formation, highlighting the importance of Nod-factor recognition during root nodule symbiosis. The kinase domain of *Lj*NFR5 was reported to be inactive in contrast to *Lj*NFR1 (Madsen et al., 2011). *In vitro* kinase assays evidenced that *Lj*NFR1 undergoes auto-phosphorylation and is also capable of phosphorylating the cytoplasmic domain of *Lj*NFR5.

Recognition of Myc and Nod-factors, which is required prior to intracellular invasion of the endosymbionts, results in the induction of an oscillatory Ca^{2+} spiking that is initiated in cell nuclei (Ehrhardt et al., 1996; Kosuta et al., 2008; Sieberer et al., 2012; Kelner et al., 2018). In *M. truncatula*, *MtNFP*, *MtCERK1*, and *MtLYR4* are all required to generate nuclear Ca^{2+} oscillations following recognition of symbiotic elicitors (Genre et al., 2013; Sun et al., 2015; Feng et al., 2019). As induction of nuclear Ca^{2+} oscillations is a common feature of mycorrhizal and rhizobial responses, it suggests they follow the same signalling pathway.

1.2.5 Early signalling of AM and root nodule symbioses share a common signalling pathway

One of the first genetic evidences that AM and root nodule symbioses share a common signalling pathway came through the characterization of the *M. truncatula* RLK Does not Make Infection 2 (*DMI2*, also known as *NORK*), ortholog of the symbiosis receptor-like kinase (*SymRK*) in *L. japonicus* (Endre et al., 2002; Stracke et al., 2002). *Mtdmi2* and *Ljsymrk* null-mutants are defective in both AM and root nodule symbioses and thus evidenced a common signalling pathway between mycorrhizal and rhizobial symbioses. Similarly, *Mtdmi2* null-mutant showed no Ca^{2+} responses upon treatment with symbiotic elicitors (Sun

et al., 2015). Nonetheless, the precise function of *MtDMI2*/*LjSymRK* has not yet been established. The extracytoplasmic region of *Mt*DMI2/*Lj*SymRK comprises a three leucine-rich repeats (LRRs) and a malectin-like domain (MLD) and *Lj*SymRK can associate with the Nod-factor receptors *Lj*NFR1 and *Lj*NFR5 *in planta* (Antolín-Llovera et al., 2014; Ried et al., 2014). A negative feedback loop via ubiquitination of *Lj*SymRK by an E3 ligase which leads to its degradation, was demonstrated to regulate endosymbiosis in *L. japonicus* (Den Herder et al., 2012; Yuan et al., 2012). Likewise, the plant U-box E3 ubiquitin ligase 1 (PUB1) in *M. truncatula* can interact with *Mt*DMI2 *in planta* and reduction of PUB1 enzymatic activity increases AM colonization (Vernié et al., 2016). Taken together, these studies showed that the presence of *Mt*DMI2/*Lj*SymRK at plasma membrane is required to transduce the symbiotic signal. Interestingly, ectopic expression of the intracellular kinase domain of *Mt*DMI2 is sufficient to induce nodule organogenesis in absence of rhizobia, though the full-length is necessary for proper rhizobial colonization (Saha et al., 2014). An interactor of *Mt*DMI2 has been identified via yeast-two-hybrid screen: the *M. truncatula* 3-hydroxy-3-methylglutaryl CoA reductase 1 (HMGR1), which functions in the production of mevalonate (MVA) in the MVA pathway (Kevei et al., 2007). Silencing *MtHMGR1* results in reduction of rhizobial infection. However, whether *MtHMGR1* is also involved in AM colonization has not been investigated. Interestingly, application of MVA induced nuclear Ca^{2+} oscillations in wild-type root hairs of *M. truncatula, L. japonicus* and *Daucus carota* but not in *Arabidopsis thaliana* (Venkateshwaran et al., 2015). Because carrot is only capable of AM symbiosis and *A. thaliana* cannot achieve endosymbiosis with AM fungi nor rhizobia, it was suggested that MVA would act as a secondary messenger during root endosymbiosis. The MVA-induced nuclear Ca^{2+} is significantly altered in *Mtnfp* and *Mtdmi2* mutants (Venkateshwaran et al., 2015), suggesting that MVA acts in concert with the Nod-factor receptor complex *Mt*LYK3/*Mt*NFP and the symbiosis co-receptor *Mt*DMI2 for transduction of the symbiotic signal and activation of the nuclear Ca^{2+} signalling. The study of MVA was indicative but the exact nature of the secondary messenger during root endosymbiosis as well as the underlying molecular mechanisms responsible for transduction of the symbiosis signal remain elusive. Symbiosis-activated nuclear Ca^{2+} oscillations initiate in nuclei of root cells (Kelner et al., 2018). Thus, it implicates that a signal transduction mechanism connects the plasma membrane to the nucleus.

1.2.6 Identification of nucleoporins essential for root endosymbiosis

On the path between cytoplasm and nucleoplasm, genetic screens in *L. japonicus* allowed for the identification of three components of the nuclear pore complex referred to as NUP85 (nucleoporin 85), NUP133, and NENA, and these were shown to be involved in rhizobial and mycorrhizal endosymbioses (Kanamori et al., 2006; Saito et al., 2007; Groth et al., 2010). Truncation of *Lj*NUP85 or *Lj*NUP133 as well as deleterious amino acid substitution of *Lj*NENA, are associated with the absence of Ca^{2+} spiking after Nod-factor treatment (Kanamori et al., 2006; Saito et al., 2007; Groth et al., 2010). Thus, it is likely these nucleoporins are involved in the transduction of a secondary messenger that goes from the cytoplasm to the nucleoplasm during symbiosis signalling. Symbiosis defects in *Ljnup85* and *Ljnup133* mutants are temperature sensitive with strongest impairment at higher temperature, namely 18 °C versus 22 °C and 22 °C versus 26 °C, respectively (Kanamori et al., 2006; Saito et al., 2007). Interestingly, *LjNENA* was shown to be exclusively involved in epidermal infection of AM fungi and rhizobia (Groth et al., 2010). Nodule development was not impaired in *Ljnena* mutant though the root nodules were not colonised. This observation highlights a differential regulation of rhizobial infection and nodule organogenesis.

1.2.7 Nuclear Ca^{2+} machinery required for root endosymbiosis and downstream response

The nuclear Ca^{2+} encoding machinery required for the generation of nuclear Ca^{2+} oscillations during root endosymbiosis, includes the cation-permeable channel *Mt*DMI1, the Ca^{2+}-permeable cyclic-nucleotide gated channels (CNGCs) 15a/b/c and the calcium ATPase MCA8 in *M. truncatula* (Ané et al., 2004; Capoen et al., 2011; Charpentier et al., 2016). Similarly, there are two cation-permeable channels in *L. japonicus* known as POLLUX and CASTOR, homologs of *MtDMI1*, and both are required for rhizobial and mycorrhizal symbioses (Charpentier et al., 2008). Full-length *MtDMI1* can complement the symbiotic mutant phenotype of the *castor pollux* double mutant (Venkateshwaran et al., 2012). All these components are localised at the nuclear envelope and govern the generation of nuclear Ca^{2+} oscillations in response to Myc and Nod-factors (Wais et al., 2000; Charpentier et al., 2008; Capoen et al., 2011; Sun et al., 2015; Charpentier et al., 2016). In *M. truncatula*, *Mt*DMI1 and the *Mt*CNGC15s interact with each other *in planta* (Charpentier et al., 2016). Based on mathematical modelling, it was predicted that upon transmission of a secondary messenger

into the nucleus, simultaneous activation of *Mt*DMI1 and *Mt*CNGC15s leads to a weak release of K^+ and Ca^{2+}, respectively (Charpentier et al., 2013). A following positive feedback of Ca^{2+} on *Mt*DMI1 would then fully activate the *Mt*CNGC15s. Subsequently, sustainment of the nuclear Ca^{2+} oscillation was predicted to require feedback from calmodulin and Ca^{2+}. In agreement with these suggestions, Ca^{2+} binding pockets have been identified on *Lj*CASTOR and the *M. truncatula* calmodulin 2 was shown to control closure of the *Mt*CNGC15s during symbiosis response (Kim et al., 2019; del Cerro et al., 2022). Besides, the role of *Mt*MCA8 is to replenish the nuclear Ca^{2+} store –the lumen between the inner and outer nuclear envelops contiguous with the endoplasmic reticulum– (Capoen et al., 2011).

Activation of nuclear Ca^{2+} signalling results in transcriptional reprogramming and expression of symbiosis genes essential for AM and root nodule symbioses (reviewed in Oldroyd, 2013). The decoding machinery that perceives nuclear Ca^{2+} spiking involves the nuclear-localised calcium and calmodulin-dependent serine/threonine protein kinase *Lj*CCaMK and *Mt*DMI3 in *L. japonicus* and *M. truncatula*, respectively (Levy et al., 2004; Mitra et al., 2004). *LjCCaMK*/*MtDMI3* are required for AM and rhizobial symbioses and they are hypothesised to be the main decoders of the nuclear Ca^{2+} oscillations. Once activated, they phosphorylate the transcription factors *Lj*CYCLOPS and *Mt*IPD3/*Mt*IPD3-like (interacting protein of DMI3) in *L. japonicus* and *M. truncatula*, respectively (Messinese et al., 2007; Yano et al., 2008; Singh et al., 2014; Jin et al., 2018a). Phosphorylation of *Lj*CYCLOPS/*Mt*IPD3/*Mt*IPD3L leads to their activation and thus to their binding to DNA to induce expression of symbiosis genes essential for AM and root nodule symbioses.

Although multiple components required for the encoding or decoding of symbiosis-induced nuclear Ca^{2+} oscillation have been identified, the molecular signals transducing the information from the plasma membrane RLKs to activate the ion channels at nuclear envelope remain unknown. Heterotrimeric G proteins have been shown to mediate RLK-dependent downstream responses in various signalling pathways (Pandey, 2020). Notably, the heterotrimeric G protein β subunit was shown to positively regulate nodulation in three legumes including *Glycine max*, *M. truncatula* and *Pisum sativum* (Choudhury and Pandey, 2013; Bovin et al., 2022). Thus, I explore further the role of this heterotrimeric G protein subunit in *M. truncatula* during root endosymbioses comprising both AM and root nodule symbioses.

1.3 Heterotrimeric G proteins in plants

1.3.1 The heterotrimeric G protein subunits

Heterotrimeric G proteins (hereafter G proteins) are key signalling components in eukaryotes involved during the regulation of a multitude of growth and developmental processes (see for instance Simon et al., 1991; Urano et al., 2012a; Urano et al., 2016b; Chakravorty and Assmann, 2018; Lengger and Jensen, 2020). Most discoveries related to plant G proteins come largely from studies in *A. thaliana* and *O. sativa* although knowledge regarding G protein signalling have been expanded through studies in other plant species. Plant G proteins are involved in numerous signalling pathways, including developmental processes such as seed germination, growth and cell division (reviewed in Perfus-Barbeoch et al., 2004; Urano et al., 2016b), phytohormone response (reviewed in Jose and Roy Choudhury, 2020), ion channel opening (Wang et al., 2001; Fan et al., 2008; Jeon et al., 2019), light response (see references in Urano et al., 2012a), abiotic stress response (reviewed in Zhang et al., 2021), and plant innate immunity (reviewed in Zhong et al., 2019 and Zhang et al., 2021).

The core G protein complex consist of three subunits (Gα, Gβ and Gγ). Gα is capable of binding either guanosine diphosphate (GDP) or guanosine triphosphate (GTP) and Gβ and Gγ subunits form together a dimer (see for instance Urano and Jones, 2014). The three subunits form all together a heterotrimeric complex at the plasma membrane. According to the classical paradigm that largely derives from the mammalian system, the G protein complex switches between inactive and active states depending on the nucleotide-bound form of Gα (Sprang, 1997). During resting phase, Gα is GDP-bound and remains associated with the Gβγ dimer in a trimeric conformation. Upon activation of cell-surface receptors, the latter stimulate GDP release from Gα and GTP-bound Gα dissociates from Gβγ dimer due to conformational change. Both the GTP-Gα monomer and Gβγ dimer can interact with a variety of downstream protein targets to transduce signals for distinct cellular and physiological functions (Offermanns, 2003; McCudden et al., 2005; Wettschureck and Offermanns, 2005; Smrcka and Fisher, 2019).

Plant G proteins have been similarly shown to interact with numerous protein targets (see Urano and Jones, 2014 and Pandey, 2019). Plant Gα, Gβ and Gγ subunits are predominantly localised at plasma membrane but can be detected in inner membranes and

intracellular organelles (Roy Choudhury et al., 2020). *Arabidopsis* Gα and Gγ harbour a prenylation motif for membrane anchoring at their N-terminal and C-terminal, respectively, and both *At*Gα and *At*Gγ are independently trafficked to the plasma membrane (Adjobo-Hermans et al., 2006; Trusov et al., 2012). *Arabidopsis* Gβ requires to interact with Gγ for its proper localization and this is achieved prior to their trafficking to the plasma membrane (Wang et al., 2008). *Arabidopsis* Gβγ dimer has been localised at the plasma membrane in transformed mesophyll protoplasts and detected at the endoplasmic reticulum via western-blot (Wang et al., 2007; Wang et al., 2008). *At*Gβ alone has been detected within the nucleus of transformed tobacco and *Arabidopsis* leaves via immunoprecipitation and fluorescence microscopy, respectively (Peškan and Oelmüller, 2000; Anderson and Botella, 2007). Rice Gβ and Gγ have been similarly detected both at the plasma membrane and within nuclei in onion epidermal cells and rice root cells (Yadav et al., 2014; Liu et al., 2018).

1.3.2 Plant G proteins are auto-active

In contrast to their mammalian counterparts, plant Gα subunits rapidly release GDP without any stimulus and the rate of GTP hydrolysis is >100-fold slower in comparison (Johnston et al., 2007; Jones et al., 2011b; Choudhury et al., 2012; Urano et al., 2012b). X-ray crystallography of *Arabidopsis* Gα and computational-based molecular dynamics simulations enabled deducing that, despite high structural homology with mammalian Gα, its helical domain displays pronounced intrinsic disorder and dynamic motion, resulting in self-activation (i.e., GDP release and binding to GTP) (Jones et al., 2011a). Notably, a chimeric mammalian Gα in which its helical domain was replaced by the *Arabidopsis* Gα helical domain was sufficient to confer rapid activation (Jones et al., 2012). Plant Gαs are therefore considered as self-activating and this property is presumably conserved throughout the plant kingdom (Johnston et al., 2007; Choudhury et al., 2012; Urano et al., 2012b). It also implies that regulation of G proteins in plants is rather directed on the deactivation of Gα instead of its activation. The ability of Gβγ dimer to stabilize Gα in GDP-bound conformation is presumably not sufficient to counter-balance Gα self-activation (Urano et al., 2012b). Accordingly, protein regulators that accelerate the GTP hydrolysis reaction of plant Gαs are required to maintain a pool of GDP-bound Gα subunits within plant cells. Two GTPase-accelerating proteins (GAPs) have been identified and shown to mediate Gα self-activation. These include the regulator of G protein signalling (RGS) proteins and the phospholipase D

α1 (PLDα1) (Chen et al., 2003; Zhao and Wang, 2004; Urano et al., 2012b). RGS proteins and PLDα1 accelerate the GTPase activity of plant Gα subunits and therefore promote Gα binding to GDP. RGS proteins localize at plasma membrane and consist of a predicted seven-transmembrane domain and a cytoplasmic C-terminal tail that harbours a GAP domain (Chen et al., 2003; Urano et al., 2012b). Notably, RGS protein in *Arabidopsis* is essential to stabilize Gαβγ subunits in their heterotrimeric conformation (Liang et al., 2018).

1.3.3 G protein signalling in plants

Despite the wide range of G-protein-mediated signalling in plants, the diversity of G protein subunits is surprisingly low. This is exemplified in *A. thaliana* and *O. sativa*, whose genomes encode one Gα, one Gβ, and respectively three and five Gγs allowing for three and five heterotrimeric combinations, respectively (Kato et al., 2004; Perfus-Barbeoch et al., 2004; Thung et al., 2012; Trusov et al., 2012). This is in contrast to the human genome that encodes numerous Gαβγ subunits allowing for 1380 unique potential combinations of heterotrimeric G proteins (Xu et al., 2016).

Specificity of plant G protein signalling arises first from the diversity of Gγ subunits (Thung et al., 2012; Sun et al., 2018). Plant genomes encode three types of Gγs (A, B and C) that differentiate according to their varying C-terminal structure (Trusov et al., 2012). The type A Gγ subunits have similar structures than those of non-plant Gγs, while Gγs of types B and C are unique and only found in the plant kingdom (Trusov et al., 2012). Besides, many plant species are polyploid and have retained multiple G protein subunits (Pandey and Vijayakumar, 2018). For example, the soybean genome that is allotetraploid encodes four Gα, four Gβ and ten Gγ subunits (Choudhury et al., 2011).

The repertoire of plant G proteins is also uniquely extended as plant genomes encode unique and unusual extra-large G proteins, known as XLGs (Lee and Assmann, 1999; Ding et al., 2008; Pandey, 2019). XLG proteins have a C-terminal domain that is homologous to canonical Gα subunits, but also have a unique N-terminal domain extension (absent in canonical Gα subunits) that is about four-hundred amino-acid long and highly conserved among XLGs. All plant XLGs are presumably capable of GTP binding and can form heterotrimeric complex with plant Gβγ dimers (Heo et al., 2012; Urano et al., 2016a; Pandey, 2019). They function both redundantly and independently of canonical Gα proteins (Urano et al., 2016a; Pandey, 2019; Roy Choudhury et al., 2020). Thus, XLGs are often referred to

as non-canonical Gα proteins. For clarity, I won't refer further to non-canonical Gα subunits in this introduction as only canonical Gα (hereafter Gα) was reported to participate in the regulation of root nodule symbiosis (Choudhury and Pandey, 2013)

Plant G protein signalling is predicted to function via either one of the two following modes of action: (i) activation and dissociation of the heterotrimeric complex of which Gα and Gβγ bind to different protein targets and function in parallel, synergistically, or antagonistically; (ii) activation of either Gα or Gβγ while one inhibits the other's action via sequestration and vice-versa (Pandey et al., 2010; Roy Choudhury et al., 2020). Activation and/or regulation of plant G protein signalling involve stimulus-dependent activation of RLKs (Pandey, 2020), controlled activity of GAP proteins including RGS and PLD1α (Urano et al., 2012c; Urano et al., 2012b; Roy Choudhury and Pandey, 2016; Watkins et al., 2021), and post-translational modifications including phosphorylation of the G protein subunits (Chakravorty and Assmann, 2018; Oliveira et al., 2022).

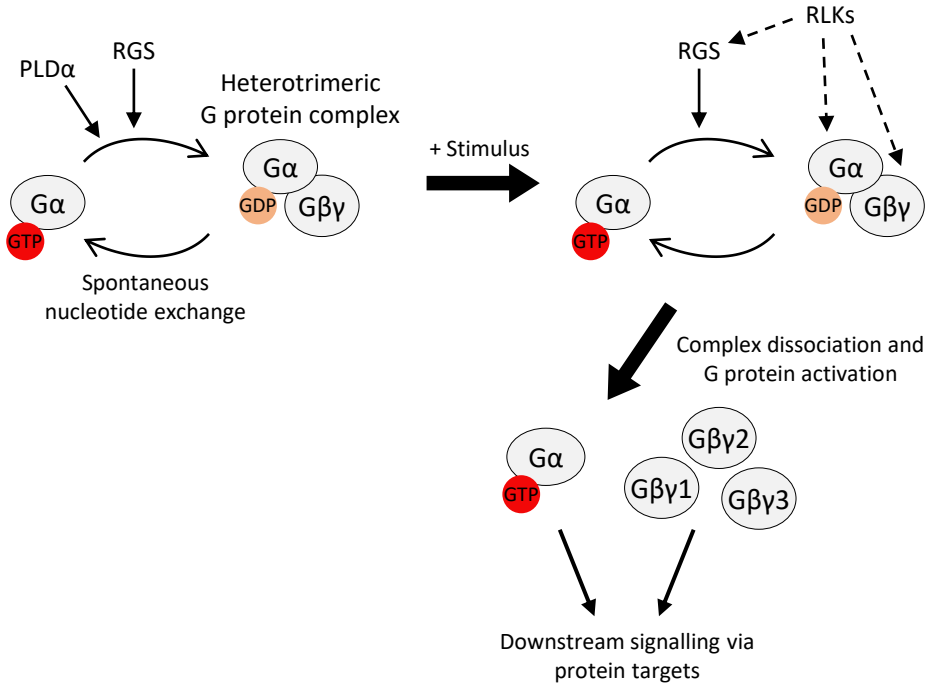

Figure 1.3 | Schematic representation of the G protein signalling in plants.
(Left panel) During the resting phase, the heterotrimeric G protein complex consists of the Gα subunit in a GDP-bound state, along with the Gβ and Gγ subunits forming a dimer. Plant Gαs undergo spontaneous nucleotide exchange, transitioning to the GTP-bound state. GTPase-accelerating proteins such as Phospholipase D alpha 1 (PLDα1) and Regulator of G-protein Signalling (RGS) play essential roles in regulating Gα self-activation, facilitating the exchange of GTP for GDP, and reforming the heterotrimeric complex. (Right panel) Upon stimulus, Receptor-Like Kinases (RLKs) interact with and regulate G protein subunits and/or RGS protein. (Bottom panel) Upon activation, the heterotrimeric complex dissociates, enabling transduction of downstream signalling via the interaction of GTP-Gα and/or Gβγ dimer with protein targets. Several Gβγ dimers are shown to underscore the diversity of Gγ subunits in plants, providing signal specificity.

1.3.4 G-protein-mediated regulation of nodulation

The G protein subunit *Gβ* was shown to positively regulate root nodulation in *G. max*, *M. truncatula* and *P. sativum* (Choudhury and Pandey, 2013; Bovin et al., 2022), whereas the soybean *GmGα* subunits were shown to negatively influence the development of root nodules (Choudhury and Pandey, 2013). No protein targets of either Gβ or Gα during nodulation have been identified. Their precise role was therefore not known as one or the other may simply inhibit the other's action via sequestration. Interestingly, the soybean Nod-factor receptor *Gm*NFR1α (ortholog of *MtLYK3*/*LjNFR1*) interacts with *Gm*Gα proteins and *Gm*RGS1/2 *in planta* (Choudhury and Pandey, 2013; Choudhury and Pandey, 2015). *Gm*NFR1α phosphorylates *Gm*RGS2 *in vitro*, and *Gm*NFR1α-mediated phosphorylation of *Gm*RGS2 increases its GAP activity toward *Gm*Gα1 (Choudhury and Pandey, 2015). Besides, constitutive expression of native *GmRGS2* and phosphomimic *GmRGS2* significantly increased nodule number compared with wild-type plants expressing empty-vector, the phosphomimic *GmRGS2* displaying a greater efficiency in that regard, whereas gene silencing of *GmRGS1/2* negatively affected root nodulation (Choudhury and Pandey, 2015). Thus, it was postulated that *Gm*NFR1α-dependent phosphorylation of *Gm*RGS2 promotes root nodule development via sequestration of the Gα subunits in their GDP-bound conformation (Choudhury and Pandey, 2015). In accordance with this, it was later shown that the symbiosis co-receptor *Gm*SymRKα (ortholog of *MtDMI2*/*LjSymRK*) interacts with and phosphorylates *Gm*Gα proteins (Roy Choudhury and Pandey, 2022). *Gm*SymRKα-dependant phosphorylation of *Gm*Gα1 renders it incapable of GTP binding. Phosphomimic *Gm*Gα1 also loses its ability to interact with Gβγ dimers *in planta*, whereas phospho-deficient *Gm*Gα1 is still capable of interacting with its heterotrimeric partners (Roy Choudhury and Pandey, 2022). Constitutive expression of phosphomimic *GmGα1* and phospho-deficient *GmGα1* resulted in significantly more and fewer number of root nodules, respectively. Taken together, it suggested that Gα subunits in soybean negatively impact root nodulation via sequestration of the Gβγ dimers. It also revealed that Gβ proteins may positively regulate root nodulation via binding to protein targets, as *Gm*SymRKα-dependant phosphorylation of *Gm*Gαs ultimately results in release of the Gβγ dimer from its heterotrimeric complex. Nonetheless, at which step of root nodule symbiosis G protein signalling would intervene, either during rhizobial infection or root nodule organogenesis, or both, remained enigmatic. Besides,

whether G protein signalling regulates the symbiosis signalling that is common to mycorrhizal and rhizobial endosymbioses remained also unknown.

1.4 Thesis outline and objectives

The role of G proteins during root nodulation prompted us to speculate that G protein signalling mediates rhizobial and mycorrhizal symbioses, and that Gβ would participate in the symbiosis signal transduction that leads to activation of nuclear Ca^{2+} signalling during root endosymbiosis. First, genetic analyses of *M. truncatula* mutants to characterize the role of *MtGβ* in root endosymbiosis will be described (chapter 3). Second, characterization of *MtGβ* function in regulating nuclear Ca^{2+} signalling, symbiosis-activated gene expression and symbiosis-activated root nodule organogenesis will be presented (chapter 4). Finally, identification of *Mt*Gβ interactors to regulate root endosymbiosis will be detailed (chapter 5).

Chapter II

Material and Methods

2.1 Plant materials and growth conditions

Medicago truncatula cv. *Jemalong* A17 (Barker et al., 1990) was used as wild-type. Mutants *dmi1-1* (C71) and *dmi2-1* (TR25) were reported previously (Sagan et al., 1995; Penmetsa and Cook, 1997; Catoira et al., 2000). TILLING mutants were identified from a population of 3,162 individual lines (cultivar A17) generated by Le Signor and co-authors (2009) and reverse screened by RevGenUk (John Innes Centre). TILLING $G\beta^{L31F}$ and $G\beta^{D35N}$ mutants were backcrossed with *M. truncatula* A17:YC3.6 (Feng et al., 2019) and homozygote progenitures were used for calcium imaging and symbiosis phenotyping, respectively.

For seed sterilization, seeds were scarified with sandpaper and surface-sterilised in 10% sodium hypochlorite solution for 2 min. Seeds were washed 5 times with sterile water before plating on water agar. Seeds were stratified and placed at 4ºC for 5-7 days in the dark and subsequently germinated overnight at room temperature in the dark.

For growth in sterile condition, germinated seeds were moved onto sterile square plates (clear polystyrene petri dish, 120/120/17 mm, Greiner Bio-One, item No. 688161) containing appropriate medium agar and sealed with micropore surgical tape. Plates were placed vertically in growth cabinet under controlled environment (16/8-hour day-night cycle at 23ºC, with 32% humidity, light intensity of 300 μmol/m^2/s).

For symbiosis assays and seed production, seedlings were first grown in sterile condition and then moved into plastic pots (4×4×6 cm). Pots were placed in greenhouse under controlled environment (16/8-hour day-night cycle at 22ºC, light intensity of 300 μmol/m^2/s). For symbiosis assays, a 1:1 v/v autoclaved mixture of Terragreen (Oil-Dri Ltd., UK) and sand was used. For seed production, a peat-and-loam-based mix with added grit (65% peat, 25% loam, 10% grit, 3kg/m^3 dolomitic limestone,1.3kg/m^3 PG mix, 3kg/m^3 osmocote exact) was used. After 2-3 weeks, plants for seed production were moved to larger pots (9×9×11 cm) for flowering and self-fertilization.

2.2 Genotyping of TILLING population

A leaf of each plant for genotyping was collected 7-10 days after planting on soil. The leaves were frozen at -20 °C and then extracted using the QIAamp® 96 DNA QIAcube HT kit (Qiagen) 96-well plate kit following manufacturer's instructions, with elution in 50 µL sterile dH_2O. Genotypes were assessed via fluorescence-based competitive allele specific PCR (He et al., 2014). Wild-type- and mutant-specific primers were labelled with VIC (Victoria) and FAM (6-Carboxyfluorescein) fluorescent dyes, respectively. Primer mix was prepared as follows; 12 µL of each allele-specific forward primer 100 µM (FAM and VIC), 30 µL of common reverse primer 100 µM, diluted with dH_2O up to 100 µL. Reaction mix was made of 0.3 µL primer mix, 2.1 µL PACE® polymerase 2X 150 nM (3CR BIOSCIENCE), 2.1 µL dH_2O, and 1 µL genomic DNA. The conditions of PCR were the following: initial denaturation (15 min at 94°C), followed by 10 cycles of first amplification (20 sec at 94°C; 1 min at 54°C), and 35 cycles of second amplification (20 sec at 94°C; 1 min at 55°C). Fluorescence was measured on PHERAstar plate reader. Excitation and emission wavelengths of FAM and VIC dyes are 485/520 nm and 520/570 nm, respectively. Data were analysed on KulsterCaller genotyping software. Genotypes of selected individuals were confirmed through sequencing of PCR products. Primers are listed on Table 2.3.

2.3 CRISPR-CAS9

Vectors were produced using the Golden Gate cloning strategy as described in this chapter (section 2.13.5). *Mt*U6.6 promoter and terminator (Kim and Nam, 2013), single guide RNAs (sgRNAs), and scaffold for sgRNAs (Castel et al., 2019) were *de novo* synthesised. *Mt*U6.6 promoter and terminator and sgRNA scaffold were cloned into modified pL1F-3~5 vectors with an internal *RFP* gene for negative selection, flanked with Esp3I restriction sites for sgRNA insertion. The synthetic DNAs corresponding to the sense and antisense sequences of the sgRNAs were diluted 1000X and mixed 1:1. The mix was heated up in a water bath to 95 ºC and slowly cooled down to room temperature. Double-strand sgRNAs were inserted into pL1F-3~5 (1 µL sgRNA mix in 15 µL final volume with Esp3I enzyme (ThermoFisher Scientific) as opposed to BsaI to generate sgRNA-containing pL1F-3~5 vectors). Level 0 vector containing *Cas9* gene is the pICSL90017 from The Sainsbury Laboratory (TSL, Norwich) with N- and C-termini nuclear localised sequence (NLS) and Arabidopsis-codon-optimised sequence with potato intron (Castel et al., 2019). Final level 2 vectors are described

in Table 2.4. Roots were transformed via *Agrobacterium-rhizogenes*-mediated root transformation and subsequently screened for nodulation assay. Nodules were counted on fully transformed roots at 25 days post-inoculation and roots were sampled in liquid nitrogen for DNA extraction. DNA was extracted with the DNeasy® Plant Mini Kit (Qiagen) according to the manufacturer's instructions. DNA was amplified via PCR using GoTaq® and amplified fragments were gel extracted for sequencing. When individuals had multiple fragments of different size, those were extracted and sequenced separately. In some cases, noise in the sequencing chromatograms was too elevated for the sequences to be called. Accordingly, individuals with ambiguous sequences were classified as chimera and removed from the final data set. Primers are listed in Table 2.3.

2.4 Symbiosis assays

2.4.1 Microsymbiont material

Sinorhizobium meliloti strain 2011 (Sm2011) expressing *LacZ* reporter gene (Sm2011:*LacZ*), reported previously (Ardourel et al., 1994), was used for all rhizobial infection and nodulation assays. *LacZ* encodes a β-galactosidase enzyme that cleaves β-galactosides. X-Gal (5-Bromo-4-chloro-3-indolyl-β-D-glucuronic Acid) is used as substrate and its cleavage results in a dark blue precipitate. Blue coloration reports the presence of bacteria. For mycorrhization assays, *Rhizophagus irregularis* spores were contained in a granulate mixture (Endorize, Agrauxine, France) used as inoculum (12.5% of final volume) in all mycorrhization assays.

2.4.2 Rhizobial infection assay

Germinated seeds were grown in sterile condition on square plates containing BNM (Table 2.1) 1% agar covered with sterilised filter paper (WHA10334365, Sigma-Aldrich) to prevent roots from penetrating the medium. Sm2011:*LacZ* was grown on selective TY (Table 2.1) plate containing 100 µM Spectinomycin and 4 µM tetracycline for 2-3 days at 28ºC. Single colony was inoculated in selective TY liquid for 2 days at 28ºC. The culture was spun down by centrifugation (5 minutes at 4000 rpm) and resuspended in sterile dH_2O. 1-day old roots were sprayed with 1 mL of Sm2011:*LacZ* prepared at OD_{600}=0.01 using an Intranasal Mucosal Atomization MAD Nasal™ device and grown in sterile condition for five more days. Plants were then stained via LacZ staining as described below. Infection pocket and infection thread were visualised by the blue-stained bacteria and the numbers were counted using a light microscope. The number of infections is relative to the length of root.

2.4.3 LacZ staining

Roots were fixed in fixative solution made of Z' buffer (100 mM Sodium Phosphate buffer (75 mM $Na_2HPO_4 \cdot 7H_2O$; 25 mM $NaH_2PO_4 \cdot H_2O$), 10 mM KCl, 1 mM $MgCl_2$) supplemented with 2.5% v:v glutaraldehyde. This was gently vacuum-infiltrated for 30 min. Fixative solution was replaced with fresh and samples were kept at room temperature for 1 hour. Samples were washed three times for 5 min with Z' buffer. Staining solution was added (1 mM X-Gal, 5 mM $K_3[Fe(CN)_6]$, 5 mM $K_4[Fe(CN)_6]$, mixed in Z' buffer) and samples were kept in the dark for 2-4 hours at 30ºC. Staining reaction was stopped by replacing staining solution with Z' buffer.

2.4.4 Nodulation assay

To assess the nodulation phenotypes of the TILLING mutants, germinated seeds were grown in sterile condition for 6 days on square plates containing BNM 1% agar. Plants were then transferred into pots for symbiosis assay and grown one more day before inoculation with rhizobium. 5 mL of Sm2011:*LacZ* prepared at OD_{600}=0.01 was spread onto the soil surface of each plant. Root nodules were counted using a light microscope. Number of nodules is relative to the root dry mass. Roots were dried out at 37 ºC for 2 days. Number of days of inoculation are indicated in figure legends.

2.4.5 Mycorrhization assay

To assess the mycorrhization phenotypes of the TILLING mutants, germinated seeds were grown in sterile condition for 6 days on square plates containing BNM 1% agar. Plants were then transferred into pots for symbiosis assay supplemented with 1:8 v/v (12.5%) of granulate mixture containing *Rhizophagus irregularis* spores (Endorize; Agrauxine, France). Fungal structures were blue stained in acidic ink as follows; roots were cleared in 10% KOH 15 min at 95°C, washed 3 times in water and subsequently stained in acidic ink (5% ink, 5% acetic acid) for 4 min at 95°C. The percentage of root colonization was quantified using the grid line intersect method (Giovannetti and Mosse, 1980). Briefly, roots were cut into small segments and spread randomly in plastic petri dishes in which a grid with 1×1 cm squares was affixed to the base. At least one hundred and twenty intersections for each root sample were counted to measure roots with or without AM-associated structures using a light microscope. Number of days of inoculation are indicated in figure legends.

2.4.6 Complementation of TILLING mutant

For complementation of $G\beta^{L29F}$ mutant, wild-type and mutant were transformed via *Agrobacterium-rhizogenes*-mediated root transformation as described below. Four weeks post-transformation, transformed roots were screened via fluorescence and inoculated as indicated above for nodulation or mycorrhization assays. Root nodules and AM-associated structures were scored as described above using a Leica MZFLIII with fluorescence screening for counting nodule on transformed roots or selecting transformed material for AM blue staining.

2.5 *Agrobacterium-rhizogenes*-mediated root transformation

2.5.1 Transformation of *Agrobacterium rhizogenes*

T-DNA vectors were generated via Golden Gate as described below. *Agrobacterium rhizogenes* electrocompetent cells AR1193 (Stougaard et al., 1987) were transformed by electroporation (200 Ω, 1.25 V, 25 µF; Gene Pulser Bio-Rad) with 1.5 µL plasmid DNA (250 $ng.\mu L^{-1}$) and 20 µL cell aliquot in an electroporation cuvette (Geneflow). Cells were afterwards incubated in 300 µL SOC medium (Table 2.1) at 28ºC and 220 rpm for 2 hours, then plated on LB medium (Table 2.1) supplemented with appropriate antibiotics and incubated at 28ºC for 3 days.

2.5.2 Root transformation procedure

Each plant had their root cut off and regenerated into transgenic roots via *Agrobacterium-rhizogenes*-mediated transformation, while the shoot system of the plants remained non-transgenic. Each transformed root system should be considered as an independent transformant as it results from independent T-DNA insertion event. For each assay, new sets of transgenic roots were prepared. The transformation efficiency varied between 10% and 60%.

To prepare the agrobacterium, *A. rhizogenes* AR1193 expressing the T-DNA of interest were first grown on selective LB plates for 3 days at 28ºC. On the morning prior to root transformation, single colonies were incubated for 24 hours in multiple 10 mL liquid LB medium supplemented with appropriate antibiotic selection (about 50 mL of agrobacterium culture to transform ~300 seedling roots). The day after, cells were spun down at 4000 rpm for 5 min and resuspended in sterile dH_2O.

M. truncatula seedlings were germinated overnight at room temperature. The transformation was performed in sterile condition under a laminar flow cabinet. Germinated seeds were kept in sterile dH_2O to prevent them from drying out. Seed coats were removed to avoid subsequent fungal contamination. Roots are 1-2 cm long and approximately 3-5 mm of root tip was cut off after which the seedlings were dipped into the cell suspension of agrobacteria for 5 min. 20 seedlings were dipped into 1.5 mL of cell suspension while a next batch of 20 seedlings was prepared. Cell suspensions were changed regularly to reduce the risk of fungal contamination. After dipping, seedlings were placed into square plates containing Mod FP (Table 2.1) 1% agar and 2 µg/mL nystatin and grown in sterile condition for 5-7 days. The following week, roots that had regenerated were cut off as those are mostly non-transgenic. Plants were then placed into new squares plates containing Mod FP 1% agar and 2 µg/mL nystatin and covered with sterilised filter paper (WHA10334365, Sigma-Aldrich) to prevent roots from penetrating the medium. Plants were grown in sterile condition for 1 up to 4 weeks depending on the assay. Fluorescent probes were used as transgenic marker. Transformed roots were screened using a fluorescence stereo microscope (MZFL III Leica). Roots with no fluorescence or chimeric fluorescence were cut off. Plants with fully fluorescent roots were kept for further analyses.

2.6 Spontaneous nodulation

To assess spontaneous formation of nodule-like structures in wild-type and *dmi2-1* mutant using different combinations of heterotrimeric G proteins, wild-type and mutant were transformed via *Agrobacterium-rhizogenes*-mediated root transformation as described above. Three weeks post-transformation, transformed roots were screened via fluorescence and transferred into sterile phytatrays™ (L×W×H 11.4 cm×8.6 cm×10.2 cm, Sigma-Aldrich; 4 plants/phytatrays) containing 1:1 v/v autoclaved mixture of Terragreen (Oil-Dri Ltd., UK) and sand. *dmi2-1* plants were inoculated with Sm2011:*LacZ* as described above in nodulation assay procedure. Plants were uprooted after 70 days of growth in phytatrays™. Nodule-like structures were counted using a light microscope. For sectioning, nodule-like structures were embedded in 5% agarose and sectioned with a VT1000 vibratome (Leica) using 100 µM sections. Cross-sections were imaged on a Leica DM6000 microscope.

2.7 Quantification of gene expression

2.7.1 RNA extraction

Roots were sampled in liquid nitrogen and grinded with mortar and pestle. Total RNA was extracted using the RNeasy® Plant Mini Kit (QIAGEN) according to the manufacturer's instructions. Samples were treated with DNase I (BIORON) for 25 min twice. Absence of genomic DNA was validated via PCR amplification of intronic fragments. Concentration and purity were determined by spectrophotometry (A260/280 and A260/230 ratios) and integrity was confirmed by gel electrophoresis (2% w/v agarose).

2.7.2 cDNA synthesis

cDNA was obtained from 550-1000 ng of RNA using the SuperScript™ III Reverse Transcriptase (Invitrogen) according to the manufacturer's instructions.

2.7.3 Quantitative PCR

Quantitative PCR (qPCR) was performed using a CFX96 Touch™ Real-Time PCR Detection System (BIO-RAD) with SYBR® Green JumpStart™ Taq ReadyMix™ (Sigma-Aldrich). For each primer set, amplification efficiency (E) was first determined through a cDNA dilution series standard curve (two technical replicates per data point and five data points corresponding to 20X, 40X, 80X, 160X, 320X dilutions of cDNA, in 10 µL reaction mix, including 0.2 mM of each primer). The conditions of the qPCR were the following: initial denaturation (2 min at 95ºC), followed by 40 cycles of amplification and quantification (20 seconds at 95ºC; 20 seconds at 60ºC, and 20 seconds at 72ºC, with a single fluorescence measurement). A melt curve was also generated to verify the specificity of the amplification reaction (50 ºC to 95 ºC, with a fluorescence measurement every 0.5 ºC). Calculation of the normalised expression and fold change ratio was performed using the mathematical model described by Pfaffl (2001). Primers used for qPCR are listed in Table 2.3.

2.8 Calcium imaging

For calcium phenotyping of the F2 segregating population of YC3.6×$G\beta^{L31F}$ mutant, F2 homozygous wild-types and mutants were grown in sterile condition for 2 days on square plates containing BNM 1% agar and 100 nM aminoethoxyvinylglycine (AVG) covered with sterilised filter paper. For calcium imaging of transformed roots co-expressing *YC3.6* with *NES-Gβ* or *NLS-Gβ*, or *NLS-RGECO* with $MtRGS^{PentaD}$, wild-type plants were transformed

via *Agrobacterium-rhizogenes*-mediated root transformation. Site-directed mutagenesis via overlapping PCR was conducted on *MtRGS* coding sequence to replace the five phosphorylation sites with aspartate residues (*Mt*RGS^{PentaD}). Transformed roots were screened via fluorescence at 17-20 days post transformation. A chamber of 48×64 mm coverglass (Solmedia) using high-vacuum grease (Dow Corning GMBH) was used to place the roots in 1-2 mL dH_2O. Only the root was covered with a coverslip to leave space for Nod-factor application at a final concentration of 10^{-8} M. Nod-factors were produced as previously described (Morieri et al., 2013). For induction of *MtRGS*^{PentaD} expression, plants were placed in sterile 6-well plates and roots were incubated in 5 mL liquid BNM complemented with 25 µM dexamethasone. During incubation, plants were kept in growth cabinet for the indicated time (18-24 hours). Calcium imaging was performed using a Nikon ECLIPSE FN1 equipped with an emission image splitter (Optosplit, Cairn Research, UK) and an electron multiplying cooled charge coupled camera (Rolera™ Thunder EMCDD, QImaging). CFP was excited at wavelength of 436±20 nm by a light emitting diode (OptoLED, Cairn) and emitted fluorescence was detected at of 480±40 nm for CFP and 535±30 nm for YFP. RGECO was excited at 561 nm and emitted fluorescence captured in the 571–640 nm range. Images were collected in 3 sec intervals using MetaFluor software. Nod-factor-activated calcium oscillations were recorded for at least 30 min. Spontaneous nuclear calcium spiking was recorded for at least 30 min. Calcium imaging traces shown in this study are non-detrended.

2.9 Confocal microscopy

Localization experiment for *Mt*Gβs-GFP was performed using a Zeiss 780 confocal laser scanning microscope equipped with an Argon Krypton laser (Zeiss). Wild-type plants were transformed via *Agrobacterium-rhizogenes*-mediated root transformation and transformed roots were imaged at 21 days post-transformation. Nod-factor treatment was performed in 5 mL dH_2O complemented with mock or Nod-factors at 10^{-7} M. The 488 nm excitation line of the argon ion laser was used to excite GFP, and emission spectra were collected between 490 and 535 nm. For mCherry, excitation wavelength was 561 nm and emission imaged between 575-625 nm. The experiment was conducted with at least three plants for each construct and condition, and one or two root hairs per plant were imaged. Images were processed in Zen 3.1 lite software. Protein expression and integrity was assessed by protein extraction and immunoblotting.

2.10 Yeast-two-hybrid

The gal4-based yeast two-hybrid assay was performed in the yeast strain AH109. Protein coding sequences were amplified from *M. truncatula* cultivar A17 root cDNA. The murine p53 and its interacting partner SV40 large T-antigen were used as control (CLONTECH PT3024-1). The vector pBD-GAL4-GW and pAD-GAL4-GW (CLONTECH) were used to sub-clone sequences via BP/LR gateway cloning (Invitrogen) as described below (section 2.13.6). Yeast strain was transformed using the lithium acetate method (Gietz and Woods, 2002). Briefly, 50 mL of yeast culture was grown at 30 ºC in YPAD medium (Table 2.1) until an OD_{600} of 0.6-0.8, centrifuged for 5 min at 1000 g, resuspended in sterile dH_2O, centrifuged for 5 min at 1000 g, and pellet carefully resuspended in 1.5 mL of 100 mM lithium acetate. For each transformation reaction, 100 µL of yeast cells were carefully added to 300 µL of transformation mix (40% polyethylene glycol, 0.12 M lithium acetate, 0.16 $mg.mL^{-1}$ salmon sperm DNA, and 2-3 µL of plasmids (300-500 $ng.mL^{-1}$)). The mixture was vortexed vigorously for 2 min, incubated at 30 ºC for 30 min, then at 42 ºC for 30 min, centrifuged for 5 min at 700 g and gently resuspended in 100 µL 0.9% NaCL. Co-transformed yeasts were grown on synthetic dropout SD medium (Table 2.1) lacking leucine and tryptophan (-LW) for 2 days at 28 °C. Positive transformants were grown in liquid SD medium -LW overnight at 28 °C and resuspended in sterile dH_2O. Pairwise interactions were assessed on synthetic dropout SD medium lacking adenine, histidine, leucine, and tryptophan (-AHLW) after 7 days of growth at 28 °C.

2.11 Co-immunoprecipitation

Co-immunoprecipitation (co-IP) was performed to assess interaction of *Mt*Gβ and *Mt*AUK *in planta*. Constructs were generated via Golden Gate cloning (see section 2.13.5). Genomic sequence of *MtAUK* was domesticated by L. Grubb (Charpentier's lab) to create the Golden Gate vector. The latter construct was domesticated by L. Grubb to generate *Mt*AUKΔGβ. Protein coding sequences of *MtGβ* and *MtDMI3* were used to create the Golden Gate vectors. *Mt*AUK and *Mt*AUKΔGβ were C-terminally fused to modified C-terminal YFP including HA epitope. *Mt*Gβ and *Mt*DMI3 were C-terminally fused to modified N-terminal YFP including MYC epitope. All recombinant genes were driven by constitutive promoters except for *Mt*Gβ-MYC-nYFP that was driven by *MtGβ* native promoter. Final level 2 vectors are listed in Table 2.4. *Agrobacterium-rhizogenes*-mediated root transformation was performed

in *M. truncatula* cultivar A17. Four weeks post-transformation, approximately 40 plants were transferred into plastic pots (4×4×6 cm) filled with a 1:1 v/v autoclaved mixture of Terragreen (Oil-Dri Ltd., UK) and sand. Plants were further cultured in sterile growth cabinet for another week. Plants were then inoculated with Sm2011:*LacZ* as described above. Two days post-inoculation, plants were uprooted, washed in water, roots cut apart and flash frozen in liquid nitrogen. For co-IP analysis, roots were pulverised in liquid nitrogen with mortar and pestle and resuspended in lysis buffer (10% glycerol, 50 mM Tris-HCl pH 8.0, 150 mM NaCl, 1% Igepal ca-630, 250 mM Mannitol, 1 mM PMSF, 20 µM MG-132 with the addition of cOmplete^{TM} EDTA-free protease inhibitor cocktail tablets (Roche) (1 tablet per 50 mL)) at a ratio of 10 mL per 3 g root material. The material was further homogenised using a Potter tube homogenizer and then supernatant was clarified by centrifugation 3 times at 2,558 × g for 10 min each. An input fraction was collected and then the supernatant was incubated with µMacs HA-trap beads (µMACS^{TM} HA Isolation Kit, Miltenyi Biotec) for 2 h at 4 °C. Supernatant was then applied to a µ column in a µMacs magnetic stand and then beads were washed 4 times with 1 mL wash buffer (50 mM Tris-HCl pH 8.0, 150 mM NaCl, 0.1% Triton X-100, with the addition of cOmplete^{TM} EDTA-free protease inhibitor cocktail tablets (Roche) (1 tablet per 50 mL)). Following washes, beads were eluted by two additions of 40 µL µMacs elution buffer (50 mM Tris HCl (pH 6.8), 50 mM DTT, 1% SDS, 1 mM EDTA, 0.005 bromphenol blue, 10% glycerol) preheated to 80°C and beads were allowed to sit in buffer for 1 min prior to elution from columns. Input and IP samples were then loaded on an SDS-PAGE gel and immunoblotted with αHA or αGFP^{Nterm} antibodies (see Section 2.13.9 and Table 2.2). Immuno-band intensity was quantified using imageJ (see detailed method in Chapter 11, section 3.5 of Stael et al., 2022). The regions of interest were equal for each immuno-band.

2.12 Protein expression in heterologous system

2.12.1 Purification from *Escherichia coli*

Protein coding sequences were cloned into pOPIN-M vector including a 3xHis:MBP tag by In-Fusion cloning (see section 2.13.7) followed by transformation into *E. coli* Rosetta DE3 expression strain (Sigma-Aldrich) via heat shock (see section 2.13.8). Cell cultures were grown in 8 L liquid LB at 30 °C with 210 rpm shaking until OD_{600} 0.6-0.8 was reached (3-6 hours) followed by transfer to 16 °C overnight. Overnight culture was complemented with 1 mM IPTG to induce protein expression. Cells were harvested by centrifugation in a Sorvall

Lynx centrifuge at 5,663 x g and resuspended in buffer A1 (50 mM HEPES, 50 mM glycine, 0.5 M NaCl, 20 mM imidazole, 5% (v/v) glycerol) with the addition of cOmplete™ EDTA-free protease inhibitor cocktail tablets (Roche) (1 tablet per 50 mL). Cells were lysed by sonication using a VibraCell sonicator (SONICS) at 40% maximum amplitude with 1 s pulse and 3 s interval between pulses. Whole cell lysate was centrifuged at 38,724 x g for 30 min at 4 °C in a Sorvall Lynx centrifuge. Clarified cell lysate was then injected onto a 5 mL Ni2+-NTA column (GE Healthcare) equilibrated in A1 buffer, followed by step-elution with elution buffer B1 (50 mM Tris-HCl pH 8.0, 50 mM glycine, 0.5 M NaCl, 500 mM imidazole, 5% (v/v) glycerol), and transfer to a Superdex 200 16/60 gel filtration column equilibrated in buffer A4 (20 mM HEPES pH 7.5, 150 mM NaCl, 1 mM TCEP). Fractions of 2 mL were collected, those corresponding to an absorbance peak were separated via SDS-PAGE, and those containing the protein of interest were pooled and concentrated to 1-3 mg/mL using VivaSpin® centrifugal concentrators (30K for 3xHis:MBP:Gβs). For cleavage of the 3xHis:MBP tag, 3C protease (Thermo Fisher Scientific, 1:100 ratio of protein:protease) was added to the concentrated proteins and incubated overnight at 4 °C for cleavage of the tag.

2.12.2 Purification from insect cells

Insect cells of *Spodoptera frugiperda* strain *Sf9* were maintained at a density of 1×10^6 cells/mL by passaging in 20 mL of 1 × SF-900™ (SFM; Gibco) every 3-5 days, with density measured using an automated cell counter instrument (Countess 3 FL Automated Cell Counter, Invitrogen). Disposable Countess™ Cell Counting Chamber Slides (Invitrogen) were prepared with a mix of 10 µL of insect cell sample with 10 µL of trypan blue before inserting the slide into the instrument for cell counting. The cells were grown at 26 °C with 200 rpm shaking.

For protein production from insect cells, protein coding sequences were subcloned into pOPIN-M as described above and then pFASTBAC1 (Invitrogen) by In-Fusion cloning (Takara BioSciences). Briefly, coding sequences including MBP tag and genes of interest were created by PCR using Phusion® High Fidelity DNA Polymerase (New England Biolabs) with the pOPIN-M-Gβs vectors as DNA template, and specific primers to generate overhangs with BamHI and HindIII as digestion sites. pFASTBAC1 vector was linearised with BamHI and HindIII restriction enzymes. In-Fusion cloning reaction followed the same procedure than described below (section 2.13.7). Briefly, the constructs were transformed into STELLAR *E. coli,* transformants selected and plasmids purified to isolate plasmid DNA

followed by confirmation by sequencing. Next, recombinant bacmid was generated by transforming via heat shock purified plasmid into DH10Bac competent cells (Thermo Fisher Scientific) expressing YFP as a transformation marker. Positive colonies were selected and isolated using a modified plasmid purification protocol. From a 5 mL culture incubated overnight at 37 °C with 200 rpm shaking, cells were pelleted at 2,558 × g for 5 min and resuspended in 300 µL buffer P1 (50 mM Tris-Cl pH 8, 10 mM EDTA, 100 µg/mL RNase A, Qiagen plasmid prep kit). Following addition of 300 µL buffer P2 (200 mM NaOH, 1% SDS (w/v)), mixture was incubated at room temperature for 5 min. 400 µL of P3 (3 M potassium acetate, pH 5.5) was added and mixed by inversion. This was allowed to rest on ice for 6 min and then centrifuged at 2,558 × g for 10 min and then an additional 2 min. Supernatant was removed and 500 µL of 70% ethanol was added to the pellet and inverted before centrifugation at 2,558 × g for 5 min at room temperature. This was repeated twice more. Supernatant was removed and pellet was air-dried for 1 min. DNA was then dissolved in 50 µL buffer EB (10 mM Tris-Cl, pH 8.5) and bacmid concentration was determined with a NanoDrop One (Thermo scientific). Sequence was confirmed via sequencing. Next, recombinant baculovirus was produced using *Sf9* cells cultured in 1 × SF-900™ (SFM; Gibco). Cells in log phase were added to wells containing 2 mL SFM medium and seeded at 0.5 $\times 10^6$ cells/mL in a 6-well plate. Cells were allowed to attach for 15 min at room temperature. 6 µL of FuGENE HD transfection reagent (Promega) was added to 4 µg of bacmid in 200 µL SFM medium and incubated for 15 min at room temperature. This was then added dropwise to the cells in 6-well plates and incubated for 3 days at 27 °C for production of the P1 viral stock. P1 virus was harvested and P2 was produced by addition of 1:100 P1 to 50 mL *Sf*9 cells at density of 1-2 × 10^6 cells/mL. This was incubated for 3 days at 27 °C with 200 rpm shaking to produce the P2 viral stock. P2 viral stock was harvested by centrifugation at 1000 × g for 10 min at 4 °C. Supernatant was used (1:100 ratio) to infect 1 L culture at 2 $\times 10^6$ cells/mL and incubated for 60 hours at 27 °C with shaking at 200 rpm. Cells were harvested at 2 000 ×g for 15 min and washed in PBS.

For protein purification, cells were centrifuged again at 2,000 × g for 10 min, resuspended and lysed in 30 mL ice-cold lysis buffer (25 mM Tris, pH 7.5, 200 mM NaCl, 1mM DTT) with the addition of cOmplete™ EDTA-free protease inhibitor cocktail tablets (Roche) (2 tablets per 50 mL). Cells were lysed by sonication using a VibraCell sonicator (SONICS) at 40% maximum amplitude with 1 s pulse and 3 s interval between pulses. Whole cell lysate was centrifuged at 500 x g for 10 min at 4 °C in a Sorvall Lynx centrifuge.

Supernatant was centrifuged again at 30,000 x g for 30 min at 4 °C. Supernatant was added to a 5 mL MBP-Trap column (GE) and washed with 15 mL lysis buffer without DTT. Proteins of interest were eluted with 20 mL lysis buffer without DTT supplemented with 10 mM of maltose. Protein presence and purity was then assessed via SDS-PAGE and Western-blot.

2.13 Molecular biology methods

2.13.1 Polymerase chain reaction and DNA migration

PCR using GoTaq® G2 Green Master Mix (Promega) was prepared in 25 µL final volume (5 to 50 ng of DNA template, 12.5 µL 2X GoTaq® Green Master Mix, 0.4 µM primers, mixed in dH_2O). The conditions of PCR were the following: 5 minutes at 95°C, followed by 30-40 cycles of amplification (30 sec at 95°C; 30 sec at primer's annealing temperature; 60 sec per kb of amplified fragment at 72°C), and a final extension of 5 min at 72°C.

PCR using Phusion™ High-Fidelity DNA Polymerase (ThermoFisher Scientific) was prepared in 20 µL final volume (5 to 50 ng of DNA template, 0.25 µL Phusion™ High-Fidelity DNA Polymerase, 4 µL 5X Buffer HF, 0.25 µM dNTPs, 0.4 µM primers, mixed in dH_2O). The conditions of PCR were the following: 2 minutes at 98°C, followed by 30-40 cycles of amplification (30 sec at 98°C; 30 sec at primer's annealing temperature; 15/30/40 sec per kb of amplified fragment at 72°C for plasmid/genomic/complementary DNA template, respectively), and a final extension of 10 min at 72°C.

Overlapping PCR, for sequence domestication using two separate PCR fragments upstream and downstream of the domestication site, was prepared using Phusion™ High-Fidelity DNA Polymerase in a 2-step fashion in 20 µL final volume as described above using two PCR-amplified fragments as templates and without primers. The conditions of overlapping PCR were the same as described above with the following modifications: 12 cycles of amplification (step one, without primers), followed by 5 minutes at 42°C while the 5' and 3' end primers were added at 0.4 mM final concentration, then 32 cycles of amplification (step two, with primers), with a final extension of 10 min at 72°C. PCR products were isolated via gel DNA extraction.

Whole plasmid amplification, for sequence domestication of a given plasmid, was prepared using Phusion™ High-Fidelity DNA Polymerase in 20 µL final volume as described above with 10 ng of DNA template. The conditions of PCR were the same as above. Amplified plasmids were digested with DpnI restriction enzyme (15 µL PCR reaction, 2 µL

enzyme, 1.5 µL CutSmart Buffer) to cleave remaining plasmid template for 1 hour 30 minutes at 42°C and 15 minutes at 80°C.

PCR products were resolved in 1% (w/v) agarose Tris-Acetate-EDTA (TAE) buffer gels (Melford), along with a 2-log DNA ladder (New England Biolabs®) and stained for 10-15 min in a 10 $mg.mL^{-1}$ ethidium bromide solution.

2.13.2 Gel DNA extraction

Agarose gel was moved onto UV box and DNA-containing gel slices were cut and kept in Eppendorf tubes. DNA was extracted with QIAquick® Gel Extraction Kit (Qiagen) according to the manufacturer's instructions with the following modification: DNA was precipitated with 100 µL isopropanol prior to applying sample to the column and DNA was eluted with 17 µL Buffer EB.

2.13.3 Plasmid purification

Plasmids were purified with QIAprep Spin Miniprep Kit (Qiagen) according to the instructions of the manufacturer. Pellets from 4 mL overnight-grown bacterial culture (10 min centrifugation at 2,558 × g) were used for purification. Plasmids were eluted with 30 µL Buffer EB.

2.13.4 Sequencing of PCR product and plasmid

Sequencing tube reaction was prepared in 1.5 mL Eppendorf tube with 1 µL PCR product or 2 µL purified plasmid, 2.5 µL of 10 mM primer, in 10 µL final volume mixed with dH_2O. Tubes were sent to Genewiz (Azenta, UK) for Sanger sequencing.

2.13.5 Golden Gate cloning

Golden gate cloning followed the principles previously outlined (Engler et al., 2008; Engler et al., 2009; Weber et al., 2011). Level 0 modules were synthesised by Life Technologies (Thermo Fisher Scientific). Coding sequences were amplified from *M. truncatula* cultivar A17 cDNA using Phusion™ DNA Polymerase. Where necessary, Golden Gate incompatible restriction sites were removed by site directed mutagenesis via overlapping PCR. When possible, Golden Gate vectors were created via whole plasmid amplification (e.g., plasmid containing wild-type *MtGβ* sequence mutated into $MtG\beta^{L29F}$ sequence by mutating one single nucleotide). Level 1 vectors were generated in a 15 µL reaction mix containing 100 ng of each level 0 plasmid, 100 ng backbone plasmid, 1.5 µL CutSmart Buffer, 1.5 µL 10X T4

buffer, 1 µL BsaI (New England Biolabs), and 1 µL T4 DNA ligase (New England Biolabs). The reaction was incubated for 25 cycles of 3 min at 37 ºC and 4 min at 16 ºC, followed by 5 min at 50 ºC and 5 min at 80 ºC, to allow digestion and ligation of the different DNA modules. Level 2 vectors were generated in the same way, using 1 µL BpiI (ThermoFisher Scientific), as opposed to BsaI. Level 2 vectors used in this work are listed in Table 2.4.

2.13.6 Gateway cloning

Protein coding sequences were created by PCR using Phusion™ High-Fidelity DNA Polymerase (ThermoFisher Scientific) as described above with *M. truncatula* cultivar A17 cDNA as template and specific primers to generate overhangs for BP reaction. The amplicon size was confirmed on a 1.5% agarose gel, and gel extraction used to purify desired DNA fragments. A BP reaction was then performed with the reaction mix as described in this sesction to clone the fragment into pDONR207 entry vector (Invitrogen). After sequence verification by sequencing, DNA fragments were cloned into pBD-GAL4-GW and pAD-GAL4-GW via LR reaction. *In vitro* DNA recombination BP and LR reactions were performed in minimal reaction volume as follows; BP reaction: 2.5 µL purified PCR product, 1 µL entry vector (150 ng.µL^{-1}), 1 µL BP enzyme; LR reaction: 1 µL entry vector (150 ng.µL^{-1}), 1 µL destination vector (150 ng.µL^{-1}), 1 µL LR enzyme. Reaction was incubated for at least 2 hours at 25 ºC prior to competent cell transformation via heat chock.

2.13.7 In-Fusion cloning

In-Fusion HD (Takara Bio Europe) cloning was used to generate pOPIN-M (Addgene) construct for expression of *Mt*Gβ$^{WT/L29F/L31F}$ proteins in heterologous system. Protein coding sequences were created by PCR using Phusion® High Fidelity DNA Polymerase (New England Biolabs) with *M. truncatula* cultivar A17 cDNA as DNA template, and specific primers to generate overhangs with KpnI and HindIII as digestion sites. PCR products were separated on agarose gel and gel extracted. DNA concentration was determined with a NanoDrop One (Thermo Scientific). pOPIN-M vector was linearised with KpnI and HindIII restriction enzymes. In-Fusion cloning reaction was prepared using 1× In-Fusion HD enzyme premix, 50-100 ng linearised vector and 10-50 ng of purified PCR fragment. The reaction was incubated at 50°C for 15 min and used to transform 50 µL chemically competent STELLAR *E. coli* cells (Clontech) by heat shock. Cells were then plated on LB agar plates containing appropriate antibiotic, 200 µg/mL X-Gal for antibiotic and blue-white selection

and grown overnight at 37 °C. White colonies were grown in 5 mL LB containing appropriate antibiotic overnight at 37 °C. Plasmids were purified and sequenced as described above. pOPIN-M vectors for *Mt*Gβ^{L29F} and *Mt*Gβ^{L31F} proteins were created via whole plasmid amplification using pOPIN-M-Gβ^{WT} as DNA template.

2.13.8 *Escherichia coli* transformation by heat shock

Plasmids were amplified and purified from different *Escherichia coli* strains as indicated. Chemically competent *E. coli* strain DH5α (Invitrogen), or other *E. coli* strains as specified, were transformed by adding 2.5 µL of reaction mix to a 25 µL cell aliquot, incubating on ice for 10 min, followed by a 45 sec heat shock at 42ºC and 2 min on ice. Cells were then incubated 1 hour with 100 µL SOC medium at 37ºC and 220 rpm, plated on selective LB medium and incubated overnight at 37ºC. Single colonies were grown overnight in 5 mL selective LB medium at 37ºC and 220 rpm. Plasmids were purified using QIAprep® Spin Miniprep Kit (Qiagen) and subsequently sequenced (Genewiz by Azenta, UK) as indicated above.

2.13.9 SDS-PAGE and immunoblotting

Protein samples were run on a 10% SDS-PAGE pre-cast gel (Bio-Rad for Western blots, Expedeon or Merck for *in vitro* protein samples) using 1 × Tris-Glycine running buffer for 20 min at 75 V then 1 h at 120 V. For immunoblotting, the proteins were transferred from the gel onto PVDF (polyvinylidene difluoride) membrane (BioRad) with 1 × transfer buffer in 20% EtOH overnight at 30 V. The next day membranes were blocked for 1 h in 5% milk in TBS-T (20 mM Tris, 150 mM NaCl, 0.1 % Tween 20, pH 7.5) at room temperature and then blotted with appropriate primary antibody (see Table 2.2) overnight in TBS-T 1 % milk at 4 °C. For antibodies that were not HRP-conjugated, the blots were washed in TBS-T 3 times for 10 min followed by 2 h incubation with appropriate secondary antibody (see Table 2.2). The blots were then washed 3 times with TBS-T for 15 min each before imaging with Pico ECL (ThermoFisher) on an ImageQuant8000.

2.14 Computation methods

2.14.1 Design of DNA, protein and primer sequences *in silico*

Gene, protein, and coding sequences were retrieved from Phytozome V12 portal (*Medicago truncatula* genome Mt4.0v1). DNA sequences were manipulated *in silico* using ApE plasmid

Editor tool (M. Wayne Davis). Primers were designed manually or with Primer-BLAST tool (NCBI).

2.14.2 Transcriptomic analysis

For *MtGβ* expression (Medtr3g116500) assessment in several tissues, transcriptomic data were retrieved from the *M. truncatula* Gene Expression Atlas web server (MtGEA) (Benedito et al., 2008) using the probe ID "Mtr.10712.1.S1_at".

2.14.3 Protein sequence alignment

Protein sequences were retrieved from Phytozome V12 portal. Protein sequence alignment was generated using T-Coffee web portal (EMBL-EBI) and formatted using Boxshade software.

2.14.4 Protein homology modelling of *Mt*Gβ

The homology modelling was made using the SWISS-MODEL and Phyre^2 web servers according to the online tutorials (https://swissmodel.expasy.org/docs/tutorial; http://www.sbg.bio.ic.ac.uk/phyre2/html/help.cgi?id=help/interpret_normal). The template 'c2pbiB' gave the best z-score among all templates identified to build *Mt*Gβ homology structure. The template 'c2pbiB' was used to generate the final predicted model of *Mt*Gβ using EzMol 2.1 software (Reynolds et al., 2018). Homology model of the *Arabidopsis* heterotrimeric G protein complex built by Ullah and co-authors (2003) was used in this thesis (chapter 3) with permission of Oxford University Press (Licence number: 5459460457915).

2.14.5 Statistical analysis

Statistical analyses were performed using GraphPad Prism version 8.0 for Windows (GraphPad Software, La Jolla California USA, www.graphpad.com). Two-group comparison tests were conducted using two-tailed t-test with a prior F-test for homoscedasticity. Multiple comparison tests were calculated by ANOVA by using Tukey's post-test. The confidence intervals are shown in the figure legends.

2.15 Material tables

Table 2.1 | list of media used for culture of plants, bacteria and yeast

Medium	Recipe for 1 L
BNM (Buffered Nodulation Medium)	390 mg MES hydrate, 340 mg $CaSO_4 \cdot 2H_2O$, 61 mg $MgSO_4 \cdot 7H_2O$, 34 mg KH_2PO_4, 2.3 mg $ZnSO_4 \cdot 7H_20$, 1.6 mg H_3BO_3, 5.8 mg $MnSO_4 \cdot 4H_20$, 0.25 mg $Na_2MoO_4 \cdot 2H_20$, 0.025 mg $CuSO_4 \cdot 5H_20$, 0.025 mg $CoCI_2 \cdot 6H_2O$, 9.35 mg Na_2EDTA, 6.95 mg $FeSO_4 \cdot 7H_2O$, pH 6 with KOH.
Mod FP (Modified FP)	40 mg NH_4NO_3, 40 mg $CaCl_2 \cdot 2H_2O$, 40 mg $MgSO_4 \cdot 7H_2O$, 30 mg KH_2PO_4, 45 mg $Na2HPO_4 \cdot 12H_2O$, 2.5 mg $C_6H_5FeO_7$, 2.8 mg H_3BO_3, 2 mg $MnSO_4 \cdot 4H_20$, 0.22 mg $ZnSO_4 \cdot 7H_20$, 0.08 mg $CuSO_4 \cdot 5H_20$, 0.08 mg H_2MoO_4, pH 6 with KOH.
TY (Rhizobium complete medium)	5 g Tryptone, 3 g Yeast Extract, 1.32 g $CaCl_2$ $6H_2O$.
LB (Lysogeny Broth)	10 g Tryptone, 5 g Yeast Extract, 5 g NaCl, pH 7 with NaOH.
SOC (Super Orbital broth with Catabolite repression)	20 g Tryptone, 5 g Yeast Extract, 0.58 g NaCl, 0.19 g KCl, 2.03 g $MgCl_2$, 2.46 g $MgSO_4 \cdot 7H_2O$, 3.6 g glucose.
SD (Synthetic Dextrose minimal media)	6.9 g Yeast Nitrogen Base without Amino Acids (Formedium), 20 g glucose, 30 mg L-isoleucine, 150 mg L-valine, 20 mg L-adenine hemisulphate, 20 mg L-arginine, 30 mg L-lysine, 20 mg L-methionine, 50 mg L-phenylalanine, 200 mg L-threonine, 30 mg L-tyrosine, 30 mg L-tyrosine, 20 mg L-histidine, 100 mg L-leucine, 20 mg L-tryptophan, 20 mg uracil. pH 5.8 with NaOH. For solid medium, 2% agar.
YPAD (Yeast Peptone Adenine Dextrose medium)	10 g Yeast Extract, 20 g peptone, 20 g glucose, 20mg L-adenine hemisulphate. For solid medium, 2% agar.

Table 2.2 | List of antibodies used in this work

Antibody	Titre Used	Vendor
αGFP Nterm (G-1544)	1:1 000	Sigma
αHA-HRP (3F10)	1:1 000	Roche
αMBP-HRP (E8038S)	1:2 500	NEB
α-rabbit-HRP sc-2357 (A0120)	1:10 000	Santa Cruz Biotechnology

Table 2.3 | List of primers

Name	Sequence (5' to 3')		Additional Comments
Genotyping of TILLING population			
-fluorescence-based allele-specific primers (KASP)			
L29F-WT-VIC	gaaggtcggagtcaacggattACGTTTGAAGCAAAGACGCC	Fwd	
L29F-mut-FAM	gaaggtgaccaagttcatgctACGTTTGAAGCAAAGACGCT	Fwd	
S30F-WT-VIC	gaaggtcggagtcaacggattCGTTTGAAGCAAAGACGCCTCTC	Fwd	
S30F-mut-FAM	gaaggtgaccaagttcatgctCGTTTGAAGCAAAGACGCCTCTT	Fwd	
L31F-WT-VIC	gaaggtcggagtcaacggattGTTTGAAGCAAAGACGCCTCTCTC	Fwd	
L31F-mut-FAM	gaaggtgaccaagttcatgctGTTTGAAGCAAAGACGCCTCTCTT	Fwd	
D35N-WT-VIC	gaaggtcggagtcaacggattGACGCCTCTCTCTTCTTGATACAG	Fwd	
D35N-mut-FAM	gaaggtgaccaagttcatgctGACGCCTCTCTCTTCTTGATACAA	Fwd	
KASP-commun-1	AATGAAACTCGAACTCAGAACT	Rev	Commun Reverse for L29F, S30F, L31F, D35N mutations
A123V-WT-VIC	gaaggtcggagtcaacggattCCCCAACTGGTCAATCTGTTGC	Fwd	
A123V-mut-FAM	gaaggtgaccaagttcatgctCCCCAACTGGTCAATCTGTTGT	Fwd	
D128N-WT-VIC	gaaggtcggagtcaacggattTGTTGCATGCGGTGGCCTTG	Fwd	
D128N-mut-FAM	gaaggtgaccaagttcatgctTGTTGCATGCGGTGGCCTTA	Fwd	
KASP-commun-2	CTATCAGTGGGTGAATTAAGATTGAA	Rev	Commun Reverse for A123V and D128N mutations
W184X-WT-VIC	gaaggtcggagtcaacggattGTTCTGGTGATCAAACATGTGTTTTATG	Fwd	
W184X-mut-FAM	gaaggtgaccaagttcatgctGTTCTGGTGATCAAACATGTGTTTTATA	Fwd	
E198K-WT-VIC	gaaggtcggagtcaacggattAGAACATCTGTTTTTGGAGGTG	Fwd	
E198K-mut-FAM	gaaggtgaccaagttcatgctAGAACATCTGTTTTTGGAGGTA	Fwd	
D206N-WT-VIC	gaaggtcggagtcaacggattTTTCAGTCTGGACATACTGCAG	Fwd	
D206N-mut-FAM	gaaggtgaccaagttcatgctTTTCAGTCTGGACATACTGCAA	Fwd	
KASP-commun-3	CTACTATTAAAACAACTTAAACAATACCTAAGT	Rev	Commun Reverse for W184X, E198K and D206N mutations
S301F-WT-VIC	gaaggtcggagtcaacggattCAACGAAATGGCACATGTGACCTC	Fwd	
S301F-mut-FAM	gaaggtgaccaagttcatgctCAACGAAATGGCACATGTGACCTT	Fwd	
KASP-commun-4	GAGGTCACATGTGCCATTTCGTTG	Rev	Commun Reverse for S301F mutation

-PCR amplification for sequencing			
TILLING-seq-1	AGTTCGATCCATCCATCCAT	Fwd	L29F, S30F, L31F, D35N mutations
TILLING-seq-2	TCCGGTATGACCTTGGAGAG	Rev	
TILLING-seq-3	CCATTGACGAAATTTTACAGGTT	Fwd	A123V, D128N, W184X, E198K, D206N, S301F mutations
TILLING-seq-4	GCAACAATTACCTTAGCCAATAAA	Rev	
CRISPR-CAS9			
-sgRNAs			
sgRNA1-sense	aaCGTCTCacttGCTGGCTATGCAAAGTCTCAgtttaGAGACGaa	Fwd	
sgRNA1-antisense	ttCGTCTCtaaacTGAGACTTTGCATAGCCAGCaagtGAGACGtt	Rev	
sgRNA2-sense	aaCGTCTCacttGACATACTGCAGATGTACTTgtttaGAGACGaa	Fwd	
sgRNA2-antisense	ttCGTCTCtaaacAAGTACATCTGCAGTATGTCaagtGAGACGtt	Rev	
sgRNA3-sense	aaCGTCTCacttGTAGAACTCTCCAAGGTCATACgtttaGAGACGaa	Fwd	
sgRNA3-antisense	ttCGTCTCtaaacGTATGACCTTGGAGAGTTCTACaagtGAGACGtt	Rev	
-Genotyping of CRISPR-CAS9-transformed roots (PCR amplification & Sequencing)			
CRISPR-1-F	GTCAGTTACGGAGCTGAAGGAACG	Fwd	PCR amplification of PAM1~3 sites and sequencing of PAM1~2 sites
CRISPR-2-R	CCGCACTGCTCGACTTGCCAC	Rev	
CRISPR-3-F	GCATGCGGTGGCCTTGACAGTG	Fwd	Sequencing of PAM3 site
CRISPR-4-R	CTAACTCAGTTACGGAATGCTTGGTAC	Rev	PCR amplification of PAM1~2 sites
CRISPR-5-F	GTACCAAGCATTCCGTAACTGAGTTAG	Fwd	PCR amplification of PAM3 site
RT-qPCR			
UBC9-F	GGTTGATTGCTCTTCTCTCCCC	Fwd	E = 97.4%
UBC9-R	AAGTGATTGCTCGTCCAACCC	Rev	
Gbeta-F	TGCGACGCGACTGCCAGATT	Fwd	E = 123.4%
Gbeta-R	TCGTTGTCACCGCTGTGTTGC	Rev	
NIN-F	GCAATGTGGGGATTTAGAGATT	Fwd	E = 110.2%
NIN-R	GGAAGATTGAGAGGGGAAGCTT	Rev	
ENOD11-F	CCACATGCAAAGATGGGACG	Fwd	E = 125.7%
ENOD11-R	CAGCCTCCACCTAGCATCCA	Rev	
Ggamma1-F	CAGCATCCGGCCCTTAAGGAAGT	Fwd	E = 108.8%
Ggamma1-R	GCTTTCCCAAGCCTTACCAGGTCT	Rev	
Ggamma4-F	GTTCCTACTCCATTTGCACAAGTTGGAACTGT	Fwd	E = 112.9%
Ggamma4-R	CATTGCAGACTGTGGAAGATTCACCTATTGT	Rev	

Table 2.4 | List of Golden Gate level 2 vectors

Identifier	Backbone	Position 1	Position 2	Position 3	Position 4	Position 5	End Linker
CRISPR-CAS9							
CAS9-Gbeta	pL2-1 (KmR)	Forward p35S:mCherry:t35S	Reverse pLjUBI1:NLS-CAS9-NLS:tACS2	Forward MtU6:sgRNA1:scaffold:tU6	Forward MtU6:sgRNA2:scaffold:tU6	Forward MtU6:sgRNA3:scaffold:tU6	pELE-6
CAS9-Control	pL2-1 (KmR)	Forward p35S:mCherry:t35S	Reverse pLjUBI1:NLS-CAS9-NLS:tACS2	-	-	-	pELE-3
Complementation and GFP Localization							
GFP-control	pL2-1 (KmR)	Reverse pAtUBI10:NLS-mCherry:t35S	Reverse pβ:eGFP:tACS2	-	-	-	pELE-3
Gbeta-GFP	pL2-1 (KmR)	Reverse pAtUBI10:NLS-mCherry:t35S	Reverse pβ:Gβ-eGFP:tACS2	-	-	-	pELE-3
OE Gbeta-GFP	pL2-1 (KmR)	Reverse pAtUBI10:NLS-mCherry:t35S	Reverse pLjUBI1:eGFP:tACS2	-	-	-	pELE-3
GbetaL29F-GFP	pL2-1 (KmR)	Reverse pAtUBI10:NLS-mCherry:t35S	Reverse pβ:GβL29F-eGFP:tACS2	-	-	-	pELE-3
GbetaL31F-GFP	pL2-1 (KmR)	Reverse pAtUBI10:NLS-mCherry:t35S	Reverse pβ:GβL31F-eGFP:tACS2	-	-	-	pELE-3
NES-Gbeta-GFP	pL2-1 (KmR)	Reverse pAtUBI10:NLS-mCherry:t35S	Reverse pLjUBI1:NES-Gβ-eGFP:tACS2	-	-	-	pELE-3
NLS-Gbeta-GFP	pL2-1 (KmR)	Reverse pAtUBI10:NES-mCherry:t35S	Reverse pLjUBI1:NLS-Gβ-eGFP:tACS2	-	-	-	pELE-3
Calcium Imaging							
NES-Gbeta	pL2-1 (KmR)	Reverse p35S:YC3.6:t35S	Reverse pLjUBI1:NES-Gβ:tACS2	-	-	-	pELE-3
NLS-Gbeta	pL2-1 (KmR)	Reverse p35S:YC3.6:t35S	Reverse pLjUBI1:NLS-Gβ:tACS2	-	-	-	pELE-3
RGSPentaD	pL2-1 (KmR)	Reverse pNOS:GVG:tNOS	Reverse pLjUBI1:NLS-RGECO:t35S	Reverse 3xUAS:m35S:RGSpentaD:tNOS	-	-	pELE-4

Spontaneous nodulation

Gbeta+Gamma1	pL2-1 (KmR)	Reverse p35S:mCherry:t35S	Reverse pLjUBI1:Gβ:tACS2	Reverse pNOS:Gγ1:tNOS	-	-	pELE-4
Gbeta+Gamma4	pL2-1 (KmR)	Reverse p35S:mCherry:t35S	Reverse pLjUBI1:Gβ:tACS2	Reverse pNOS:Gγ4:tNOS	-	-	pELE-4
RGSPentaD	pL2-1 (KmR)	Reverse p35S:mCherry:t35S	Reverse pLjUBI1:RGSpentaD:tACS2	-	-	-	pELE-3
DMI2 KD	pL2-1 (KmR)	Reverse p35S:mCherry:t35S	Reverse pLjUBI1:DMI2-KD:tACS2	-	-	-	pELE-3
Control	pL2-1 (KmR)	Reverse p35S:mCherry:t35S	-	-	-	-	pELE-2

Co-Immunoprecipitation

AUK-Gbeta	pL2-1 (KmR)	Forward p35S:mCherry:t35S	Reverse pNOS:AUK-HA-cYFP:tNOS	Reverse pβ:Gβ-MYC-nYFP:tACS2	-	-	pELE-4
AUKΔGβ-Gbeta	pL2-1 (KmR)	Forward p35S:mCherry:t35S	Reverse pNOS:AUKΔGβ-HA-cYFP:tNOS	Reverse pβ:Gβ-MYC-nYFP:tACS2	-	-	pELE-4
AUK-DMI3	pL2-1 (KmR)	Forward p35S:mCherry:t35S	Reverse pNOS:AUK-HA-cYFP:tNOS	Reverse pLjUBI1:DMI3-MYC-nYFP:tACS2	-	-	pELE-4

Chapter III

Medicago truncatula Gβ subunit of the heterotrimeric G proteins regulates root endosymbiosis

3.1 Introduction

The role of heterotrimeric G proteins (hereafter G proteins) during root endosymbiosis has first been studied in *Glycine Max* in the context of root nodule symbiosis by Choudhury and Pandey (Choudhury and Pandey, 2013). In this study, the functions of G protein Gα, Gβ and Gγ subunits were assessed using gene silencing and overexpression strategies in *Agrobacterium-rhizogenes*-mediated transformed root. Based on the number of root nodules on transgenic roots, they demonstrated that *GmGβ* and *GmGγ* subunits are positive regulators of root nodule symbiosis. *GmGα* subunits by contrast were shown to negatively affect the number of root nodules. Thus, G protein signalling was shown to be genetically involved in root nodulation, either directly or indirectly, with antagonistic function between the different G protein subunits (Gβ/Gγ versus Gα).

In two consecutive studies, Choudhury and Pandey further explored the role of two receptor-like kinases essential for root nodule endosymbiosis, namely the Nod-factor receptor-like kinase *Gm*NFR1α (ortholog of *LYK3* in *Medicago truncatula* and *NFR1* in *Lotus Japonicus*) and the symbiosis co-receptor *Gm*SymRKα (ortholog of *MtDMI2*/*LjSymRK*).

The Nod-factor receptor *Gm*NFR1α phosphorylates *in vitro* the regulators of G protein signalling *Gm*RGS1/2 (Choudhury and Pandey, 2015). In transformed roots, phosphomimic and phospho-deficient versions of *Gm*RGS2 were beneficial and detrimental for root nodule symbiosis, respectively. This observation suggested that *Gm*NFR1α putatively promotes root nodule development via phosphorylation of *Gm*RGS2. In plants, RGS proteins catalyse GTP hydrolysis reaction of Gα subunits through their GTPase-accelerating domain, thereby controlling the GDP-binding state of Gαs (Urano et al., 2012b). Accordingly, the influence of *Gm*NFR1α-mediated phosphorylation on the inherent GTPase-accelerating activity of *Gm*RGS2 was tested. Phosphomimic *Gm*RGS2 showed a greater GTPase-accelerating activity towards the soybean *Gm*Gα1 subunit in *in vitro* assays (Choudhury and Pandey, 2015). Given the inhibitory role of *Gm*Gαs in root nodule symbiosis,

it suggested that *Gm*RGS2 attenuates the negative influence of *Gm*Gαs by maintaining them in a GDP-bound state –at least in soybean. As such, Nod-factor receptor *Gm*NFR1α would promote this inhibition via phosphorylation of *Gm*RGS2 to increase its GTPase activity towards *Gm*Gαs.

In addition, the symbiosis co-receptor *Gm*SymRKα was shown to interact with and phosphorylate *Gm*Gα1 subunit *in vitro* (Roy Choudhury and Pandey, 2022). Both native and phospho-dead *Gm*Gα1 showed equally detrimental effect on root nodule symbiosis, whereas phosphomimic *Gm*Gα1 showed a beneficial effect. These results suggested that *Gm*SymRKα putatively participates in the mitigation of *Gm*Gαs by phosphorylating them. Interestingly, phosphomimic *Gm*Gα1 also loses the ability to interact with the *Gm*Gβγ dimers as demonstrated via yeast split ubiquitin and bimolecular fluorescence complementation assays (Roy Choudhury and Pandey, 2022). The interaction between phosphomimic *Gm*Gα1 and *Gm*RGS2 still occurred in these assays.

Depending on the pathway, either Gα or Gβγ is the active signalling entity and the other is only required to maintain an inactive heterotrimeric complex, while in other cases Gα and Gβγ proteins both function as main signal transducers (Pandey et al., 2010; Roy Choudhury et al., 2020). In the context of root nodule symbiosis as studied in soybean, at least two putative regulatory mechanisms controlled by *Gm*NFR1α and *Gm*SymRKα were suggested to lock *Gm*Gαs in an inactive state through phosphorylation of *Gm*RGS2 and *Gm*Gαs. Considering the beneficial influence of *Gm*Gβ and *Gm*Gγ subunits on root nodule symbiosis, but their inability to interact with phosphorylated *Gm*Gα1 subunit, it was postulated that *Gm*Gβγ dimers would be released from their heterotrimeric configuration during root nodule symbiosis (Roy Choudhury and Pandey, 2022). The release of *Gm*Gβγ would then positively regulate the development of root nodules via interaction with downstream protein partners (Roy Choudhury and Pandey, 2022).

The beneficial role of *Gβ* in root nodule symbiosis was later established in *M. truncatula* and *Pisum sativum* via RNA interference in *Agrobacterium-rhizogenes*-mediated transformed roots (Bovin et al., 2021), indicating a ubiquitous role of *Gβ* during root nodule development in nodulating species. Nonetheless, the downstream signalling mechanism of Gβ remains elusive. Besides, whether G protein signalling also regulates arbuscular mycorrhizal (AM) symbiosis, that shares common features and molecular components with root nodule symbiosis, has not been addressed.

The aim of the research presented in this chapter was to investigate further the function of *MtGβ* in AM and root nodule symbioses in *M. truncatula*. Using genetic analyses of mutant lines derived from the targeting-induced-local-lesions-in-genomes (TILLING) method and the use of the CRISPR-CAS9-mediated gene editing strategy, I confirmed the role of *MtGβ* in root nodule symbiosis and demonstrated its role in AM symbiosis, raising the question whether the Gβ protein is part of the common symbiosis pathway.

3.2 Results

3.2.1 *MtGβ* is expressed in roots and root hairs of Medicago

A single gene encodes a Gβ subunit in *M. truncatula* genome (Urano 2012). To assess the expression pattern of *MtGβ* in *M. truncatula*, I explored the *M. truncatula* Gene Expression Atlas web server (MtGEA) (Benedito et al., 2008). I identified one specific probe for *MtGβ* transcript (Mtr.10712.1.S1_at) and determined that *MtGβ* is ubiquitously expressed in all organs including root, stem, petiole, leaf and flower (Figure 3.1, A). Importantly, *MtGβ* is expressed in root hairs cells that are the first cells to perceive rhizobial and mycorrhizal symbiotic factors. Interestingly, *MtGβ* is significantly down-regulated in nodules and particularly in mature nodules (Figure 3.1, B), while in root hairs its expression is slightly repressed after 24 hours of Nod-factor treatment (Figure 3.1, C). These results suggest that expression of *MtGβ* is repressed when the first steps of rhizobial perception and colonization are completed. On the other hand, no significant regulation of *MtGβ* expression is observed after 30 days of mycorrhization (Figure 3.1, D), indicating that the presence of AM structures in roots has no effect on the transcriptional regulation of *MtGβ* at this stage of AM colonization. Overall, the transcriptomic data indicate that *MtGβ* is expressed in root and notably in root epidermis that is the first cell layer in contact with rhizobia and arbuscular mycorrhizae during colonization.

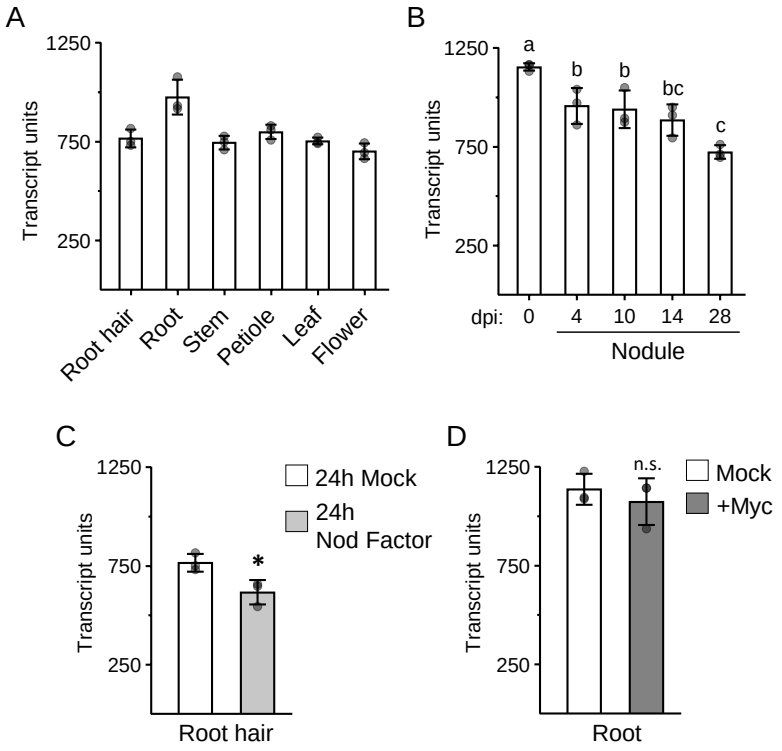

Figure 3.1 | Expression profile of *MtGβ* in *M. truncatula*.
Transcriptomic data of *MtGβ* (Medtr3g116500) was built via DNA microarray (Probeset: Mtr.10712.1.S1_at) using the Affymetrix Medicago Gene Chip ® [1]. The number of transcript units was measured in different WT *M. truncatula* tissues including root hairs at 2 days post-germination (dpg) [2] or root, stem, petiole, leaf and flower at 28 dpg [1] from non-inoculated plants (**A**), in nodule at several days post inoculation (dpi) after 15-day-old plants deprived of nitrogen for 4 days were inoculated with *Sinorhizobium meliloti* strain 2011 [1] (**B**), in root hairs of 2-day-old plants treated for 24 hours with mock solution or Nod-Factor [2] (**C**) and in roots at 30 dpi of 14-day-old plants mock-inoculated or inoculated with *Glomus intraradices* [3] (**D**). Histograms represent mean and standard deviation and circles represent single value for each dataset. N = 3 biological replicates. Different letters indicate p-value < 0.05 (multiple comparisons Turkey's test). * p-value < 0.05 (two-tailed t-test). n.s., not significant.
[1]: *Benedito et al., 2008*
[2]: *Breakspear et al., 2015*
[3]: *Gomez et al., 2009*

3.2.2 Identification of *Gβ* mutant lines

To assess the function of *MtGβ* subunit during root endosymbioses, the JIC-RevGen TILLING population of *M. truncatula* (Le Signor et al., 2009) was reverse screened to identify mutant alleles of *MtGβ.* This approach led to the identification of nine ethyl-methane-sulfonate (EMS) heterozygous mutant alleles carrying either nonsense or missense mutation in *MtGβ* (Table 3.1). To identify homozygous mutants within each segregating population, I used the Kompetitive Allele Specific PCR (KASP) genotyping method (He et al., 2014) (Figure 3.2). This method allowed for fast and cost-effective genotyping of segregating population via allele-specific PCR and fluorescence-based reporting system.

Table 3.1 | Phenotype in root nodule and AM symbioses of the TILLING mutants used in this study.

Mutation	Amino Acid Conservation	Phenotype			
		Rhizobial Infection[(1)]	Nodulation[(2)]	Early Mycorrhization[(3)]	Late Mycorrhization[(4)]
L29F	Partially Conserved (not monocots)	**– 64.12%** ***	**– 51.93%** ***	**– 56.30%** ***	**– 51.61%** ***
S30F	Variable	*Not Tested*	**– 22.79%** ***	*Not Tested*	**– 22.12%** *
L31F	Highly Conserved	**– 56.81%** ***	**– 46.89%** ***	**– 49.46%** ***	**– 40.59%** ***
D35N	Highly Conserved	**– 22.55%** *	**No Difference**	*Not Tested*	*Not Tested*
D128N	Highly Conserved	*Not Tested*	**No Difference**	*Not Tested*	*Not Tested*
W184X	Highly Conserved	-	-	-	-
E198K	Highly Conserved	**No Difference**	**+ 23.29%** **	*Not Tested*	**No Difference**
D206N	Highly Conserved	*Not Tested*	**– 18.42%** **	*Not Tested*	**– 71.25%** ***
A123V + S301F	Highly Conserved	*Not Tested*	**No Difference**	*Not Tested*	*Not Tested*

The percentages refer to the mean difference in comparison with the wild-type of [(1)]the number of infection pocket and infection thread per centimetre of root (average of the two values) at 5 days post-inoculation (dpi), [(2)]the number of nodules per milligram of dry root at 18 dpi, and [(3)(4)]the percentage of arbuscule- and vesicle-containing roots (average of the two values) at 25 and 40-45 dpi, respectively. The values correspond to the results showed in Figure 3.6 (L29F and L31F mutations), Figure 3.8 (S30F and D35N mutations), and Figure 3.9 (E198K and D206N mutations). No difference in nodulation were observed in the TILLING mutant harbouring the A123V and S301F mutations (data not shown in this thesis). * p-value < 0.05, ** p-value < 0.01, *** p-value < 0.001.

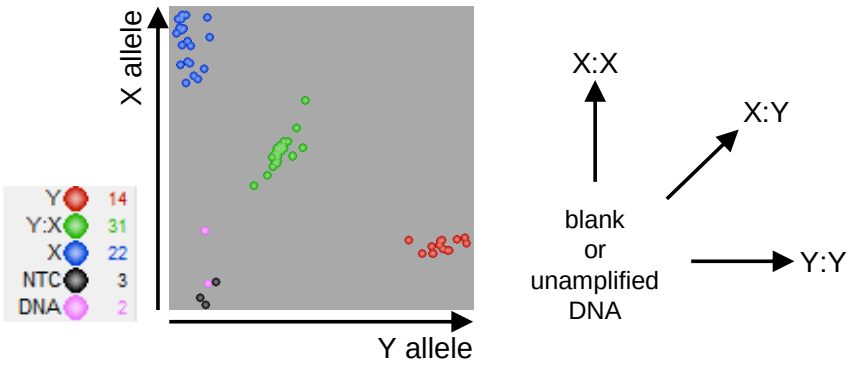

Figure 3.2 | Genotyping of single nucleotide polymorphism via the KASP method.
Representative result image of the KASP (Kompetitive Allele Specific PCR) genotyping assay used in this work to genotype TILLING mutants in segregating TILLING population in *M. truncatula*. DNA was amplified on 96-well plate with competitive allele-specific oligonucleotides fused to distinctive fluorescent reporters (one for each allele). Fluorescence was measured with a plate reader and reported on two-dimensional graph. Circles represent single individuals.

3.2.3 *Gβ* knock-out abolishes root nodule development

Among the heterozygous mutant alleles retrieved, one carries a nonsense mutation that leads to a premature stop codon at residue 184 ($G\beta^{184W\rightarrow X}$) (*Mt*Gβ protein is 378 amino acid long). The screening of one-hundred-twenty-three individuals, progenies of heterozygous $G\beta^{184W\rightarrow X}$ mutants, resulted in the identification of only two homozygous mutants that died prematurely after four weeks of growth (Figure 3.3, A-B). Those two homozygotes failed to develop a proper shoot system. Both had very stunted tiny leaves arrested in their development and stems that could not elongate. In addition, the distortion of segregation observed in the genotype distribution (Figure 3.3, A), suggests that homozygosity of $G\beta^{184W\rightarrow X}$ mutant allele causes severe defect in either zygote development or seed germination. Similar observations were made in *Oryza sativa* and maize for which seed lethality and premature leaf development arrest were associated with *Gβ* loss-of-function, respectively (Sun et al., 2018; Wu et al., 2020; Chen et al., 2022). Nonetheless, the two *M. truncatula* homozygous dwarf plants that I identified had developed a root system. The same observation was made for the loss-of-function *Gβ* mutants identified in maize (Wu et al., 2020; Chen et al., 2022). This indicates that root organogenesis in *M. truncatula* can still occur in the absence of functional *Mt*Gβ. Hence, I generated full knock-out transformed roots via *Agrobacterium-rhizogenes*-mediated root transformation using the CRISPR-CAS9 technology. In this transformation method, only the roots are stably transformed, while the shoot apical meristem remains non-transformed.

A

Genotype:		WT	Het	Hom
1st trial:	No. of Plants	20	24	0
	%	≈ 45.5%	≈ 54.5%	0%
2nd trial:	No. of Plants	34	43	2
	%	≈ 43.0%	≈ 54.4%	≈ 2.5%
TOTAL:	No. of Plants	54	67	2
	%	≈ 43.9%	≈ 54.4%	≈ 1.6%

B

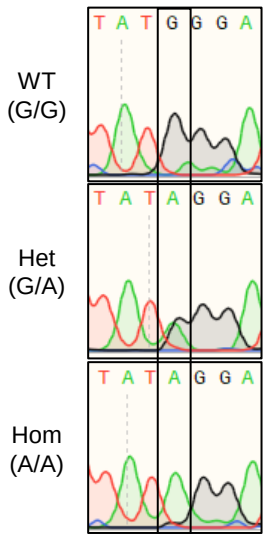

Figure 3.3 | Genotyping of TILLING $G\beta^{184W\rightarrow X}$ early stop codon mutant.

Segregating population of the TILLING mutant *Gβ*$^{184W\rightarrow X}$ coding an early stop codon at residue 184 of *Mt*Gβ protein was genotyped. (**A**) Summary table of the genotyping assays in two populations derived from heterozygous knock-out individuals. Number of plants for each genotype and percentage of each are shown. (**B**) Representative sequencing chromatograms found in **A** for each genotype. The mutation G to A causes codon TGG (tryptophan) to switch to TAG stop codon. WT, wild-type; Het, heterozygous; Hom, homozygous.

To knock-out *MtGβ*, I designed three single guide RNAs (sgRNAs) targeting either *MtGβ* exon two or exon three (Table 3.2). I considered the GC-content within nucleotides 1-10 and 4-8 of the sgRNAs, as GC-content superior to 25% within these regions showed most efficiency in mammalian system, whereas GC-content in the nucleotide 11-20 region had no statistical influence (Labuhn et al., 2018). GC-content within nucleotides 1-10 and 4-8 of sgRNA1~3, was 60 and 60%, 40 and 40%, and 50 and 20%, respectively (Table 3.2). On- and off-target of the designed sgRNAs were analysed with the CRISPR-P 2.0 tool (Liu et al., 2017). No off-targets were found with three or less mismatches as compared with the sgRNA sequences, while the number of off-targets with four mismatches for sgRNA1~3 was equal to eight, zero and eleven, respectively (Table 3.2). The secondary structure was also considered as it may interfere with editing efficiency (Liang et al., 2016a) and was calculated in accordance to this study (Table 3.2). Only the sgRNA1 had a Total Base Pairs (TBP) between the guide sequence and the scaffold sequence superior to the standard TBP, namely thirteen instead of twelve or less (Table 3.2). The sgRNAs were eventually evaluated according to the CRISPRater model (Labuhn et al., 2018) and a microhomology prediction tool to estimate the frequency of out-of-frame mutations (Bae et al., 2014). The two latter criteria were in compliance with these studies (Table 3.2). Each sgRNA was amplified and subcloned via Golden gate assembly with CAS9 enzyme and mCherry fluorochrome as plant transformation marker as described in Figure 3.4. The CAS9 enzyme used in this work was an Arabidopsis-codon-optimised *CAS*9 gene with potato intron and nuclear localization signal (NLS) peptide at both N- and C-termini, as these ameliorations were shown to elevate mutation rates (Castel et al., 2019). After validation of the T-DNA construct via sequencing, the vector was introduced into *A. rhizogenes* AR1193 for subsequent root transformation.

Table 3.2 | sgRNA characteristics for CRISPR-CAS9-mediated *MtGβ* gene editing.

position	sequence	length (+3 PAM)	Off-targets (=4 nt diff)	GC-content nt 1-10	GC-content nt 4-8	Structure features[1]	Out-of-frame Score[2]	CRISPRater score[3]	
exon 2	**GCTGGCTATG**CAAAGTCTCAAGG	*20*	8	60%	60%	3 TSL; 0 GSL; 5 CBP; 13 TBP; 0 IBP	73.8	0.8	high
exon 2	**GTAGAACTCT**CCAAGGTCATACCGG	*22*	0	40%	40%	3 TSL; 0 GSL; 4 CBP; 7 TBP; 0 IBP	70.6	0.61	med
exon 3	**GACATACTGC**AGATGTACTTAGG	*20*	11	50%	20%	3 TSL; 0 GSL; 5 CBP; 10 TBP; 0 IBP	81.1	0.69	med

[1]Criteria: TSL: Total Stem Loop of the sgRNA (equal to 3); GSL: Guide Stem Loop in the guide sequence (equal to 0); CBP: Consecutive Base Pairs between guide sequence and the scaffold sequence (no more than 7); TBP: Total Base Pairs between guide sequence an the scaffold sequence (no more than 12); IBP: Internal Base Pairs in the guide sequence (no more than 6).
[2]Criteria: superior to 66 according to Bae et al., 2014.
[3]Criteria: superior to 0.6 according to Labuhn et al., 2018.
nt: nucleotide

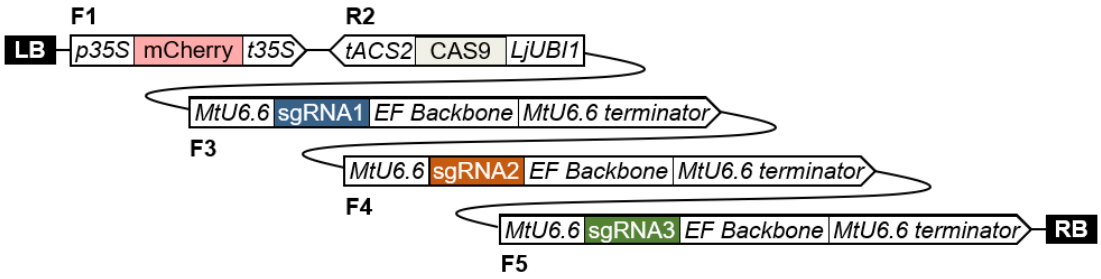

Figure 3.4 | T-DNA construct for CRISPR-CAS9-mediated *MtGβ* editing.
T-DNA-containing CRISPR-CAS9 construct used in this work for editing MtGβ via *Agrobacterium-rhizogenes*-mediated root transformation. Diagram represents Level 2 plasmid generated via the Golden Gate cloning strategy. Position and direction of each fragment are indicated above or below the boxes (F: Forward, R: Reverse). The mCherry fluorochrome was used as transformation marker. The promoter and terminator regions are shown in italics for each fragment. LB, Left Border. RB, Right Border.

After *Agrobacterium-rhizogenes*-mediated root transformation and inoculation with the rhizobia strain *Sinorhizobium meliloti*, the number of root nodules on fully transformed roots were counted and DNA of each transformed root system was extracted for genotyping (Figure 3.5). Among seventeen plants expressing the *Gβ*-targeted CRISPR-CAS9 construct, five were monoallelic or biallelic homozygous null mutants (Figure 3.5, B). No root nodules were observed on those plants at 25 days post-inoculation, while the control (free CAS9) and the plants genotyped wild-type or heterozygote presented numerous fully developed nodules on their root system (Figure 3.5, A). This result demonstrates that *MtGβ* is not only a positive regulator of root nodule symbiosis as previously reported, but is also indispensable for root nodule development.

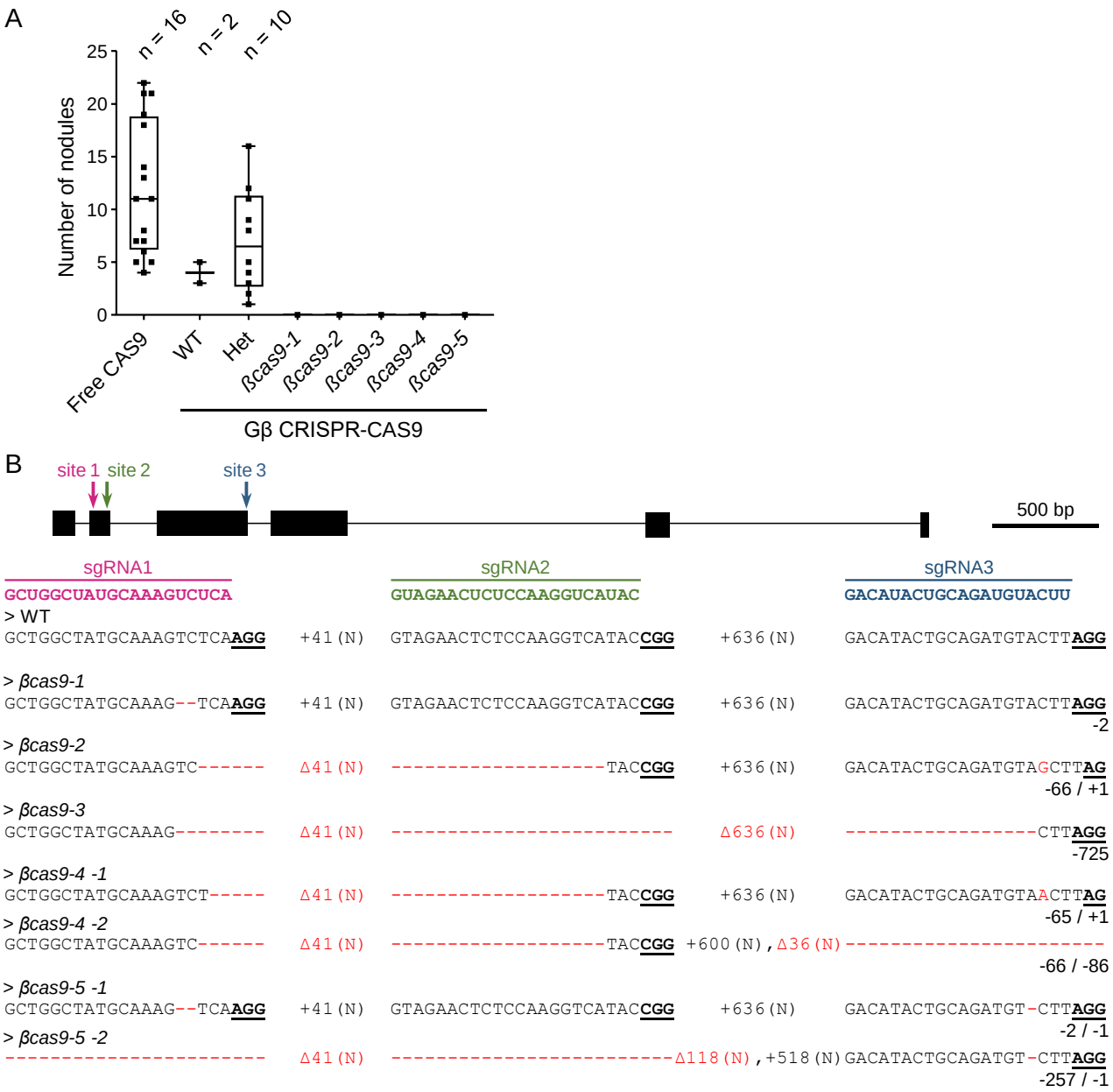

Figure 3.5 | CRISPR-CAS9-mediated *MtGβ* null alleles abolish root nodulation.
The CRISPR-CAS9 gene-editing method was used to generate *MtGβ* null mutants in hairy roots via *Agrobacterium*-mediated root transformation and transformed roots were inoculated with *Sinorhizobium meliloti* (strain Sm2011:*LacZ*). (**A**) Number of nodules at 25 days post-inoculation on transformed roots expressing the *CAS9* gene cassette alone (Free CAS9) or co-expressed with the three single guide RNAs (sgRNAs) targeting *MtGβ* exons (Gβ CRISPR-CAS9). Individual plants and their respective root system were genotyped via PCR amplification of the targeted regions and PCR bands were extracted and sequenced. Five plants were genotyped as homozygous null mutants (*βcas9-1~5*), two as wild-type (WT), and ten as heterozygous (Het). n indicates number of plants. (**B**) Genomic sequences of representative WT and the five homozygous null mutants at the location of the genomic sites targeted by the three sgRNAs (sgRNA1~3). Number of bases (+(N)) between the three sites is indicated between the sequences. Nucleotide deletions are indicated by red hyphen and by red delta (Δ) if deletions extended further from the sites. Nucleotide insertions are indicated in red. Corresponding allele names are indicated for each sequence (top-left above sequences). The null mutants *βcas9-4* and *βcas9-5* are biallelic mutants. Total number of deleted (-) or inserted (+) bases is summarised for each allele (bottom-right below sequences). Double mutations are separated with a slash. Sequences of the sgRNAs are shown above the WT sequence. Targeted sites (exons 2 and 3) are shown on representative *MtGβ* gene (top). Black rectangles and lines represent exons and introns, respectively. The PAM sites are underlined in the sequences. The sequences are 5'→3' oriented.

To identify whether any specific amino acid mutations in *Mt*Gβ could affect its function and therefore root nodule symbiosis, I assessed the nodulation phenotype of the eight remaining EMS homozygous mutant lines carrying missense mutations that lead to amino acid substitutions (Table 3.1). Among them, four mutant alleles ($G\beta^{L29F}$, $G\beta^{S30F}$, $G\beta^{L31F}$, $G\beta^{D206N}$) presented a reduction of nodulation, and one mutant allele ($G\beta^{E198K}$) displayed an increase of nodulation after 18 days post-inoculation with *S. meliloti*. These results suggest that specific amino acid substitutions in *Mt*Gβ can be sufficient to negatively or positively regulates its activity during root nodule symbiosis. This observation suggests further that understanding the effect of those point mutations could inform on the signalling mechanism of Gβ protein, and its effect on putative downstream targets required for root nodule symbiosis.

3.2.4 L29F and L31F substitutions disrupt both root nodule and AM symbioses

Gβ protein consists of a helical N-terminal tail and seven bladed β-propellers, each blade arranged around a central axis and composed of four antiparallel β-sheets (Figure 3.6, A-B). Mutant alleles $G\beta^{L29F}$ and $G\beta^{L31F}$, carry missense mutations that do not reduce or abolish $G\beta^{L29F}$ and $G\beta^{L31F}$ transcript levels (Figure 3.7). Missense mutations in $G\beta^{L29F}$ and $G\beta^{L31F}$ lead to amino acid substitutions from leucine (L) to phenylalanine (F) on residues 29 and 31, respectively. L29 and L31 residues are both located at the end of the N-terminal helix (Figure 3.6, B), and L31 is highly conserved in angiosperms while L29 is highly conserved in dicotyledons (Figure 3.6, C). As both mutations are positioned in the same domain of *Mt*Gβ and both mutants are defective for root nodule symbiosis (Table 3.1), I characterised further the defect in root nodule symbiosis of these mutants as well as the level of AM colonization.

During root nodulation in *M. truncatula*, rhizobia are first entrapped in a curled root hair forming the so-called infection pocket (IP). Then rhizobia invade intracellularly the root hairs and the underneath cells through a tubular structure called infection thread (IT). These structures can be visualised few days after inoculation with rhizobia expressing the *β-Galactosidase* (*LacZ)*. β-Galactosidase hydrolyses 5-bromo-4-chloro-3-indolyl-β-D-galactopyranoside (X-gal) into galactose and 5-bromo-4-chloro-3-hydroxyindole that spontaneously dimerizes and is oxidised into a blue component, namely the 5,5'-dibromo-4,4'-dichloro-indigo.

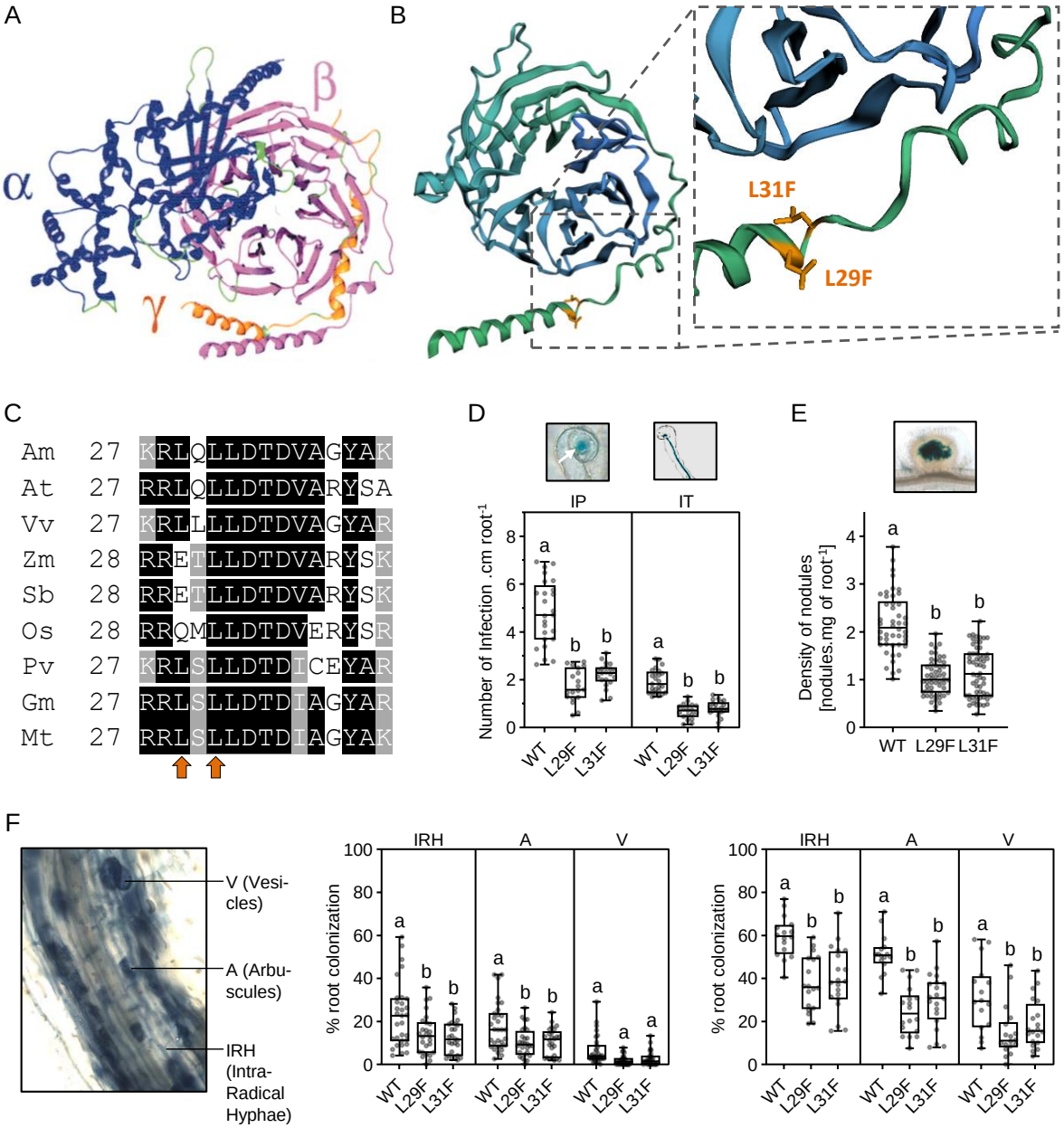

Figure 3.6 | L29F and L31F mutations impair both root nodule and AM symbioses.
(**A**) Homology model of the heterotrimeric G protein complex in *Arabidopsis* built by Ullah et al., 2003. The Gα, Gβ, and Gγ subunits are shown in blue, pink and orange, respectively. (**B**) Homology model of the Gβ protein in *M. truncatula*. The N-terminal tail and the seven-bladed beta-propeller architecture is shown from green to blue. The location of L29F and L31F amino acid substitutions are shown. (**C**) Amino acid sequence alignment (from residue 27-28 to 41-42) of Gβ protein from *Amborella trichopoda* (Am), *Arabidopsis thaliana* (At), *Vitis vinifera* (Vv), *Zea mays* (Zm), *Sorghum bicolor* (Sb), *Oryza sativa* (Os), *Phaseolus vulgaris* (Pv), *Glycin max* (Gm) and *M. truncatula* (Mt). Orange arrows underline L29F and L31F mutations. (**D-F**) Rhizobial and mycorrhizal symbiosis phenotypes of wild-type, $G\beta^{L29F}$ (L29F) and $G\beta^{L31F}$ (L31F) mutants. (**D**) Rhizobia infection assay at 5 days post inoculation (dpi) with *Sinorhizobium meliloti* (Sm2011:LacZ strain). IP, infection pocket. IT, infection thread. Representative pictures are shown above. $N \geq 19$ (3 biological rep.). (**E**) Nodulation assay at 18 dpi with *S. meliloti*. Number of nodules are relative to the root dry mass. Representative picture is shown above. $N \geq 34$ (3 biological rep.). (**F**) Quantification of AM-associated symbiotic structures per percentage of roots at 25 dpi (middle) and 40-45 dpi (right) with *Glomus intraradices*. IRH, intraradical hyphae. A, arbuscules. V, vesicles. Representative picture is shown (left). $N \geq 26$ (middle) and $N \geq 16$ (right) (3 biological rep.). Box plots show minimum, 25th percentile, median, 75th percentile and maximum. Symbols on box plots represent single value for each plant. Different letters represent p-value < 0.01 (ANOVA multiple comparison Tukey's test).

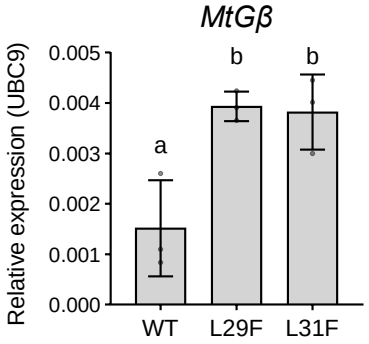

Figure 3.7 | Expression of *MtGβ* in $G\beta^{L29F}$ and $G\beta^{L31F}$ mutants.
Quantitative expression analysis of the transcript level of *MGβ* (Medtr3g116500) in wild-type (WT) and $G\beta^{L29F}$ (L29F) and $G\beta^{L31F}$ (L31F) mutants. Expression was normalised to *UBC9* (AC137602_2.4). Histogram and error bars represent mean and standard deviation, respectively. Circles represent single value. *N* = 3 biological replicates comprising 15 plants each at 2 days post-germination. Different letters indicate p-value < 0.05 (multiple comparison Turkey's test).

To assess whether rhizobial infection is impaired in $G\beta^{L29F}$ and $G\beta^{L31F}$ mutants, development of IP and IT was observed at 5 days post inoculation with *S. meliloti* 2011:*LacZ*. $G\beta^{L29F}$ and $G\beta^{L31F}$ mutants showed significantly reduced number of rhizobial infection structures at 5 days post inoculation (Figure 3.6, D), that correlates with a significant reduction in nodule number at 18 days post inoculation (Figure 3.6, E). The density of root nodules in $G\beta^{L29F}$ and $G\beta^{L31F}$ mutants is reduced by half as compared with the wild type (reduction by 52% and 47%, respectively) (Figure 3.6, E). No differences relating to the root mass were observed between wild-type and mutants (data not shown), excluding the fact that the phenotype is due to change in root architecture. Altogether these data show that *MtGβ* plays a role during the first colonization steps of root nodule symbiosis.

M. truncatula is also capable of AM endosymbiosis. AM invasion within root cells is first characterised by the penetration of intraradical hyphae (IRH), followed by the development of arbuscules in the cortical cell region and the development of vesicles at later stages (Figure 3.6, F; right panel). These AM-associated structures can be visualised via ink staining and scored using the gridline intersect method (Giovannetti and Mosse, 1980) to evaluate the percentage of roots colonised by each structure. I counted the number of AM-associated structures in wild-type, $G\beta^{L29F}$ and $G\beta^{L31F}$ mutants at 25 and 45-days post inoculation to evaluate the degree of AM colonization at an early and later stage (Figure 3.6, F). The two mutants showed a reduced percentage of IRH and arbuscule development at both stages, and vesicle at later stage (Figure 3.6, F). These results indicate that *MtGβ* is required for AM colonization. Because both mutants are impaired at early stage of AM colonization

and because the significant reduction in AM colonization persists over time, it suggests further that *MtGβ* acts early in the colonization process.

Altogether, the endosymbiosis phenotypes of mutant alleles carrying missense mutation in conserved residues of the N-terminal helix of *Mt*Gβ reveal that *MtGβ* is required for early colonization of both arbuscular mycorrhizae and rhizobia. It further suggests that the N-terminal helix of *Mt*Gβ is essential for its function in a signalling pathway common to both AM and root nodule symbioses.

3.2.5 Characterization of $G\beta^{S30F}$ and $G\beta^{D35N}$ mutants confirms the importance of the N-terminal tail of Gβ for its function

Two additional mutant lines with single amino acid substitutions located next to the internal end of the Gβ N-terminal helix were identified. The $G\beta^{S30F}$ and $G\beta^{D35N}$ mutants carry missense mutations that lead to the substitution of a serine to a phenylalanine at residue 30 (S30F) and to the substitution of an aspartate to an asparagine at residue 35 (D35N), respectively (Table 3.1). S30 residue is poorly conserved and only present in nodulating species, whereas D35 residue is highly conserved across angiosperms (Figure 3.8, B). $G\beta^{S30F}$ mutant showed a mild reduction in terms of root nodule density and percentage of AM colonization (Figure 3.8, C-D). Density of nodules was reduced by approximately 22% (Figure 3.8, C) and percentage of AM colonization was reduced from approximately 74% to 58% in comparison with wild type (Figure 3.8, D). On the other hand, $G\beta^{D35N}$ mutant showed a mild defect in terms of rhizobial infection (Figure 3.8, E), less severe in comparison to $G\beta^{L29F}$ and $G\beta^{L31F}$ mutants (Figure 3.6, D). Accordingly, the density of nodules at 18 days post-inoculation in $G\beta^{D35N}$ mutant was not significantly different from wild-type (Figure 3.7, F). This result suggests that D35N substitution has a milder effect on root nodule symbiosis. The AM phenotype of this mutant has not been tested.

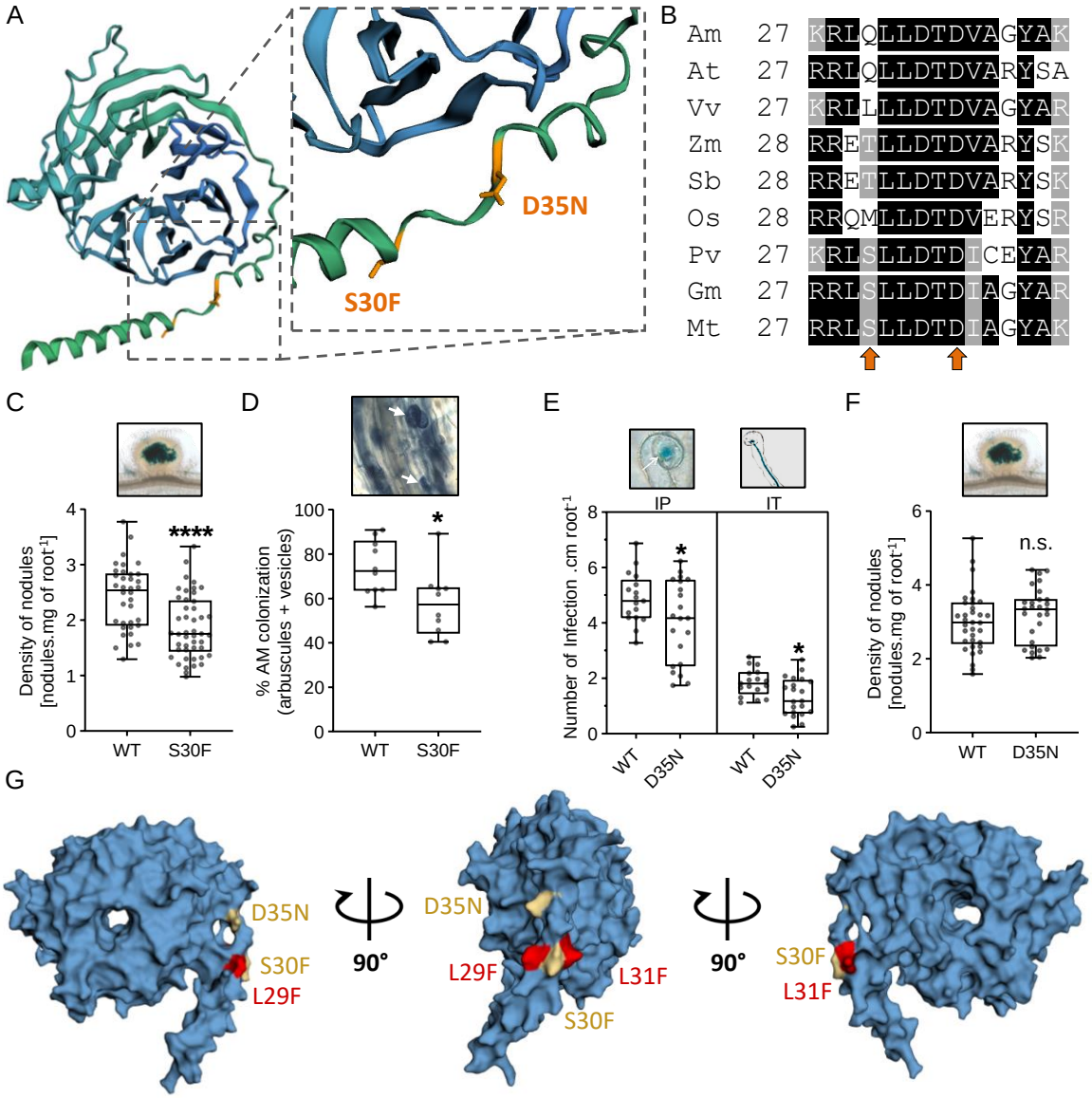

Figure 3.8 | Root endosymbiosis phenotypes of *Gβ*^{S30F} and *Gβ*^{D35N} mutants.
(**A**) Homology model of *Mt*Gβ protein in *M. truncatula*. The N-terminal tail and the seven-bladed beta-propeller architecture is shown from green to blue. The location of S30F and D35N amino acid substitutions are shown. (**B**) Amino acid sequence alignment (from residue 27-28 to 41-42) of Gβ protein from *Amborella trichopoda* (Am), *Arabidopsis thaliana* (At), *Vitis vinifera* (Vv), *Zea mays* (Zm), *Sorghum bicolor* (Sb), *Oryza sativa* (Os), *Phaseolus vulgaris* (Pv), *Glycin max* (Gm) and *M. truncatula* (Mt). Orange arrows underline S30F and D35N mutations. (**C-F**) Rhizobial and mycorrhizal symbiosis phenotypes of wild-type and *Gβ*^{S30F} (S30F) (**C-D**) and *Gβ*^{D35N} (D35N) (**E-F**) mutants. (**C,F**) Nodulation assay at 18 days post inoculation (dpi) with *S. meliloti*. Number of nodules are relative to the root dry mass. $N \geq 28$ (3 biological rep.). (**D**) Quantification of AM structures (both arbuscules and vesicles) per percentage of roots at 45 dpi with *Glomus intraradices*. $N \geq 10$ (1 biological rep.). (**E**) Rhizobia infection assay at 5 days post inoculation (dpi) with *Sinorhizobium meliloti* (Sm2011:LacZ strain). IP, infection pocket. IT, infection thread. $N \geq 17$ (3 biological rep.). Representative pictures are shown above. Box plots show minimum, 25th percentile, median, 75th percentile and maximum. Symbols on box plots represent single value. * p-value < 0.05, **** p-value < 0.0001, n.s., not significant (two-tailed t-test with a prior F-test for homoscedasticity). (**F**) Homology model of *Mt*Gβ protein in *M. truncatula* with the location of L29F, S30F, L31F and D35N amino acid substitutions shown in red or gold.

Altogether, analyses of the endosymbiosis phenotypes of $G\beta^{L29F}$, $G\beta^{S30F}$, and $G\beta^{L31F}$ mutants demonstrate that substitutions within the end of the N-terminal helix from residues 29 to 31, disrupt the function of *Mt*Gβ protein in both root nodule and AM symbioses (Figure 3.6, D-F and Figure 3.8, C-D). Nonetheless, S30F mutation has a lower impact than the L29F and L31F mutations. It raises the question whether these mutations, particularly L29F and L31F, affect differentially the function of *Mt*Gβ. The three amino acids (L29, S30 and L31) are positioned at similar location but with different orientations (Figure 3.8, G). Due to their orientation on both side of the tail, L29 and L31 might be essential to assure orientation and/or flexibility of the N-terminal tail of Gβ (Myriam Charpentier, personal communication). Overall, these data corroborate that alteration in this particular domain of *Mt*Gβ, located at the end of the N-terminal helix, impairs both root nodule and AM symbioses, and further suggest that *MtGβ* is part of the common symbiosis signalling pathway.

3.2.6 Amino acid substitutions within the fourth bladed β-propeller of Gβ subunit

Mutant lines with single amino acid substitutions located within the fourth bladed β-propeller of *Mt*Gβ were also identified. The $G\beta^{E198K}$ and $G\beta^{D206K}$ mutants carry missense mutations that lead to the substitution of a glutamate to a lysine at residue 198 (E198K) and to the substitution of an aspartate to an asparagine at residue 206 (D206N), respectively (Table 3.1). These residues are both highly conserved in angiosperms (Figure 3.9, A). $G\beta^{E198K}$ mutant showed no difference in terms of number of IP and IT in comparison with wild-type (Figure 3.9, B), but showed minor though significant increase of root nodule density by approximately 23% (Figure 3.9, C). During infection of root nodules, rhizobia progress from the infection zone to the interzone of nodules where they differentiate into nitrogen-fixing bacteroids. During infection, root nodules undergo several developmental stages that can be distinguished. This includes the development of small white bombs before rhizobia infection, followed by the establishment of more matured nodules once rhizobia infection has terminated and bacteroids have differentiated. Matured and functional nodules are characterised by their pink colour due to the presence of leghaemoglobin that is essential for maintaining a low oxygen concentration within the nodule and assure bacterial nitrogenase activity. The maturation of root nodules in $G\beta^{E198K}$ mutant was significantly increased as compared with wild-type (Figure 3.9, E), suggesting that E198K mutation could promote root nodule organogenesis and/or colonization of nodules by rhizobia.

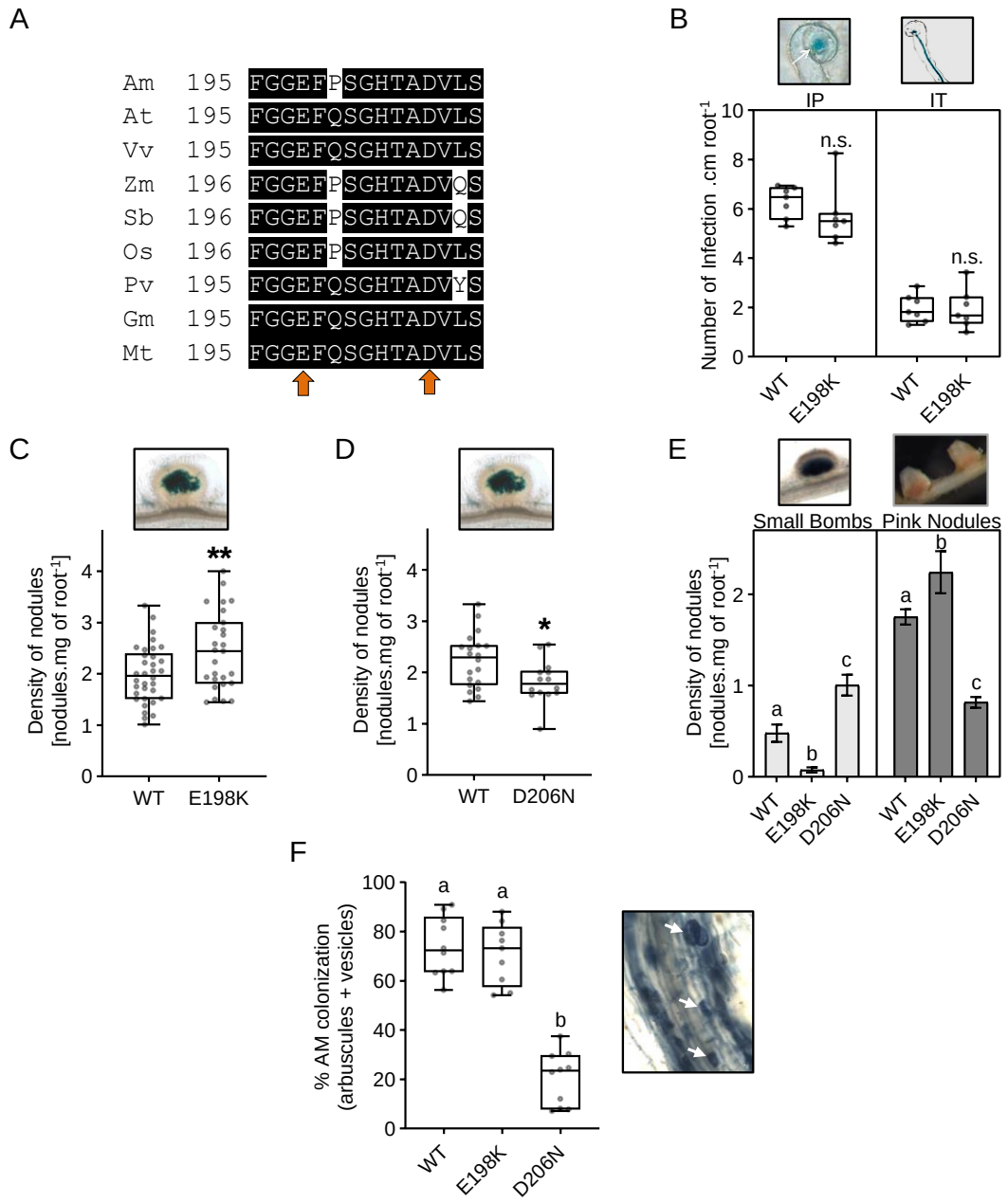

Figure 3.9 | Root endosymbiosis phenotypes of *Gβ*^{E198K} and *Gβ*^{D206N} mutants.

(**A**) Amino acid sequence alignment (from residue 195-196 to 209-210) of Gβ protein from *Amborella trichopoda* (Am), *Arabidopsis thaliana* (At), *Vitis vinifera* (Vv), *Zea mays* (Zm), *Sorghum bicolor* (Sb), *Oryza sativa* (Os), *Phaseolus vulgaris* (Pv), *Glycin max* (Gm) and *M. truncatula* (Mt). Orange arrows underline E198K and D206N mutations. (**B-F**) Rhizobial and mycorrhizal symbiosis phenotypes of wild-type (WT), *Gβ*^{E198K} (E198K) (**B-C**,**E-F**) and *Gβ*^{D206N} (D206N) (**D-F**) mutants. (**B**) Rhizobia infection assay at 5 days post inoculation (dpi) with *Sinorhizobium meliloti* (Sm2011:LacZ strain). IP, infection pocket. IT, infection thread. $N \geq 7$ (1 biological rep.). (**C-E**) Nodulation assay at 18 dpi with *S. meliloti*. Number of nodules are relative to the root dry mass. All types of nodules were counted up (**C-D**) or small bombs and pink nodules were counted separately (**E**). $N \geq 27$ (2 biological rep.) (**C**) and $N \geq 14$ (representative of 2 biological rep.) (**D-E**). (**F**) Quantification of AM structures (both arbuscules and vesicles) per percentage of roots at 45 dpi with *Glomus intraradices*. $N \geq 9$ (1 biological rep.). Representative pictures are shown (top or right). Box plots show minimum, 25th percentile, median, 75th percentile and maximum. Symbols on box plots represent single value. Values in bars are means ± s.e.m.. * p-value < 0.05, ** p-value < 0.01, n.s., not significant (two-tailed t-test with a prior F-test for homoscedasticity). Different letters represent p-value < 0.05 (ANOVA multiple comparison Tukey's test).

In contrast, $G\beta^{E198K}$ mutant showed no difference in terms of AM colonization at late stage (Figure 3.9, F), but the phenotype at earlier stage remains to be evaluated. On the other hand, $G\beta^{D206N}$ mutant had fewer root nodules than the wild-type (approximately 18% less) (Figure 3.9, D) and nodules were less developed (Figure 3.9, E), suggesting that D206N mutation alters *Mt*Gβ function during root nodule symbiosis. But the rate of rhizobial infection in $G\beta^{D206N}$ mutant remains to be evaluated to assess whether the infection process is impaired, which could explain the fewer number of root nodules. Besides, a severe reduction in AM colonization was observed in $G\beta^{D206N}$ mutant line (Figure 3.9, F) indicating a defect in AM colonization in this mutant. Overall, these results corroborate the dual function of *Mt*Gβ protein in both root nodule and AM symbioses.

3.3 Discussion

G protein signalling was shown to be involved in root nodule symbiosis (Choudhury and Pandey, 2013; Choudhury and Pandey, 2015; Bovin et al., 2022; Roy Choudhury and Pandey, 2022) but the function of *Gβ* in this plant-microbe interaction remained unknown. The interactions of *Gm*RGS proteins and *Gm*Gα subunits with the Nod-factor receptor *Gm*NFR1α and its co-receptor *Gm*SymRKα, respectively (Choudhury and Pandey, 2015; Roy Choudhury and Pandey, 2022), suggest that G protein signalling modulates the early signalling of root nodule symbiosis. *Gm*NFR1α and *Gm*SymRKα were shown to phosphorylate *in vitro* *Gm*RGS2 and *Gm*Gα1, respectively. Nonetheless, no evidence was provided to demonstrate these phosphorylation events occur in a Nod-factor-dependant manner, thereby causing concerns about whether G protein signalling was regulated during early signalling (Roy Choudhury and Pandey, 2022). Yet the influence caused by the phospho-mimic or phospho-dead versions of *Gm*RGS2 and *Gm*Gα1 on nodulation demonstrates that changes in G protein signalling affect root nodule symbiosis. Also, *Gm*Gβγ dimers were unable to interact with phospho-mimic *Gm*Gα1 (Roy Choudhury and Pandey, 2022) and *Gβ* was shown to regulate positively nodule formation in three different species (soybean, pea, and alfalfa) (Choudhury and Pandey, 2013; Bovin et al., 2022). These observations suggest that Gβ protein may actively mediate downstream signalling during nodulation. In this study, I investigated further the role of *MtGβ* in root nodule and AM symbioses.

Transcriptomic analysis indicates that *MtGβ* is expressed in root and notably in root hair cells (Figure 3.1, A), which represent the first cell layer to perceive extracellular symbiotic factors. Expression of *MtGβ* gene in root hairs was recently confirmed via promoter GUS staining by Bovin and co-authors (2022). A 2,700 bp fragment upstream of the start codon of *MtGβ* was used as putative promoter and fused to the *GUS* gene reporter to monitor expression of *Gβ* in *M. truncatula* roots in presence or absence of *S. meliloti*. They observed strong GUS-reporter signal in root hairs regardless of the presence of *S. meliloti* (Bovin et al., 2022). Transcriptomic analysis demonstrates further that *MtGβ* is down-regulated after 24h treatment with Nod-factor and during nodule maturation (Figure 3.1, B-C). Likewise, Bovin and co-workers confirmed that strong GUS expression was observed in nodule primordium and weaker GUS staining was obtained in matured nodules. Overall, this suggests that *Gβ* might play a role in early endosymbiosis signalling rather than at a later stage of colonization.

To assess the role of *Gβ* in root endosymbiosis, I characterised several mutant lines from a TILLING population in *M. truncatula* (Le Signor et al., 2009). Amongst the mutants, one carries a nonsense mutation in *MtGβ* gene that leads to an early stop codon at residue 184 (Figures 3.3 and 3.4). Homozygosity for $G\beta^{184W\rightarrow X}$ allele was lethal in Medicago as it has been observed in rice and maize (Sun et al., 2018; Wu et al., 2020; Chen et al., 2022). Maize and Medicago *Gβ* knock-out mutants exhibit similar early shoot meristem growth arrest (Wu et al., 2020; Chen et al., 2022) that was correlated with stunted tiny leaves and growth arrest of the stems. Studies in maize showed that *Gβ* knock-out induces autoimmune response, causing early arrest of shoot meristem growth (Wu et al., 2020). The *Gβ* knock-out autoimmunity phenotype in maize was suppressed after crossing the heterozygotes to a tropical line (Wu et al., 2020). Suppression of the autoimmune response in the F2s correlated with restored growth, indicating that autoimmunity is responsible for *Gβ*-knock-out-induced growth arrest. In Medicago and maize *Gβ* knock-outs, root meristem growth is by contrast not arrested and plants can survive for few weeks (Wu et al., 2020; Chen et al., 2022). To assess the nodulation phenotype of *Gβ* knock-out mutants in Medicago, I genotyped seventy-six F2 individuals within a segregation population for the $G\beta^{184W\rightarrow X}$ allele which I inoculated with *S. meliloti* (data not shown). However, no homozygous mutants were identified. Given the low percentage of homozygotes in the previous segregating populations (~1.6 %) (Figure 3.3, A) and the absence of homozygotes in this additional F2 segregating population, more than three-hundred F2 individuals would have been required to ensure sufficient amount of F2 homozygotes and assess the presence of root nodules in those.

To bypass the absence of viable *MtGβ* knock-out mutant line, I generated a CRISPR-CAS9 construct to produce *MtGβ* null mutants in Medicago transformed roots (Figures 3.4 and 3.5) as knock-out of *MtGβ* does not abolish root development. The absence of root nodules in five transformed root *MtGβ* null-mutants, while wild-type and heterozygous transformed roots formed nodules, demonstrates that *MtGβ* functions in root nodule organogenesis and/or the perception of rhizobium (Figure 3.5). Twenty-five plants expressing the CRISPR-CAS9 construct were genotyped in this assay as follows; two wild-types, ten heterozygotes, five homozygotes and eight with ambiguous sequences considered as chimeras. Those eight chimeras had sequences with high signal noise (data not shown) probably resulting from multiple sequences overlapping and could therefore not be genotyped. The total occurrence of gene editing in this assay was between 92% and 60% considering chimeras as gene editing events or not, respectively. Three different (instead of one) single guide RNAs (sgRNAs) targeting exons 2 and 3 of *MtGβ* gene were selected in an attempt to increase gene editing efficiency as previously suggested (Liang et al., 2016a; McCarty et al., 2020). But the use of multiple sgRNAs may amplify the risk of generating multiple edited alleles, thereby leading to ambiguous sequencing results. The sgRNAs were selected in accordance with several criteria (Table 3.2). I initially considered the GC-content within the nucleotides 1-10 and 4-8 of the sgRNAs, as GC-content superior to 25% within these regions showed most efficiency in mammalian system, whereas the GC-content in the nucleotide 11-20 region had no statistical influence (Labuhn et al., 2018). But it has been demonstrated in *Drosophila* that high GC-content in the proximal region of the protospacer adjacent motif (PAM) was critical (Ren et al., 2014), indicating species-specific requirements for optimal sgRNA activity. In plants, most efficient sgRNAs have total GC-content between 30% and 80% (Liang et al., 2016a) and studies in Arabidopsis and Rice recommend total GC-content between 50% and 80% (Ma et al., 2015). The sgRNA1~3 used in this work had total GC-content equal to 50%, 50% and 40%, respectively, which is in the satisfactory range described above. To reduce the amount of potential off-target effects, number of mismatches with off-target genes was tolerated from four base pair mismatches. The sgRNAs were eventually evaluated according to the CRISPRater model (Labuhn et al., 2018) and a microhomology prediction tool to estimate the frequency of out-of-frame mutations (Bae et al., 2014). The transformed root *MtGβ* null-mutants comprise ten out-of-frame mutations out of twelve total mutations (Figure 3.5, B).

To investigate further the role of *MtGβ*, additional TILLING mutants with missense mutation were phenotyped for root nodule and AM symbioses (Table 3.1). In the two mutant lines $G\beta^{L29F}$ and $G\beta^{L31F}$, reduction in number of root nodules correlated with reduced number of rhizobial infections (Figure 3.5, D-E). Because these two processes are induced and regulated by perception of Nod-factors, it suggests that *MtGβ* mediates the Nod-factor signalling pathway during the early signalling in Medicago. In four mutant lines, reduction in number of root nodules was associated with reduction in AM colonization. This includes the $G\beta^{L29F}$, $G\beta^{S30F}$, $G\beta^{L31F}$, and $G\beta^{D206N}$ mutants (Figure 3.6; Figure 3.8; Figure 3.9). The mycorrhization phenotype in these mutants was characterised by a lower percentage of AM-associated structures in roots. Particularly in $G\beta^{L29F}$ and $G\beta^{L31F}$ mutants, the presence of IRH was significantly decreased at 25 and 40-45-days post-inoculation, suggesting that *MtGβ* mediates penetration of AM fungi. Altogether these results demonstrate that *MtGβ* mediates early stage of AM and root nodule symbioses. Nodulation and mycorrhization processes share a common signalling pathway required to activate transcriptional induction of endosymbiosis-related genes upon perception of the microsymbiont-derived Nod- and Myc-factors (Parniske, 2008). As *MtGβ* mutants are impaired in the first step of colonization of the endosymbionts (IP, IT and IRH), it is tempting to speculate that *Gβ* might be part of the common signalling pathway that is activated upon perception of symbiotic elicitors by the LysM-receptor like kinases.

The use of mutants identified by TILLING for reverse genetic screen carries the risk of biased phenotyping analyses due to recurrent mutations within the genome outside the gene of interest. To reduce the risk of symbiosis phenotypes caused by alternative mutations, two or three homozygous lineages for each mutant line were used for phenotyping and consistency between the lineages was verified. In few cases, different root architectures were observed between the lineages of a given line, namely the $G\beta^{E198K}$ and $G\beta^{D206N}$ mutants, but their endosymbiosis phenotypes were all consistent. Likewise, all the lineages of the $G\beta^{D35N}$ mutant line exhibited dwarfism and roots were twice shorter (data not used in this work). Preliminary data indicated severe disruption during rhizobial infection at similar level than $G\beta^{L29F}$ and $G\beta^{L31F}$ mutants (data not shown). The $G\beta^{D35N}$ mutant was backcrossed by Myriam Charpentier and new homozygotes without dwarfism were identified and phenotyped in endosymbiosis. The backcrossed $G\beta^{D35N}$ homozygotes presented in this work still maintained a lighter root system, namely 83±33 mg versus 111±44 in the wild-type (Figure 3.9, F). Nonetheless, the similar phenotypes in several mutant lines, particularly in $G\beta^{L29F}$, $G\beta^{S30F}$,

Gβ^{L31F}, and *Gβ*^{D206N} mutants, are consistent with a dual role of *MtGβ* in nodulation and mycorrhization.

It would be interesting to speculate on the effect of the single amino acid substitutions described in this work on *Mt*Gβ protein based on studies in other eukaryotes, as the structures of eukaryotes G proteins are comparable to some extent. For example, Ullah and co-workers (2003) modelled the Arabidopsis G protein heterotrimer on the basis of experimentally determined structures of two different mammalian G protein heterotrimers (Wall et al., 1995; Lambright et al., 1996). The predicted model was overall considered as valid with high fold-recognition and self-compatibility scores, in spite of some minor differences caused by small insertions in the Arabidopsis proteins (Ullah et al., 2003). Likewise, the crystal structure of the Arabidopsis Gα was determined by Jones and co-workers (2011a) and the overall structure was found to be highly similar to previously reported mammalian Gα structures. The comparison between models revealed the existence of short, plant-specific loop inserts and variations in the lengths of secondary structure elements (Jones et al., 2011a). Similarly, in eukaryote Gβs, small deviations in some of the loops and turns between the *β*-propeller segments were reported and these seem to be specific to each Gβ protein (Sondek et al., 1996). Large insertions can also occur such as in the yeast Gβ subunit that contains a 41-amino-acid insertion within the sixth bladed *β*-propellers that is phosphorylated during mating signalling (Cole and Reed, 1991). Overall, studies of G proteins beyond plant species may give insight into the functions of the different Gβ domains in Medicago.

L29, S30, and L31 residues are located at the internal end of the N-terminal helix of *Mt*Gβ, while D35 residue is located on the region linking the N-terminal helix to the *β*-propeller (Figure 3.6, B; Figure 3.8 A). The N-terminal helix of Gβ is known to form a parallel coiled-coil with the N-terminal helix of Gγ as presented in Figure 3.6, A. The coiled-coil interface is mainly hydrophobic and is further stabilised by solvent-exposed ion pairs (Sondek et al., 1996). The segment between the N-terminal helix and the *β*-propeller in Gβ is also involved in Gγ binding and was reported as uniquely flexible, raising the possibility that the coiled coil may change position upon binding to protein targets (Sondek et al., 1996). Thus, L29F, S30F, L31F and/or D35N substitutions may change binding affinity to the Gγ subunit, or alternatively disrupt Gβ flexibility. On the other hand, single amino acid substitution within this region was also associated with abolishment of binding to protein target in yeast (Leeuw et al., 1998). Particularly, D62N substitution in yeast Gβ prevents its binding to a kinase protein target without disrupting the association with its Gγ partner. The D62 residue in yeast

corresponds to the D33 residue in Medicago (see Figure 3.6, C or Figure 3.8, B). L29F, S30F, L31F and/or D35N substitutions may similarly impair the binding affinity to an unknown protein target. Regarding the D206N substitution described in this work, the D206 residue is highly conserved in all eukaryotes (Sondek et al., 1996) and is in contact with the Gα subunit through a hydrogen bond (Lambright et al., 1996). D206N substitution may reduce the affinity with Gα and therefore impairs the formation of the heterotrimer complex. In such circumstances, it would suggest that heterotrimeric complex formation is required to prime the system before the release of Gβγ during endosymbiosis through the activation of NFR1 and SymRK. Concerning the E198K substitution, E198 residue is only present in angiosperms (Figure 3.9, A) and is part of a 5-amino-acid-long region that is totally absent from all other eukaryotes including mammalians, yeast, fly, squid and *Caenorhabditis elegans* (Sondek et al., 1996). This region is next to a partially conserved 6-amino-acid-long domain that contacts Gγ through van der Waals bonds (Sondek et al., 1996). E198 may be present in plants to form additional bonds with plant Gγs or may alternatively be involved in interaction with protein targets. As E198K substitution reverses the electrical charge from a negative to a positive charge, it may influence Gβ binding affinity to other proteins.

Chapter IV

Functional characterization of heterotrimeric G proteins during the early signalling of root endosymbiosis

4.1 Introduction

Root accommodation by rhizobia and arbuscular mycorrhizal (AM) fungi necessitates recognition by the plants of rhizobial or fungal symbiotic elicitors. Their recognition results in the activation of nuclear calcium (Ca^{2+}) oscillations leading to transcriptional reprogramming and induction of symbiotic genes. This early signalling is the first step that paves the way for the intracellular colonization of endosymbiotic microorganisms.

Rhizobia release lipochitooligosaccharides (LCOs), known as nodulation (Nod)-factors (Dénarié et al., 1996), while AM fungi produce both LCOs and short-chain chitooligosaccharides (COs), referred to as mycorrhization (Myc)-factors (Maillet et al., 2011; Genre et al., 2013). These are perceived at the root surface by plant plasma membrane receptor-like kinases (RLKs) possessing extracellular Lysine Motif (LysM) domains known to bind to *N*-acetylglucosamine polymers such as LCOs and COs (Buist et al., 2008). Nod-factor perception in *Medicago truncatula* requires two LysM-RLKs referred to as LYK3 and NFP, orthologs of the *Lotus japonicus* Nod-factor receptors NFR1 and NFR5, respectively (Limpens et al., 2003; Madsen et al., 2003; Radutoiu et al., 2003; Arrighi et al., 2006). Each of these LysM-RLKs form together a heterodimer complex at the plasma membrane in their respective plant species (Madsen et al., 2011; Moling et al., 2014). *Lj*NFR1 and *Lj*NFR5 perceive rhizobial LCOs by direct binding (Broghammer et al., 2012), and so was predicted *Mt*NFP via modelling (Mulder et al., 2006). Deletion of any of these LysM-RLKs results in full abolishment of epidermal colonization and root nodule formation, stressing the importance of Nod-factor recognition during root nodule symbiosis. Likewise, recognition of Myc-factors in *M. truncatula* involves two other LysM-RLKs: the Chitin Elicitor Receptor Kinase1 (CERK1) and the LysM Receptor 4 (LYR4) (Feng et al., 2019). *Mt*CERK1 and *Mt*LYR4 bind to mycorrhizal COs, while the mycorrhizal LCO receptors in plants remain elusive (Feng et al., 2019). Nevertheless, the transcriptional response stimulated by LCOs is partially dependant on *MtCERK1* and *MtLYK4*. Similarly, colonization of AM fungi is

partially dependant on *MtCERK1* and *MtLYK4* as well as *MtNFP*, demonstrating the presence of multiple Myc-factor receptors and/or other parallel signalling processes required for mycorrhizal colonization (Gutjahr et al., 2015). Furthermore, both rhizobial and mycorrhizal symbioses require the plasma membrane leucine rich repeat (LRR) RLK Does not Make Infection 2 (*Mt*DMI2) (ortholog of *LjSymRK*) (Endre et al., 2002; Stracke et al., 2002). *Mtdmi2* and *Ljsymrk* mutants are unable to form root nodules and arbuscular mycorrhizae, representing therefore the first evidence of a common signalling pathway leading to the intracellular accommodation of endosymbiotic microorganisms in legumes. *MtNFP*, *MtCERK1*, *MtLYR4* and *MtDMI2* are all required to activate downstream nuclear Ca^{2+} oscillations that precede recognition of symbiotic elicitors (Genre et al., 2013; Sun et al., 2015; Feng et al., 2019). Nod and Myc-factor-activated Ca^{2+} oscillations are indistinctively generated by ion channels localised at the nuclear envelope. In *M. truncatula*, these include the cation permeable channel Does not Make Infection 1 (*Mt*DMI1) and the calcium permeable Cyclic Nucleotide Gated Channels (*Mt*CNGCs) 15a/b/c (Ané et al., 2004; Charpentier et al., 2016). Similarly, suppression of nuclear Ca^{2+} oscillations by mutating one of the symbiosis ion channels results in the abolishment of root endosymbiosis (Wais et al., 2000; Charpentier et al., 2008; Capoen et al., 2011; Charpentier et al., 2016). Overall, the co-receptor *MtDMI2*/*LjSymRK*, the symbiosis ion channels at the nuclear envelope, as well as the nuclear Ca^{2+}-regulated transcriptional activators that initiate transcriptional reprograming for endosymbiosis, are part of a group of common symbiosis genes essential for rhizobial and mycorrhizal entry. This group of genes constitutes the so-called common SYM pathway (Parniske, 2008).

The characterization of the transducing signal that mediates recognition of symbiotic factors by plasma membrane receptors and activates the nuclear ion channels to generate nuclear Ca^{2+} oscillations, remains elusive. Nuclear Ca^{2+} oscillations were shown to be initiated within nuclei during symbiosis (Kelner et al., 2018), demonstrating that a signal (in the form of either single or multiple steps) originates from the plasma membrane and has to travel inside the nucleus to activate the ion channels. In the previous chapter, the characterization of various *MtGβ* mutants demonstrated that *MtGβ* regulates rhizobial and mycorrhizal colonization in *Medicago*, suggesting that *MtGβ* may be part of the early signalling. To test this hypothesis, I characterised the Ca^{2+} phenotype in $G\beta^{L31F}$ mutant and the induction of early symbiosis genes controlled by nuclear Ca^{2+} signalling. The results demonstrate that *MtGβ* regulates nuclear Ca^{2+} signalling during the early signalling. Besides,

the cellular behaviour of functional Gβ-GFP was tracked within epidermal cells and indicates that *Mt*Gβ re-localizes to cell nuclei upon Nod-factor application. In line with this result, Ca^{2+} imaging assays showed that *Mt*Gβ can spontaneously stimulate Ca^{2+} release in the nuclear region of root hair cells. Furthermore, I characterised the roles of other heterotrimeric G proteins in endosymbiosis on the basis of previous studies. The data corroborate the role heterotrimeric G proteins in mediating nuclear Ca^{2+} release and suggest a role in root nodule organogenesis.

4.2 Results

4.2.1 *MtGβ* regulates the symbiosis-activated nuclear Ca^{2+} signalling

To characterize the function of *MtGβ* in early endosymbiosis signalling, $G\beta^{L31F}$ mutant line was crossed with stably transformed wild-type expressing the Ca^{2+}-reporter Yellow Cameleon (YC) 3.6 (Nagai et al., 2004; Krebs et al., 2012). The YC3.6 probe is a Förster Resonance Energy Transfer (FRET)-based Ca^{2+} indicator, composed of a donor-acceptor pair of chromophores, CFP and YFP, respectively, linked with a calmodulin (CaM) and the CaM-binding peptide of the myosin light-chain kinase (M13) (Miyawaki et al., 1997; Nagai et al., 2002; Nagai et al., 2004). Ca^{2+} binding to CaM triggers reversible folding of the CaM-M13 hybrid protein, resulting in an increased FRET-efficiency between CFP and YFP. Hence, temporal dynamic of the YFP/CFP emission ratio correlates with the Ca^{2+} concentration dynamic within the cells. The YC3.6 sensor has already been used to track nuclear Ca^{2+} oscillations upon application of symbiotic elicitors, initially in transformed roots using the YC3.6 fused to a nuclear-localised-signal (NLS) peptide, as done for instance by Sun and co-authors (2015) in *Medicago*. Since, a stable line expressing the YC3.6 reporter (without a signal peptide) has been generated and can be similarly used (Feng et al., 2019) as the sensor diffuses within the cells including nuclei. We used this stable line to cross $G\beta^{L31F}$ mutant and assess the Ca^{2+} phenotype during symbiotic elicitor recognition. The cross was done by Myriam Charpentier. In the F2 segregation population, I selected F2 wild-type plants and F2 homozygous $G\beta^{L31F}$ expressing the YC3.6.

To assess the Ca^{2+} phenotype, 2 to 4-day old germinated seedlings were set in a chamber filled with dH_2O. Ca^{2+} imaging was performed using an OptoSplit system that enables a single camera to record images simultaneously at two different optical wavelengths

(YFP and CFP, respectively). The images were collected every 3 seconds. I imaged the root hairs in the root infection zone (above the root meristem) as this area is the most responsive to Nod-factors (Bhuvaneswari et al., 1981). Nuclear Ca^{2+} oscillations started 5 to 20 minutes after Nod-factor application (10^{-8} M). Image acquisition lasted for at least 30 minutes after application of Nod-factors. In F2 wild-type plants expressing the YC3.6 sensor, 100% of the plants responded to Nod-factor with nuclear Ca^{2+} oscillations recorded in 97.4% of nuclei (18 out of 19) (Figure 4.1, A-B). By contrast, only 54% of F2 $G\beta^{L31F}$ mutants were responsive with only 41 % (16 out of 39) nuclei that exhibited nuclear Ca^{2+} oscillations (Figure 4.1, A-B). This result reveals that $G\beta^{L31F}$ mutant is impaired in the activation of nuclear Ca^{2+} signalling upon perception of symbiotic elicitors. Interestingly, the frequency of Ca^{2+} spikes in $G\beta^{L31F}$ was significantly slower than in WT (Figure 4.1, C-E), suggesting that beyond a defect in the activation, the generation of Ca^{2+} oscillations is inefficient.

The Nod-factor-activated nuclear Ca^{2+} oscillations are decoded by the calcium and calmodulin dependent kinase (CCaMK) that further induces expression of root nodule symbiosis genes (Levy et al., 2004; Messinese et al., 2007; Jin et al., 2018b). Those include *Nodule Inception* (*NIN*) and *Early Nodulin 11* (*ENOD11*) (Charron et al., 2004; Marsh et al., 2007). I evaluated the level of expression of these two genes after 6 hours of treatment with mock or Nod-factors in the root infection zone of 2-day old seedling of $G\beta^{L29F}$ and $G\beta^{L31F}$ mutants as well as wild type as control (Figure 4.2). In mock-treated samples, *NIN* and *ENOD11* are not expressed (Figure 4.2). After 6 hours of Nod-factors induction, *NIN* and *ENOD11* were significantly expressed in wild-type as well as in the *Gβ* mutants (Figure 4.2). However, the induction of *NIN* and *ENOD11* was significantly reduced in the *Gβ* mutants in comparison with the wild-type, indicating that the defect in nuclear Ca^{2+} signalling of the *Gβ* mutants is associated with a compromised nodulation gene expression. Overall, these results demonstrate that *MtGβ* mediates the activation of the nuclear Ca^{2+} signalling and position *MtGβ* as an integral part of the early signalling during endosymbiosis.

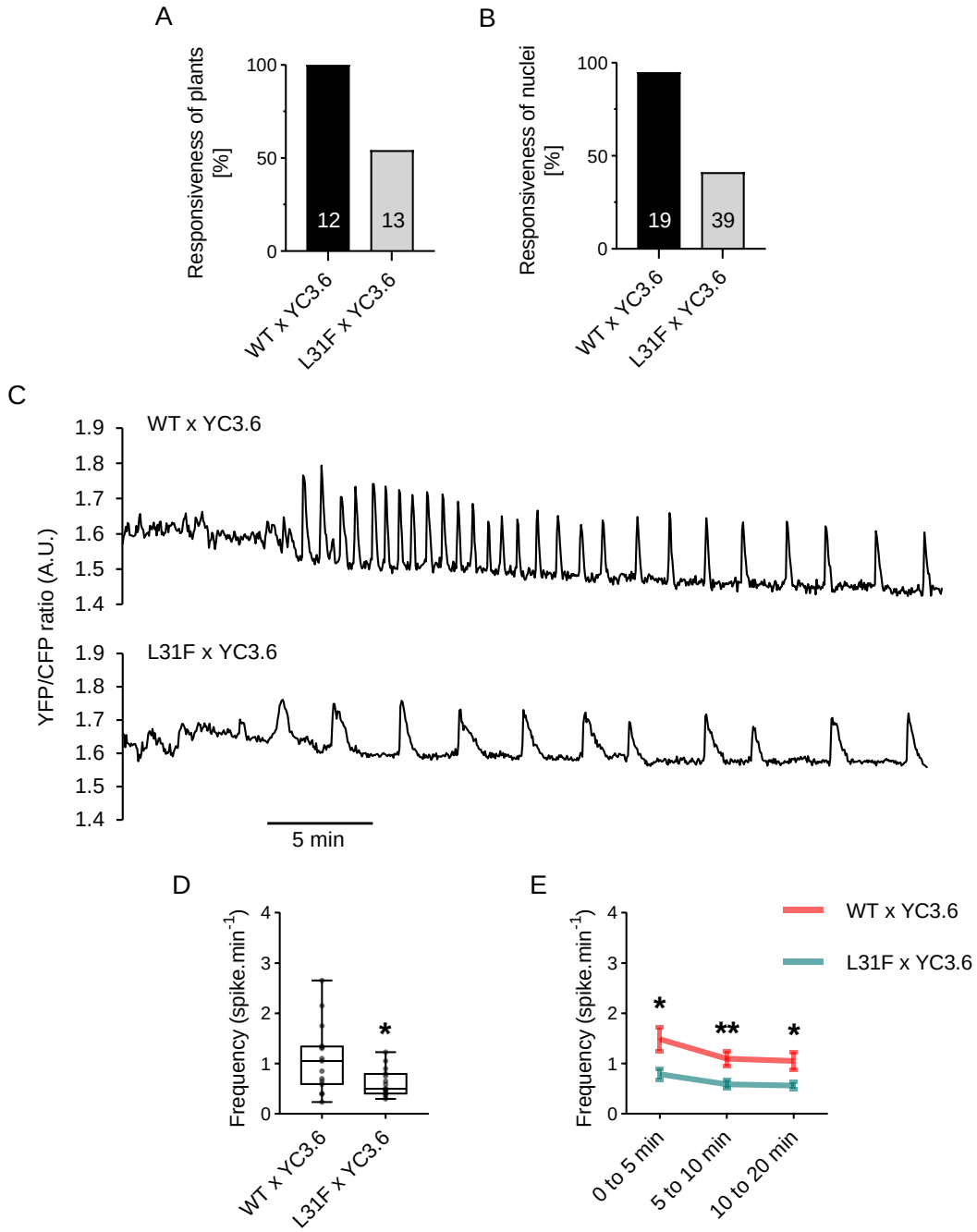

Figure 4.1 | *Gβ*^{L31F} mutant is impaired in Nod-factor-induced nuclear Ca^{2+} response.
(**A**-**B**) Percentage of responsive plants (**A**) and nuclei (**B**) exhibiting nuclear Ca^{2+} oscillations after application of Nod-factor in wild-type (WT) and *Gβ*^{L31F} mutant (L31F) stably expressing the FRET-based calcium sensor Yellow Cameleon 3.6 (YC3.6). Wild-type and homozygous *Gβ*^{L31F} plants derive from the same segregating population of YC3.6 x *Gβ*^{L31F} backcross. Number of biological replicates are indicated within bars. (**C**) Representative nuclear Ca^{2+} traces observed in **B** in wild-type (top) and *Gβ*^{L31F} (bottom). Traces start from Nod-factor application. YFP and CFP fluorescence were simultaneously acquired every 3 seconds for at least 30 minutes. Time scale is shown (bottom). (**D**-**E**) Frequency of Ca^{2+} spikes per minute during the first 20 minutes **(D)** of the nuclear Ca^{2+} oscillations, or during the 0-to-5, 5-to-10 and 10-to-20 minute segments (**E**). Sample size is equal to 15 for both genotypes in **D** and **E**. Box plots show minimum, 25th percentile, median, 75th percentile and maximum. Symbols on box plots represent single value. Connecting lines in **E** represent mean ± s.e.m. at different time segments. * p-value < 0.05, ** p-value < 0.01 (two-tailed t-test with a prior F-test for homoscedasticity).

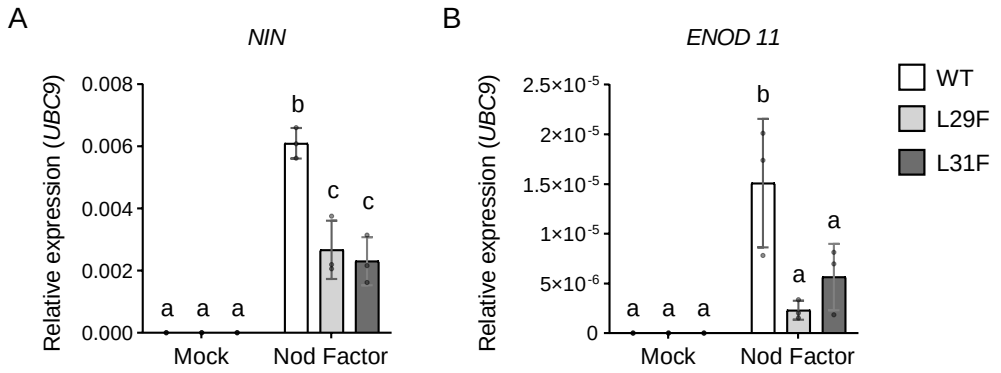

Figure 4.2 | $G\beta^{L29F}$ and $G\beta^{L31F}$ mutants are impaired in Nod-factor-induced gene expression. (**A**-**B**) Quantitative expression analysis of *NIN* (**A**) and *ENOD11* (**B**) transcript levels in roots in wild-type (WT) and $G\beta^{L29F}$ (L29F) and $G\beta^{L31F}$ (L31F) mutants after 6 hours treatment with mock or Nod-factor (10^{-7} M). Expression was normalised to *UBC9* (AC137602_2.4). Histogram and error bars represent mean and standard deviation, respectively. Circles represent single value. *N* = 3 biological replicates comprising 15 plants each at 2 days post-germination. Different letters indicate p-value < 0.05 (ANOVA multiple comparison Turkey's test).

4.2.2 *Mt*Gβ localizes to the nuclei upon Nod-factor application

To explore further the function of *MtGβ* in endosymbiosis signalling, I characterised the cellular behaviour of *Mt*Gβ protein fused with a C-terminal GFP tag. To confirm Gβ-GFP is functional, I first assessed whether Gβ-GFP can complement the symbiosis phenotype of $G\beta^{L29F}$ mutant. *Gβ-GFP* driven by *MtGβ* native promoter (*pβ:Gβ:GFP*) or by *UBIQUITIN* promoter as constitutive promoter (OE *Gβ:GFP*) were expressed in the $G\beta^{L29F}$ mutant background via *Agrobacterium*-mediated root transformation (Figure 4.3). The *pβ* promoter is composed of the 960 bp fragment upstream of *MtGβ* start codon, as opposed to the 2,700 bp fragment used in Bovin et al. (2022). According to the Mt4.0v1 *M. truncatula* genome assembly, genomic sequence from position -2,700 to -960 contains half coding sequence of Medtr3g116510. After 25 days inoculation with *S. meliloti*, over-expression of *Gβ:GFP* almost fully restored nodulation in $G\beta^{L29F}$ whereas *pβ:Gβ:GFP* partially suppressed the nodulation phenotype (Figure 4.3, A). This partial restoration of nodule density with *Gβ:GFP* expressed under its own promoter might be due to the higher expression of $G\beta^{L29F}$ in the mutant background as shown in chapter 3 (Figure 3.7), or to functional cis-elements located upstream of the selected promoter sequence. The expression of wild-type *MtGβ* in this condition may therefore be insufficient to counterbalance the presence of endogenous $G\beta^{L29F}$. On the other hand, both constructs fully restored AM colonization at wild-type level (Figure 4.3, B) except for the number of vesicles that is only partially restored with *pβ:Gβ:GFP* construct. Altogether, these results demonstrate that Gβ-GFP is functional.

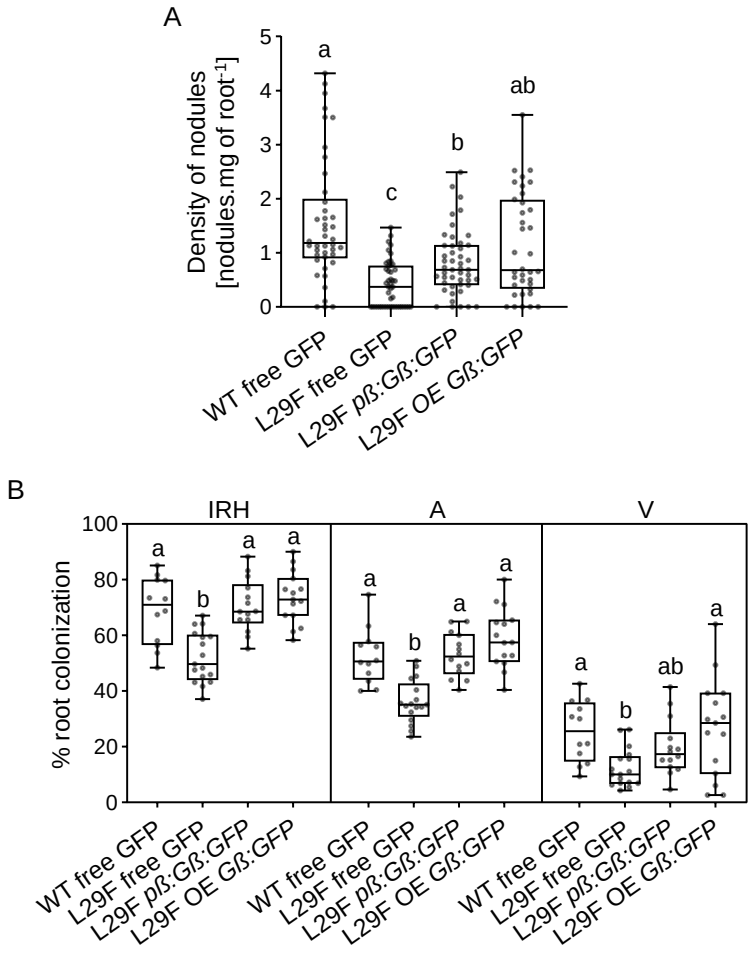

Figure 4.3 | Complementation of *Gβ*^{L29F} mutant symbiosis phenotype with functional Gβ-GFP. (**A**-**B**) Genetic constructs expressing C-terminally GFP-tagged *MtGβ* (cds sequence) driven by *Gβ* native promoter (*pβ:Gβ:GFP*) or constitutive promoter (OE *Gβ:GFP*) were used to complement nodulation (**A**) and mycorrhization (**B**) phenotypes of *Gβ*^{L29F} (L29F) mutant. Free *GFP* driven by *Gβ* native promoter (free GFP) was expressed in wild-type (WT) and *Gβ*^{L29F} as controls. (**A**) Nodulation phenotype was assessed at 25 days post-inoculation (dpi) with *Sinorhizobium meliloti*. Number of nodules is relative to the root dry mass. $N \geq 36$ (3 biological rep.). Different letters represent p-value < 0.01 (ANOVA multiple comparison Welch's test). (**B**) Mycorrhization phenotype was assessed at 48 dpi with *Glomus intraradices*. IRH, intraradical hyphae. A, arbuscules. V, vesicles. $N \geq 12$ (3 biological rep.). Different letters represent p-value < 0.05 (ANOVA multiple comparison Tukey's test). Box plots show minimum, 25th percentile, median, 75th percentile and maximum. Symbols on box plots represent single value.

The cellular behaviour of Gβ-GFP was assessed in transformed roots expressing the genetic constructs described in Figure 4.3, with the exception of the transformation marker that was replaced with *NLS-mCherry* to locate the position of nuclei within cells (Figure 4.4). I focused on root hairs to determine the effect of Nod-factor application on the cellular dynamic of Gβ-GFP. Free GFP expressed under *MtGβ* promoter was visible within cells including nuclei (Figure 4.4, A), whereas Gβ-GFP expressed with the same promoter localised at plasma membrane (Figure 4.4, A-B). By contrast, Gβ-GFP under a constitutive promoter was visible within the whole cell including the cytoplasm and nucleoplasm (Figure 4.4, A).

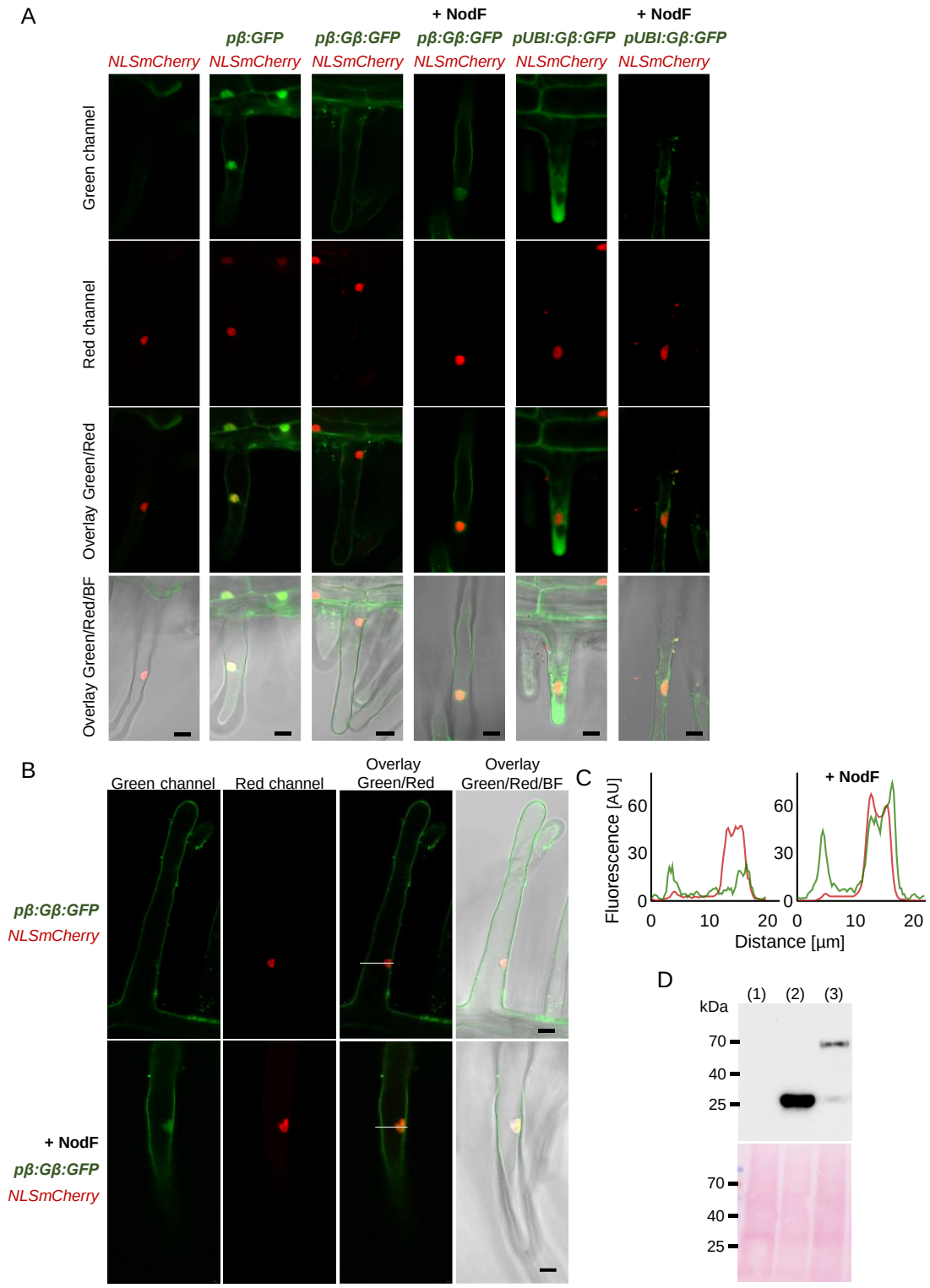

Figure 4.4 | Gβ-GFP localizes to the nucleus in root hairs upon Nod-factor treatment.
(**A**-**B**) Laser scanning confocal microscopy pictures of transformed root hairs expressing the transformation marker *NLS-mCherry* alone, or co-expressed with free *GFP* driven by *MtGβ* native promoter (*pβ:GFP*), C-terminally GFP-tagged *Gβ:GFP* (cds sequence) driven by *MtGβ* native promoter (*pβ:Gβ:GFP*) or driven by constitutive promoter (*pUBI:Gβ:GFP*) in the absence or presence of Nod-factor (+NodF). Mock or Nod-factor treatment lasted 30 minutes before imaging. Pictures are representative of at least three biological replicates. Scale bars represent 10 µm. BF, brightfield. (**C**) Fluorescence intensity distribution from vectors shown in **B** on Green/Red overlay pictures (white line). Green and red lines represent Gβ-GFP and NLS-mCherry emitted fluorescence, respectively. (**D**) Detection by immunoblot of NLS-mCherry alone (1), GFP (2), and Gβ-GFP (native promoter) (3) with αGFP antibody in total protein extracts from roots shown in **A** and **B**. Expected sizes of Gβ-GFP and GFP are 68 and 27 kDa, respectively. Top panel: immunoblot. Bottom panel: ponceau stained blot.

Another set of roots was treated with Nod-factors for 30 min and was subsequently imaged. In transformed roots expressing *pβ:Gβ:GFP* and treated with Nod-factors, fluorescence was visible at the plasma membrane and in the nucleus at equivalent level (Figure 4.4, A-C). Notably, Gβ-GFP co-localised with NLS-mCherry upon Nod-factor treatment (Figure 4.4, C). This result suggests that a pool of *Mt*Gβ is directed into nuclei of root hairs upon detection of symbiotic elicitors. This implies that *Mt*Gβ may transduce the symbiosis signal from the plasma membrane to the nucleus. Together with previous results, it indicates that *Mt*Gβ may regulates nuclear Ca^{2+} signalling directly within nuclei during the early signalling. Additionally, the localization of overexpressed Gβ-GFP (*pUBI:Gβ:GFP*, Figure 4.4, A) shifted predominantly to the nucleus after Nod-factor treatment. One could speculate on the possibility that the excess Gβ-GFP is degraded in the cytoplasm following Nod-factor treatment.

4.2.3 Constitutive expression of *NLS-Gβ* stimulates Ca^{2+} release within the nuclear region of root hairs

In *Lotus japonicus*, the overexpression of plasma membrane receptors involved in root nodule symbiosis is sufficient to induce the formation of spontaneous root nodules in the absence of rhizobia (Ried et al., 2014). These include the overexpression of *LjNFR1*, *LjNFR5* and *LjSymRK* (the latter being the most efficient among the three in inducing spontaneous nodule organogenesis). Because these genes are key regulators of nuclear Ca^{2+} signalling, it is likely that their overexpression induces constitutive activation of nuclear Ca^{2+} signalling. In accordance with this, the formation of spontaneous nodules upon overexpression of *LjNFR1*, *LjNFR5* and *LjSymRK* was dependent on the symbiosis nuclear ion channels as well as the symbiosis Ca^{2+}-regulated transcription activators (Ried et al., 2014). Similarly, an auto-active *MtDMI1* allele was shown to constitutively activate symbiosis signalling as well as spontaneous Ca^{2+} spiking, leading to the formation of root nodules in absence of rhizobia (Liu et al., 2022). Constitutive expression of wild-type *MtDMI1* is also sufficient to spontaneously induce nuclear Ca^{2+} release, though with much lower efficiency (Liu et al., 2022). I demonstrated that *MtGβ* is required to generate symbiosis-activated nuclear Ca^{2+} spiking, and that upon Nod-factor treatment, a pool of *Mt*Gβ accumulates in the nucleus. Thus, to analyse further in which compartment *Mt*Gβ functions to modulate nuclear Ca^{2+} signalling, I tested whether accumulation of *Mt*Gβ in the nucleus or in the cytoplasm could spontaneously

stimulate nuclear Ca^{2+} release. To this aim, *Mt*Gβ fused to a nuclear export signal (NES) or a nuclear localization signal (NLS) peptide was overexpressed (Figure 4.5, A) In transformed roots, NES-Gβ-GFP and NLS-Gβ-GFP correctly localised within the cytoplasm and nucleoplasm of root hair cells, respectively (Figure 4.5, A).

Next, I co-expressed the Ca^{2+} reporter YC3.6 with NES-Gβ or NLS-Gβ (without GFP tag and under the same constitutive promoters). 10 to 15-day old transformed roots were taken for Ca^{2+} imaging using the same method as described above but without Nod-factor application (Figure 4.5, B). I imaged the young root hairs in the root infection zone. In roots expressing *NES-Gβ*, the YFP/CFP ratio within the nuclear region remained at basal levels from a total of eight plants (Figure 4.5, B). By contrast, three plants out of eight expressing *NLS-Gβ* showed multiple Ca^{2+} spikes in an oscillatory fashion within the nuclear and perinuclear regions (Figure 4.5, B). Thus, it indicates that constitutive accumulation of *Mt*Gβ in nuclei triggers Ca^{2+} release within the cell in the absence of external stimuli.

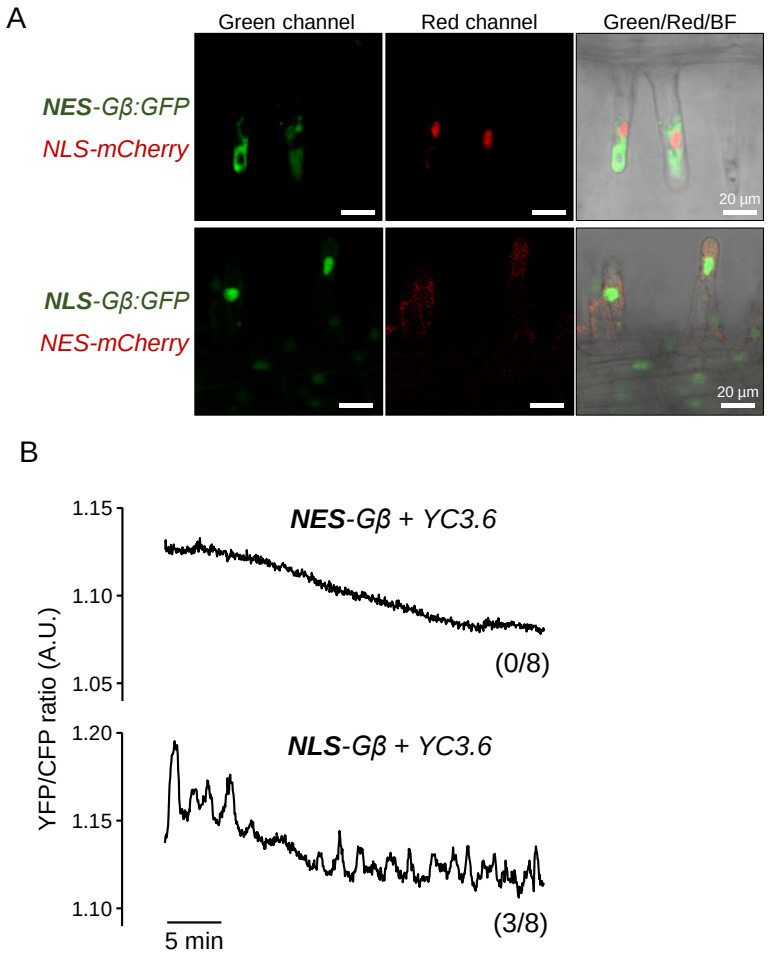

Figure 4.5 | NLS-Gβ stimulates Ca^{2+} activity within the nuclear region.

(**A**) Laser scanning confocal microscopy pictures of transformed root hairs co-expressing *NES-Gβ:GFP* and *NLS-mCherry* (top panel) or *NLS-Gβ:GFP* and *NES-mCherry* (bottom panel). Scale bars represent 20 µm. (**B**) Nuclear Ca^{2+} activity was assessed in transformed root hairs using the FRET-based Ca^{2+} reporter Yellow Cameleon YC3.6. Transformed roots were co-transformed with *YC3.6* and *NES-Gβ* (top panel) or *NLS-Gβ* (bottom panel). Representative Ca^{2+} traces for the two constructs are shown. Number of plants showing spontaneous spiking per total number of plants imaged is indicated for each construct. YFP and CFP fluorescence were simultaneously acquired every 3 seconds for at least 30 minutes. Regions of interest were focused on nuclei. Traces are non-detrended.

4.2.4 Auto-active *MtRGS* stimulates nuclear Ca^{2+} release in transformed root hairs

In *Glycine max*, *Regulators of G protein signalling* (*RGS*) were shown to positively regulate root nodule development (Choudhury and Pandey, 2015). *Gm*RGS2 also interacts with and is phosphorylated by the LysM-RLK *Gm*NFR1α (ortholog of *MtLYK3*/*LtNFR1*). A total of six *Gm*NFR1α-mediated phosphorylation sites were identified on *Gm*RGS2 C-terminus. When these sites were replaced with aspartic acid residues (*Gm*RGS^{HexaD}), the full-length phosphomimic *GmRGS2*^{HexaD} was more efficient in promoting root nodule development in comparison with its wild-type counterpart (Choudhury and Pandey, 2015). Notably, the authors tested whether *GmRGS2* could restore nodulation in the non-nodulating mutant *nod49* lacking functional *Gm*NFR1α (Indrasumunar et al., 2011; Choudhury and Pandey, 2015). Interestingly, overexpressing phosphomimic *GmRGS2*^{HexaD} in the presence of rhizobia is sufficient to supress the mutant phenotype of *nod49* mutant. It demonstrates that *GmRGS2*^{HexaD} constitutively induces the symbiosis signalling downstream of *GmNFR1α* resulting in the development of root nodules in the absence of functional *Gm*NFR1α. It is worth noting that *GmRGS2*^{HexaD} is less efficient than *GmNFR1α* in restoring nodulation in *nod49* mutant, indicating that *Gm*NFR1α is necessary for optimal activation of the symbiosis signalling. Altogether, it suggests that phosphomimic *Gm*RGS2^{HexaD} may be functionally sufficient to induce nuclear Ca^{2+} signalling activation, a hallmark of endosymbiosis signalling. Thus, I characterised the putative role of *MtRGS* in stimulating nuclear Ca^{2+} signalling in *Medicago* roots.

M. truncatula genome possesses a single gene coding a RGS protein (*MtRGS*) (Urano et al., 2012b). The protein sequence alignment between *Mt*RGS and *Gm*RGS2 (Figure 4.6, A) revealed that *Mt*RGS has retained five of the six phosphorylation sites identified by Choudhury and Pandey (2015), that are conserved, namely the Thr-269, Ser-279, Ser-407, Thr-430, and Ser-439 residues (Figure 4.6, A).

I generated a phosphomimic version of *MtRGS* by replacing these sites with aspartate residues (*MtRGS*^{PentaD}) in order to test its effect in transformed roots. Besides, I used the

glucocorticoid-mediated transcriptional induction (GVG) system (Aoyama and Chua, 1997) to control the expression of phosphomimic *MtRGS*^{PentaD} in transformed roots. This system functions through two key components: the hybrid gene *GVG* (GAL4-VP16-GR), that comprises the DNA-binding and transactivating domains of the yeast transcription factor GAL4, the transactivating herpes viral protein VP16, and the hormone-binding domain of the glucocorticoid receptor (GR); the second key component is the GAL4 upstream activating sequence (GAL4 UAS). The hybrid gene *GVG* is constitutively expressed while a gene of interest (here *MtRGS*^{PentaD}) is under the control of a GAL4-UAS-containing promoter (*pGAL4-UAS*). The hybrid protein GVG can bind to glucocorticoids. When it does, it binds to *pGAL4-UAS* promoter resulting in transcriptional expression of the gene of interest. Without application of glucocorticoids, the gene of interest is undetectable (Aoyama and Chua, 1997). Accordingly, this system allows for transcriptional induction of target genes with the advantage that it limits pleiotropic effects (Aoyama and Chua, 1997). Dexamethasone is a synthetic glucocorticoid that is used to activate the GVG system. Dexamethasone easily permeates plant cells and has already been used in *Medicago truncatula* transformed roots using similar induction system (Liu and Yoder, 2016).

To assess whether *Mt*RGS^{PentaD} is sufficient to activate nuclear Ca^{2+} release, I expressed *MtRGS*^{PentaD} under the control of *pGAL4-UAS* and tested after application of dexamethasone the activation of nuclear Ca^{2+} release in roots expressing the nuclear localised Ca^{2+} sensor NLS-RGECO under the control of a constitutive promoter (*LjUBI1*). GECOs (Genetically Encoded Ca^{2+} indicators for Optical imaging) are circularly permutated single fluorescent protein fused to a M13 and CaM proteins at the N- and C-termini, respectively (Nakai et al., 2001; Zhao et al., 2011). The GECOs are dim in the absence of Ca^{2+} and emits light when bound to Ca^{2+} due to conformational change, which triggers a fluorescent response. RGECO has similar Ca^{2+} binding affinity than its counterpart YC3.6 (Nagai et al., 2004; Zhao et al., 2011). Despite RGECO not being a ratio metric sensor, it has the benefit of having a greater dynamic range upon Ca^{2+} binding than YC3.6. NLS-RGECO has already been used in *Arabidopsis* and *M. truncatula*, and has been found suitable to monitor nuclear Ca^{2+} oscillations during symbiosis response (Kelner et al., 2018).

A

```
Gm_RGS2  239 VVAFFSISSSQPLLSQISLRRRESREFRTMSQALGIPDSGVIAESEPISRIDPNEPLDKL
Mt_RGS   241 VLAFFSISSSQPLLSQISLRRRESREFRTMGQALGIPDSGVITQSEPISRVDPNEPLDKL

Gm_RGS2  299 LLNKRFRQSFMAFADSCLAGESVHFFDEVYELSKIPEDDCVKRIYMARHIIEKYIVAGAA
Mt_RGS   301 LLNKKFRQSFMGFADSCLAGESVHFFDEVHELSKISEHDCVRRIYMARHIIEKYMVAGAA

Gm_RGS2  359 MEVNISHRSRQEILSTSNLTRPDLFHNALNEITQLMRTNLARDYWSSMFFLKFQEDSNVR
Mt_RGS   361 MEINISHRSKQEILSTSDLARADLFHNALNEIVHLMKTNLAKDYWSSMFFLKFQEECDMR

Gm_RGS2  419 SNEYELEQITGWNFSPRLSSVHGTDDPFHQDHLLKSSGCSNDTTNL
Mt_RGS   421 CNGYELEQMTGWNYSPRLSSVHGTDDPFHHDHLLKNSECGNDTDS-
```

B

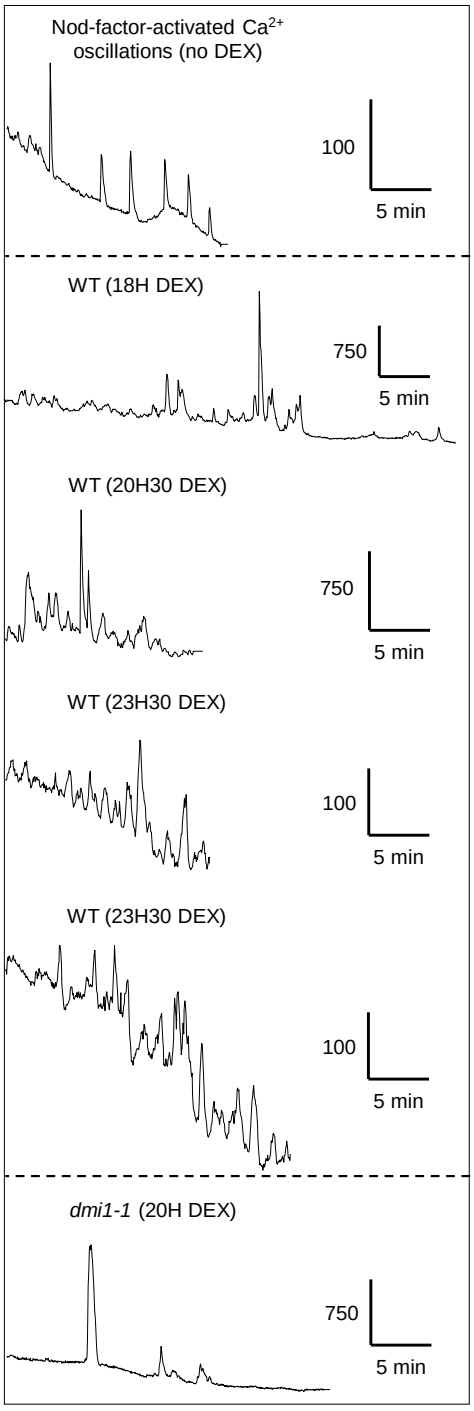

C

	WT n=7	*dmi1-1* n=7
No. Nuclei	48	62
No. Nuclear Ca^{2+} spiking	10	1
Ratio	20.8 %	1.6 %

Figure 4.6 | Phosphomimic *MtRGS^{PentaD}* stimulates nuclear Ca^{2+} activity within root hairs.

(**A**) Protein sequence alignment of *Gm*RGS2 *(G. max*) and *Mt*RGS *(M. truncatula*). The six *Gm*NFR1α-mediated phosphorylation sites identified by Choudhury and Pandey (2015) are highlighted in blue or red if absent in *Mt*RGS. (**B**-**C**) Nuclear Ca^{2+} activity was assessed in wild-type (WT) and *dmi1-1* mutant transformed roots in root hairs, using the nuclear Ca^{2+} reporter NLS-RGECO (Red GECO). Transformed roots were co-transformed with *NLS-RGECO* and phosphomimetic *MtRGS^{PentaD}* (the five phosphorylation sites shown in **A** in blue were replaced with aspartate residues) under the control of a glucocorticoid-activated promoter (*pGAL4-UAS*). Transformed roots were incubated with 25 µM dexamethasone (DEX) between 18 and 24 hours to induce the transcription of *MtRGS^{PentaD}*. (**B**) Representative nuclear Ca^{2+} traces observed in WT (middle panel) and *dmi1-1* (bottom panel) after incubation in DEX. The durations of incubation are indicated. Top panel: representative Nod-factor-induced nuclear Ca^{2+} oscillations in WT without DEX. Red fluorescence was collected every 3 seconds. Scale bars indicate fluorescence intensity (vertical bar, arbitrary unit) and time (horizontal bar, minutes). Traces are non-detrended. (**C**) Summary table with number of nuclei recorded and number of nuclei exhibiting nuclear Ca^{2+} spiking in each genetic background as shown in **B**. The ratios are indicated. 7 plants were recorded for each genotype.

10 to 15-day old transformed roots were treated in liquid medium containing 25 µM of dexamethasone for 18-24 hours to induce expression of *MtRGS*^{PentaD} as these concentration and time parameters were shown to be effective in *M. truncatula* roots (Liu and Yoder, 2016). Emitted fluorescence was collected every 3 seconds for at least 60 minutes. Dexamethasone does not induce Ca^{2+} change in elongating root hairs (Myriam Charpentier, unpublished). In wild type root expressing *MtRGS*^{PentaD} and *NLS-GECO*, 20.8% of the nuclei displayed spontaneous and rapid nuclear Ca^{2+} spiking similarly to that observed in plant expressing *NLS-Gβ* (Figure 4.6, B-C; Figure 4.5, B). To test whether the *MtRGS*^{PentaD}-induced nuclear Ca^{2+} response is dependent on *MtDMI1* (Figure 4.6, B-C), I expressed *MtRGS*^{PentaD} and *NLS-GECO* in a *dmi1* mutant background (*dmi1-1*). From seven *dmi1-1* plants, only one nucleus out of sixty-two nuclei showed rapid nuclear Ca^{2+} spiking (Figure 4.6, B-C). The single Ca^{2+} spiking observed in *dmi1-1* was considerably different in terms of number of spikes and frequency, suggesting that *MtRGS*^{PentaD}-induced nuclear Ca^{2+} response is very inefficient in the absence of *MtDMI1*. Altogether, it suggests that inducible expression of phosphomimic *MtRGS*^{PentaD} stimulates the activation of nuclear Ca^{2+} response in *Medicago* root hairs, and this is partially-dependant on *MtDMI1*. But the transcriptional induction of *MtRGS*^{PentaD} in this assay needs to be confirmed to fully demonstrate its ability to spontaneously activate nuclear Ca^{2+} release. Yet, it corroborates a function of the heterotrimeric G proteins in modulating nuclear Ca^{2+} signalling in root cells.

4.2.5 Identification of heterotrimeric G protein γ subunits in *Medicago truncatula*

The heterotrimeric G protein γ subunits (hereafter Gγs) were shown to be positive regulators of root nodule development in *G. max* in the same vein as *GmRGS2* and *GmGβs* (Choudhury and Pandey, 2013). *Gγs* in *M. truncatula* were therefore identified to characterize their function in root endosymbiosis. *MtGγ* genes were retrieved from the NCBI (National Centre for Biotechnology Information) web portal and the corresponding nucleotide and protein sequences were searched to certify there were no other *MtGγ* genes. Six *MtGγs* were identified and are hereafter referred to as *MtGγ1*, *MtGγ2*, *MtGγ3*, *MtGγ4*, *MtGγ9* and *MtGγ10* (Figure 4.7).

Plant Gγ proteins can be divided in three groups according to their C-terminal structure (Trusov et al., 2012). Briefly, the group I (or type A) are small Gγ proteins (100-120 residues) with a conserved 'CaaX' prenylation motif, the group II (or type B) is highly

similar to group I but lacks the prenylation motif and possesses instead a C-terminal motif variant, the group III (or type C) has relatively large cysteine-rich C-terminal extension (~70-350 residues) made of 20-40% cysteine residues. It is worth noting that all these groups have a conserved Gβ-interacting domain.

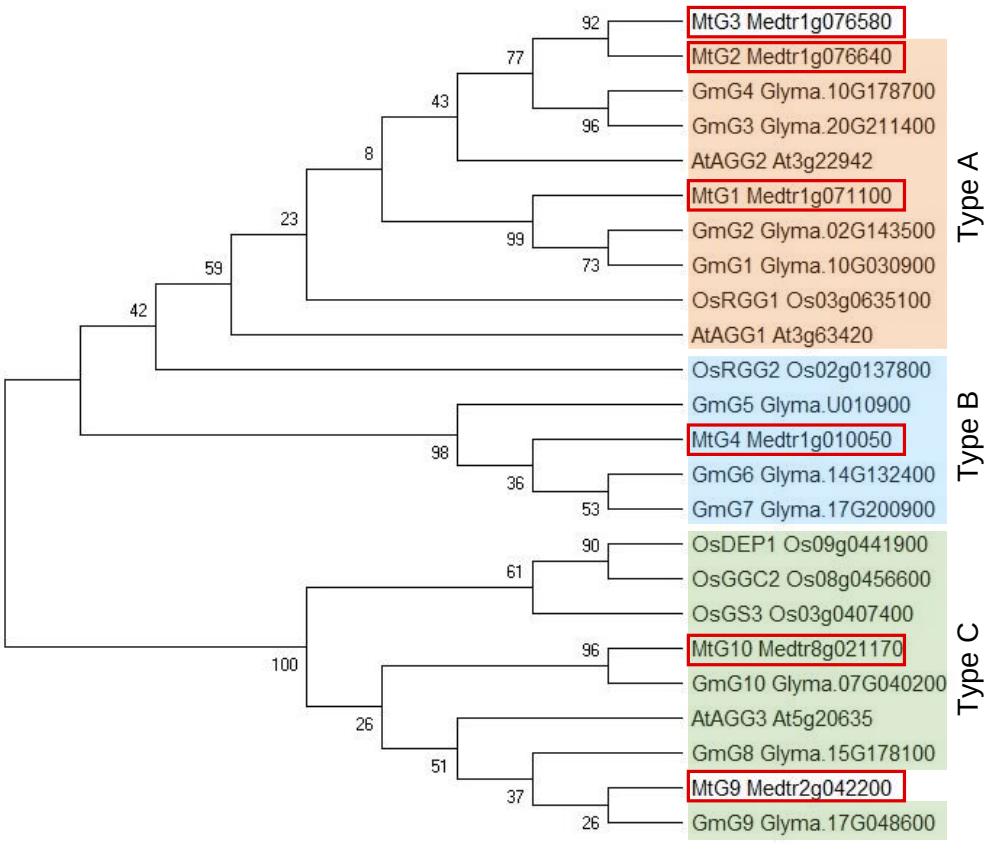

Figure 4.7 | Protein sequence similarity tree of heterotrimeric G protein γ subunits.
The tree was inferred by using the Maximum Likelihood method and JTT matrix-based model (Jones et al., 1992). The tree with the highest log likelihood (-7290.37) is shown. The percentage of trees in which the associated taxa clustered together is shown next to the branches. The tree is drawn to scale, with branch lengths measured in the number of substitutions per site. This analysis involved 24 amino acid sequences of heterotrimeric G protein γ subunits identified in *M. truncatula* (Mt), *Arabidopsis thaliana* (At), *Glycine max* (Gm) and *Oryzae sativa* (Os). The type A, B and C proteins according to the classification of Trusov et al. (2012) are highlighted in orange, blue and green, respectively. *Mt*Gγs are surrounded by red rectangles.

*Mt*Gγ1 and *Mt*Gγ2 were classified type A as they have conserved the 'CaaX' prenylation motif (Figure 4.7). *Mt*Gγ3 was by contrast unclassified (Figure 4.7) as it lacks any conserved C-terminal motifs despite 82.7% protein sequence identity to *Mt*Gγ2. It is also the shortest among the six *Mt*Gγ proteins (89 amino acid long). *Mt*Gγ4 was classified type B as it has the C-terminal 'KRWI' motif that is characteristic of type B Gγs in eudicots (Trusov et al., 2012) (Figure 4.7). *Mt*Gγ10 has a C-terminal extension with approximately 20% cysteine residues and was therefore classified as type C (Figure 4.7). *Mt*Gγ9 was also

unclassified as it has a 150-amino-acid long C-terminal extension that only contains 0.02% cysteine residues (Figure 4.7). To my knowledge, Gγ proteins similar to *Mt*Gγ3 or *Mt*Gγ9 have not been characterised in plants.

In *Glycine max*, the type A and the type B *GmGγs* were shown to promote root nodulation albeit with different efficiencies (Choudhury and Pandey, 2013). Silencing all type A and all type B *GmGγs* resulted in about 70% and 40% reduction of root nodule number, respectively, while constitutive expression of *GmGγ4* and *GmGγ5* as representatives of type A and B resulted in 42% and 14% increase of root nodule number, respectively (Choudhury and Pandey, 2013). The type A *GmGγs* and the type B in a lesser extent, were therefore shown to be positive regulators of root nodulation in *G. max* (Choudhury and Pandey, 2013). Accordingly, *MtGγ1* and *MtGγ4* were selected as representatives of type A and type B, respectively, to determine their roles in endosymbiosis in *Medicago*. *Mt*Gβ interacts with *Mt*Gγ1 and *Mt*Gγ4 in heterologous system (chapter 5, Figure 5.3). I tested the ability of different heterotrimeric G protein genes to promote root nodule organogenesis. I assumed that *MtGγ1* and *MtGγ4* should be co-expressed with *MtGβ*, as Gβ and Gγ subunits have so far been shown to function conjointly as a dimer and they are no instances where they function alone (Thung et al., 2012; Khan et al., 2016). But it is worth noting that *MtGβ* and the *MtGγ1,4* should have been tested independently.

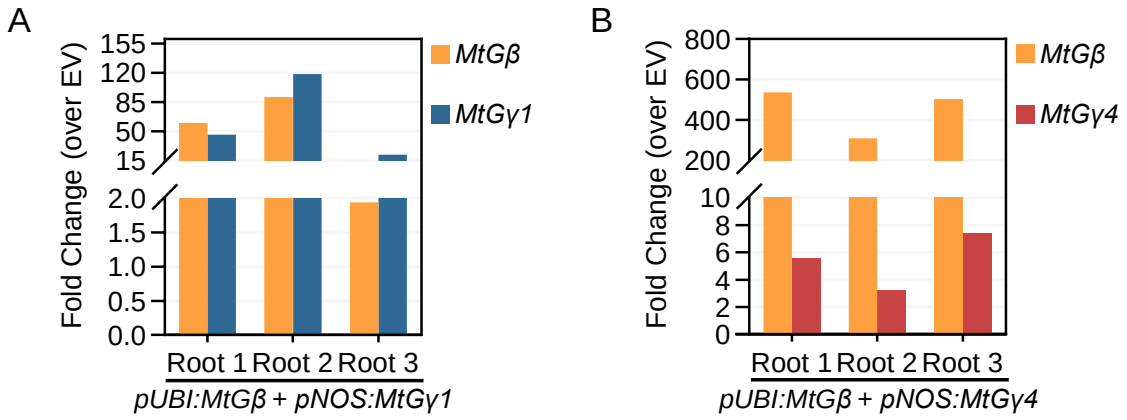

Figure 4.8 | *MtGβGγ1* and *MtGβGγ4* constitutive expression in *Agrobacterium*-mediated transformed roots.
(**A**-**B**) Quantitative expression analyses by qRT-PCR in *dmi2-1* transformed roots co-expressing *MtGβ* with *MtGγ1* (**A**) or *MtGγ4* (**B**) driven by constitutive promoters (*pUBI*, *pNOS*). Expression was assessed in three separate plants (Root1~3) and is shown as fold change over samples expressing empty vector (EV) (n=3). All relative expressions were first normalised to *UBC9* (AC137602_2.4). Bars represent average of two technical replicates.

4.2.6 Characterization of *MtRGS* and *MtGβγ* functions in root nodule organogenesis

As mentioned above, spontaneous formation of root nodules in *L. japonicus* can be initiated by overexpressing *LjNFR1*, *LjNFR5*, and *LjSymRK* via *Agrobacterium*-mediated root transformation in the absence of rhizobia (Ried et al., 2014). Spontaneous nodules and/or nodule primordia were observed in 11% (182 plants), 22% (133 plants), and 89% (129 plants) of these transformed roots, respectively. Of note, expression of *LjSymRK* driven by its innate promoter was ineffective in promoting nodule organogenesis. It therefore demonstrates that ectopic and constitutive (but not basal) expression of the symbiosis RLKs, spontaneously drives the transcriptional reprogramming required for root nodule formation. Besides, the restoration of nodulation by overexpressing phosphomimic $GmRGS^{HexaD}$ in *nod49* mutant in the presence of rhizobia (Choudhury and Pandey, 2015) leads to similar conclusion. As shown in figure 4.4, a pool of *Mt*Gβ translocates to the nucleus upon Nod-factor application, and expression of *NLS-Gβ* and phosphomimic $MtRGS^{PentaD}$ are sufficient to induce spontaneous Ca^{2+} oscillations in the nuclear region (Figure 4.5; Figure 4.6). Thus, I tested whether constitutive expression of $MtRGS^{PentaD}$ and *MtGβγ1,4* dimers via *Agrobacterium-rhizogenes*-mediated root transformation were sufficient to induce root nodule organogenesis in the absence of rhizobia or in the absence of the symbiosis co-receptor *MtDMI2* (ortholog of *LjSymRK*). Quantitative expression analyses via qRT-PCR confirmed that *MtGβγ1* and *MtGβγ4* were overexpressed in these assays (Figure 4.8), but the up-regulation of phosphomimic $MtRGS^{PentaD}$ (driven by the same constitutive promoter) remains to be confirmed.

Wild-type roots were non-inoculated to assess the formation of spontaneous nodules in the absence of rhizobia (Table 4.1; Figure 4.9). To prevent rhizobia contamination, the plants were grown in sterile phytatrays filled with a sterile mix of sand and terragreen. 21 days after *Agrobacterium*-mediated root transformation, plants with transformed roots were transferred into phytatrays and dug out after 70 days. Spontaneous nodulation in *L. japonicus* was assessed at 60 days post-transformation (Ried et al., 2014). Likewise, *Mtdmi2* null-mutant plants (*dmi2-1*) were grown in same condition but they were inoculated with *Sinorhizobium meliloti* to assess the ability of $MtRGS^{PentaD}$ and *MtGβγ1,4* to restore nodulation (Table 4.1; Figure 4.10). The kinase domain of *Mt*DMI2 (DMI2 KD) was used as positive control (Saha et al., 2014) and is sufficient to promote formation of root nodules (Table 4.1). Overexpressing *DMI2 KD* leads to the formation of spontaneous rood nodules in

31% of non-inoculated wild-type plants, while 36% of *dmi2-1* mutants (inoculated) had restored nodule organogenesis with the formation of uninfected nodules (Table 4.1; Figure 4.9, a-b; Figure 4.10, i-j). Ectopic expression of *MtRGS*^{PentaD}, *MtGβγ1* and *MtGβγ4*, resulted in emergence of nodule-like or nodule-primordium-like structures in 25%, 14% and 21% of non-inoculated wild-type plants, respectively (Table 4.1; Figure 4.9, c-h). Some of these structures were rather large, spherical, and undoubtedly different from lateral root primordium (Figure 4.9, c, d, f, h). Similarly, ectopic expression of *MtRGS*^{PentaD}, *MtGβγ1* and *MtGβγ4* in inoculated *dmi2-1* plants resulted in the formation of nodule-like or nodule-primordium-like structures in 11%, 14% and 7% of plants, respectively (Table 4.1; Figure 4.10, k-s). The longitudinal sections of some of the ectopic root structures observed in *dmi2-1* confirmed that these structures are distinct from lateral root primordium (Figure 4.10, o, p, s). Overall, these results suggest that overexpression of *MtRGS*^{PentaD}, *MtGβγ1* and *MtGβγ4* leads to inefficient nodule-like structure formation. However, a precise characterization of these ectopic structures shown in figures 4.9 and 4.10 must be completed to precisely distinguish and quantify the differences in terms of cellular organization between the observed structures and nodule organogenesis. Additionally, the effect of overexpressing *MtGβ* alone will need to be assessed in the future.

Table 4.1 | Root-nodule-associated structures in WT and *dmi2-1* transformed roots constitutively expressing different gene combinations of heterotrimeric G proteins.

Genotype	Construct	No. of Plants	Total No. of Plants Forming Nodule-Like Structures[1]
WT (non-inoculated)	EV	10	0 / 10
	DMI2 KD	16	6 / 16
	RGS^{PentaD}	20	5 / 20
	Gβγ1	21	3 / 21
	Gβγ4	19	4 / 19
dmi2-1 (inoculated)	EV	29	0 / 29
	DMI2 KD	38	14 / 38
	RGS^{PentaD}	60	7 / 60
	Gβγ1	28	4 / 28
	Gβγ4	26	2 / 26

[1]: *Agrobacterium*-mediated transformed roots of wild-type (WT) and *dmi2-1* were non-inoculated and inoculated with *Sinorhizobium meliloti*, respectively. Formation of nodule-like structures was assessed 70 days after the plants were transferred to soil (WT plants) or 70 days post-inoculation (*dmi2-1* mutants). EV, empty vector; *DMI2 KD*, *Mt*DMI2 kinase domain.

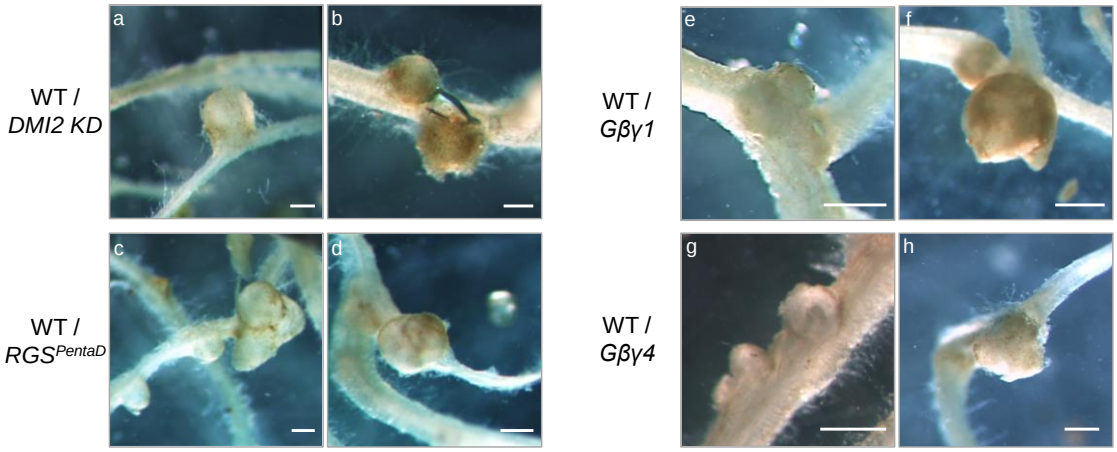

Figure 4.9 | Constitutive expression of different gene combinations of heterotrimeric G proteins in non-inoculated wild-type.
Agrobacterium-mediated transformed roots of wild-type (WT) expressing different gene combinations of heterotrimeric G proteins were assessed at 70 days after the plants were transferred to soil to test the ability of heterotrimeric G proteins to activate nodule organogenesis. (**a-h**) Representative pictures of nodule-like structures in WT transformed roots expressing the kinase domain of *Mt*DMI2 (*DMI2 KD*) used as positive control (**a-b**), phosphomimic *MtRGS*^{PentaD} (**c-d**), *MtGβ* co-expressed with *MtGγ1* (*Gβγ1*) (**e-f**), and *MtGβ* co-expressed with *MtGγ4* (*Gβγ4*) (**g-h**). WT plants were non-inoculated and grown in sterile conditions. Total number of nodule-like structures is summarised in Table 4.1. White bars represent 0.5 mm.

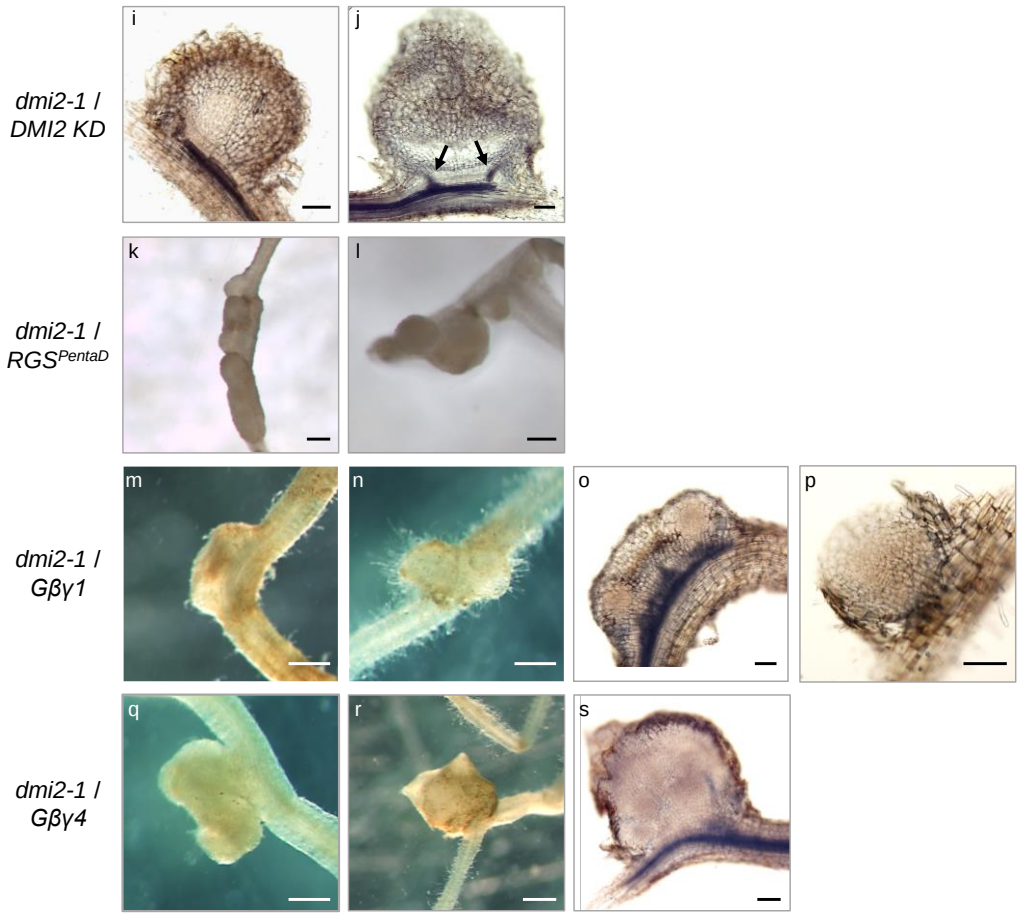

Figure 4.10 | Constitutive expression of different gene combinations of heterotrimeric G proteins in the non-nodulating *dmi2-1* mutant.
Agrobacterium-mediated transformed roots in the non-nodulating *dmi2-1* mutant expressing different gene combinations of heterotrimeric G proteins, were assessed at 70 days post-inoculation with

Sinorhizobium meliloti to test the ability of heterotrimeric G proteins to suppress the Nod- phenotype of *dmi2-1*. (**i-s**) representative pictures of nodule-like structures in *dmi2-1* transformed roots expressing the kinase domain of *Mt*DMI2 (*DMI2 KD*) used as positive control (**i-j**), phosphomimic $MtRGS^{PentaD}$ (**k-l**), *MtGβ* co-expressed with *MtGγ1* (*Gβγ1*) (**m-p**), and *MtGβ* co-expressed with *MtGγ4* (*Gβγ4*) (**q-s**). (**i-j, o-p, s**) Longitudinal section pictures of nodule-like structures in indicated transformed roots. Pictures **o** and **s** are the longitudinal sections of the structures shown in **m** and **r**, respectively. Black arrows in **j** point to the dual peripheral vascular bundles, a hallmark of root nodules. Total number of structures is summarised in Table 4.1. White and black bars in pictures represent 0.5 mm and 100 µm, respectively.

4.3 Discussion

In the previous chapter, characterization of various *MtGβ* mutants demonstrated that *MtGβ* regulates both root nodule and AM symbioses in *Medicago*. Notably, the lower number of infected epidermal cells by rhizobia and AM intra-radical hyphae in $G\beta^{L29F}$ and $G\beta^{L31F}$ mutants (Figure 3.6) indicated that early stages of colonization were impaired. The deregulated symbiosis-activated nuclear Ca^{2+} signalling in $G\beta^{L31F}$ (Figure 4.1) and the impaired up-regulation of symbiosis genes in $G\beta^{L29F}$ and $G\beta^{L31F}$ (Figure 4.2) demonstrated that *MtGβ* is part of the common SYM pathway upstream of the nuclear Ca^{2+} signalling and is likely to regulate the latter. Besides, cellular imaging of functional Gβ-GFP revealed that a pool of the protein relocates to nuclei in root hair cells upon Nod-factor treatment (Figure 4.4), suggesting that *Mt*Gβ may be actively translocated into the nucleus after detection of symbiotic elicitors.

Gβγ translocation to inner membranes have been evidenced in mammalian cells (Khan et al., 2016). All mammalian Gγ subunits are capable of supporting Gβγ translocation (Ajith Karunarathne et al., 2012) with varying kinetics depending on the Gγ C-termini and their affinity for membranes (O'Neill et al., 2012). Gβγ translocation is reversible and meets several purposes. It maintains a steady intracellular pool of free Gβγ that regulates response intensity at the plasma membrane (Chisari et al., 2009; O'Neill et al., 2012) but also allows for transduction of signal at inner membranes by Gβγ direct binding to target proteins (Malik et al., 2015; Khater et al., 2021). In addition, external stimuli can induce Gβ translocation into nuclei to regulate gene expression by Gβ direct binding to transcription modulators (Bhatnagar et al., 2013). In plants, Gβγ translocation has not been studied to my knowledge. But the *Arabidopsis* Gβ was shown to bind to various proteins in different cell compartments such as the nuclei (Kobayashi et al., 2012; Yu et al., 2016; Xu et al., 2017; Zhang et al., 2018) suggesting that Gβ function in plants is not limited to the plasma membrane.

The role of *MtGβ* in modulating symbiosis-activated nuclear Ca^{2+} signalling (Figure 4.1; Figure 4.2) in addition to the nuclear localization of Gβ-GFP after Nod-factor treatment (Figure 4.4), prompted us to speculate that Gβ may regulate nuclear ion channels. This was tested through constitutive expression of *NES-* and *NLS-Gβ* with the YC3.6 Ca^{2+} reporter (Figure 4.5). The results showed that overexpression of *NLS-Gβ* is sufficient to induce oscillatory Ca^{2+} spiking within the nuclear region of root hairs contrary to *NES-Gβ* (Figure 4.5), suggesting that nuclear-Gβ may be capable of inducing opening of ion channels at the nuclear envelope. Furthermore, transcriptional induction of phosphomimic $MtRGS^{PentaD}$ resulted in similar observations, and $MtRGS^{PentaD}$-induced nuclear Ca^{2+} spiking was significantly less efficient in the absence of the nuclear ion channel *MtDMI1* (Figure 4.6). These results imply that heterotrimeric G proteins regulate nuclear Ca^{2+} signalling through Gβ during endosymbiosis.

In plants, heterotrimeric G proteins have been shown to regulate ion channel opening. *Arabidopsis Gα* and *Gβ* were shown to redundantly function regulating ABA (Abscisic Acid)-activated anion channel opening during stomatal closure (Wang et al., 2001; Fan et al., 2008). By contrast, *Arabidopsis Gα* and *Gβ* have antagonist effects on cytoplasmic Ca^{2+}-induced Ca^{2+} oscillations in guard cells (Jeon et al., 2019). *AtGα* inhibits the oscillatory Ca^{2+} release while *AtGβ* is required for its activation. The *AtGβ*-dependant Ca^{2+} response in this system was presumed to be induced by *At*Gβ binding to phospholipase C. Altogether, these studies suggest that heterotrimeric G proteins regulate ion channel activity through distinct pathways. Nevertheless, several ambiguities remain regarding NLS-Gβ and *Mt*RGS^{PentaD}-induced Ca^{2+} release within root hairs. Whether NLS-Gβ-activated Ca^{2+} spiking depends on *MtDMI1* was not assessed and should be established in future. One may argue that ectopic expression of *NLS-Gβ* may trigger pleiotropic effects such as transcriptional remodelling as Gβ was shown to interact and modulate the activity of transcription factors (Xu et al., 2017; Zhang et al., 2018) and might therefore lead to unexpected effects on Ca^{2+} signalling. The use of an inducible system to control *NLS-Gβ* expression would be more elegant. Furthermore, if *Mt*Gβ transduces the symbiosis signal via nuclear translocation, it remains to be determined by which mechanism *Mt*RGS^{PentaD} triggers *Mt*Gβ translocation. Numerous studies on plant RGS proteins give some insight into how this scenario could be explained (discussed in more details in general discussion). In any case, it should be verified whether *Mt*RGS^{PentaD} induces *Mt*Gβ nuclear translocation in the absence of symbiotic elicitors.

The use of the GVG system in this study for transcriptional induction may be questionable since GVG-induced toxicity was reported in several plant species (Kang et al., 1999; Ouwerkerk et al., 2001; Andersen et al., 2003). Growth and developmental defects in both shoot and root systems were reported particularly upon DEX application whereas no chemical treatment resulted in almost no observable phenotype. But the phenotypes were observed after long period of DEX treatment (>2 weeks) while short treatment (1-4 days) was reported to have no effect on 1-week-old rice seedlings (Ouwerkerk et al., 2001), and no detrimental effects were observed after 24 hours of DEX treatment in this study.

Ectopic and constitutive expression of *MtRGS*^{PentaD} and *MtGβγ1,4* in *Agrobacterium*-mediated transformed roots resulted in subtle stimulation of nodule-like organogenesis (Table 4.1; Figure 4.9; Figure 4.10). Some of the structures are undeniably different from lateral roots and to a certain extent comparable to root nodules or nodule primordia. In *M. truncatula*, lateral roots and nodules equally originate from pericycle, endodermal, and inner-cortical anticlinal cell divisions as a result of local auxin accumulation (Herrbach et al., 2014; Xiao et al., 2014). Both developmental programs share 75% overlapping transcriptional changes (Schiessl et al., 2019). The distinction between lateral root and nodule development rather relies on distinct processes that produce local auxin accumulation (Schiessl et al., 2019). Shared genes in lateral root and nodule development are exemplified by *MtLBD16* and *LjASL18a/b* (Schiessl et al., 2019; Soyano et al., 2019). It is worth noting that *MtLBD16* and *LjASL18a/b* expression are regulated by and downstream of *NIN*. Interestingly, constitutive expression of *MtLBD16* and *LjASL18a/b* induced the formation of ectopic root structures similar to those observed in *MtRGS*^{PentaD} and *MtGβγ1,4*-expressing roots (Schiessl et al., 2019; Soyano et al., 2019). Thus, dissection of the transcriptional changes associated with constitutive expression of *MtRGS*^{PentaD} and *MtGβγ1,4*, would allow for the identification of the genetic program that initiates ectopic root organogenesis in this study. Notably, activation of *NIN* and *MtLBD16* in *MtRGS*^{PentaD} and *MtGβγ1,4*-expressing roots would demonstrate that heterotrimeric G proteins regulate both epidermal entry and nodule organogenesis as *MtDMI2* does. Furthermore, it would be interesting to assess *DMI2 KD*-induced spontaneous nodule formation in *Gβ*^{L29F} and *Gβ*^{L31F} mutants. Lower appearance of spontaneous nodules in the mutants would bring another piece of evidence that *MtGβ* is part of the common SYM pathway.

Chapter V

Identification of Gβ protein interactors for the activation of nuclear Ca^{2+} signalling during root endosymbiosis

5.1 Introduction

Activation of nuclear calcium (Ca^{2+}) oscillations during endosymbiosis upon detection of symbiotic elicitors initiates from the nucleus (Kelner et al., 2018). The nuclear Ca^{2+} machinery regulating the endosymbiotic response in *Medicago truncatula* comprises the cation-permeable channel Does Not Make Infections 1 (DMI1), the Ca^{2+}-permeable cyclic nucleotide-gated channels (CNGCs) 15a/b/c and the Ca^{2+}-dependant adenosine triphosphatase (Ca^{2+}-ATPase) MCA8 (Ané et al., 2004; Capoen et al., 2011; Charpentier et al., 2016). According to mathematical modelling, the CNGC15s control the Ca^{2+} release while DMI1 acts as a counter ion channel to counter-balance the flow of positive charges delivered in the nucleoplasm (Charpentier et al., 2013). The elevation of nucleoplasmic Ca^{2+} causes Ca^{2+}-bound calmodulin 2 (CaM2) to bind to the CNGC15s closing the channels, while MCA8 pumps back Ca^{2+} into the interspace of the nuclear envelope (Charpentier et al., 2013; del Cerro et al., 2022). It is hypothesised that the cycle would repeat itself as the CNGC15s and DMI1 remain in an active state (Charpentier et al., 2013; del Cerro et al., 2022). Nonetheless, the primary activation mechanism that initiates the nuclear Ca^{2+} machinery when symbiotic elicitors are detected remains unknown. DMI1 and CNGC15 proteins physically interact and this may support synchronous activation (Charpentier et al., 2016). It was also hypothesised that upon activation of either DMI1 or CNGC15, both ion channels undergo a structural change, putatively unlocking CNGC15 from DMI1 (del Cerro et al., 2022). Ca^{2+} leak through CNGC15 is predicted to positively feedback on DMI1, increasing its counter-balance flux, and by consequence the Ca^{2+} release via CNGC15. In agreement with this prediction, Ca^{2+}-binding pockets were identified in one of the homologs of *MtDMI1*, *LjCASTOR* (Kim et al., 2019).

Work presented in chapter 4 shows that the heterotrimeric G protein *Mt*Gβ subunit regulates the nuclear Ca^{2+} signalling following application of a symbiotic elicitor (Figure 4.1), in line with *Mt*RGS^{PentaD} and NLS-Gβ-activated spontaneous Ca^{2+} release within the nuclear

region of root hair cells (Figure 4.5; Figure 4.6). Intriguingly, a pool of C-terminally GFP-fused *Mt*Gβ rapidly relocates to nuclei when roots are treated with Nod-factors (Figure 4.4), suggesting that *Mt*Gβ undergoes nuclear translocation to putatively activate the symbiosis ion channels. Thus, I investigated the protein-protein interactions between *Mt*Gβ and nuclear proteins to determine the precise role of Gβ during root endosymbiosis.

5.2 Results

5.2.1 *Mt*Gβ does not interact with *Mt*DMI1 or *Mt*CNGC15c in a yeast-two-hybrid assay.

In human cells, three ion channels are regulated by Gβγ via direct binding to the intracellular amine- or carboxyl-termini of the channels (Zamponi and Currie, 2013; Dascal and Kahanovitch, 2015; Behrendt et al., 2020). Thus, the ability of *Mt*Gβ to bind to the intracellular domains of DMI1 and CNGC15s was tested using the yeast-two-hybrid system. This system uses the *Saccharomyces cerevisiae* heterologous system to investigate specific pairwise protein interactions based on the transcription activator GAL4 (Fields and Sternglanz, 1994; Matiolli and Melotto, 2018). Briefly, a protein (bait) is cloned in-frame with the DNA-binding domain of GAL4 (BD), while a second protein (prey) is cloned in-frame with the transcription activation domain of GAL4 (AD). If the bait and prey proteins interact, the resulting BD-bait/AD-prey complex reconstitutes the transcription factor GAL4 that binds specifically to GAL4 upstream activating sequences (UAS) and TATA boxes to induce transcription of marker genes (e.g., alanine and histidine-metabolizing enzymes to complement a specific yeast auxotrophy). Using a selective medium, bait-prey interaction is detected from restoration of yeast growth. The yeast-two-hybrid system enables therefore to screen for direct interaction between two proteins.

The coding sequences (CDS) of the amine or carboxyl-termini of *MtDMI1* and *MtCNGC15c* were cloned in-frame with GAL4 BD domain, while the CDS of *MtGβ* was cloned in-frame with GAL4 AD domain (Figure 5.1). No yeast growth was detected on selective medium (Figure 5.1, A), indicating that *Mt*Gβ does not bind to *Mt*DMI1 nor *Mt*CNGC15c.

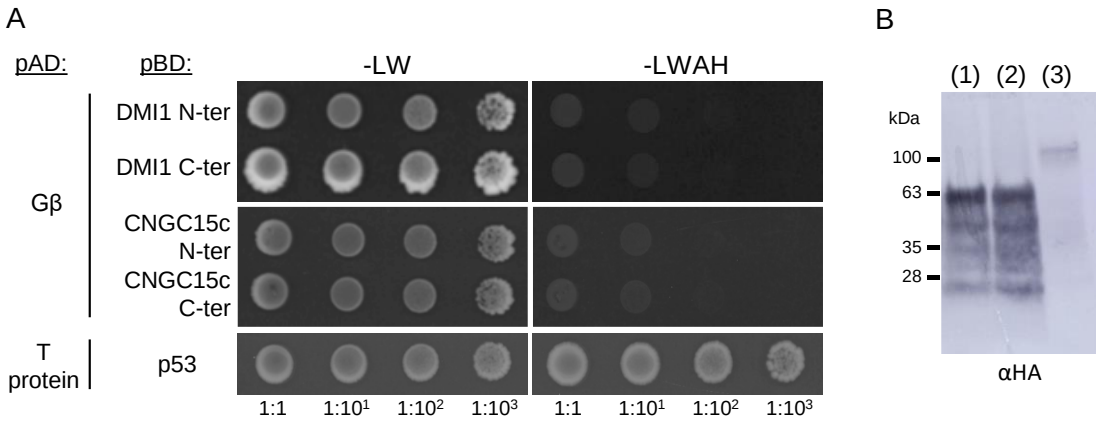

Figure 5.1 | Gβ does not interact with DMI1 and CNGC15c in GAL4-based yeast-two-hybrid assay.
(A) GAL4-based yeast two-hybrid assays to assess pairwise interactions between *Mt*Gβ fused to GAL4 activator domain (AD) and the N-terminus (N-ter) or C-terminus (C-ter) of DMI1 and CNGC15c fused to the GAL4 binding domain (BD). Dilution series of co-transformed yeast were grown on synthetic dextrose minimal (SD) medium lacking Leucine and Tryptophan (-LW). Positive interactions were detected on SD medium lacking Alanine, Histidine, Leucine and Tryptophan (-LWAH) at 7 days post growth. The mouse p53 protein known to interact with the SV40 large T-antigen (T) was used as positive control. Pictures are representative of three replicates. (**B**) Western blot analysis to assess expression of AD:HA:Gβ co-expressed with BD:Myc:CNGC15c N-ter (1) or BD:Myc:CNGC15c C-ter (2) and AD:HA:T co-expressed with BD:Myc:p53 (3). Both AD:HA:Gβ and AD:HA:T were detected on the immunoblot. Expected sizes for AD:HA:Gβ and AD:HA:T are 62 and 102 kDa, respectively.

In parallel to this study, AUK (Auxiliary Unit Kinase) protein was identified in Myriam Charpentier's laboratory and interacts with *Mt*DMI1 (Grubb et al., in preparation). *Mt*AUK localizes at the nuclear envelope and controls root endosymbiosis upstream of *MtDMI1*. Constitutive expression of *MtAUK* in *Agrobacterium*-mediated transformed roots induces spontaneous nuclear Ca^{2+} oscillations dependently to *MtDMI1*. Interestingly, the closest *Mt*AUK putative protein homolog in *Arabidopsis* (67.2% identity) was shown to interact with *At*Gβ and its kinase activity was dependent on *At*Gβ in *in vitro* assays (Yu et al., 2016). Thus, the interaction between *Mt*AUK and *Mt*Gβ was investigated.

5.2.2 *Mt*Gβ interacts with *Mt*AUK, a newly identified DMI1-interacting protein.

*Mt*AUK is a newly identified nuclear localised protein that interacts with *Mt*DMI1 and is required to activate nuclear Ca^{2+} oscillation (Grubb et al, in preparation). *Mt*AUK has a kinase domain on its carboxyl-terminus. Protein-protein interaction between *Mt*Gβ and *Mt*AUK was first assessed via GAL4-based Y2H assay. The CDS of *MtAUK* C-terminal or *MtAUK* kinase domain only were cloned in-frame with GAL4 BD, while *MtGβ* was cloned in-frame with GAL4 AD (Figure 5.2, A). Yeast cell growth was observed with both baits,

indicating that *Mt*Gβ binds to the carboxyl-terminus of *Mt*AUK and more specifically to the kinase domain of *Mt*AUK.

To confirm the interaction *in planta*, *Mt*AUK and *Mt*Gβ proteins were fused to HA (Human influenza Hemagglutinin) and N-terminus YFP (Yellow Fluorescent Protein) epitopes, respectively, and co-expressed in *M. truncatula* roots via *Agrobacterium-rhizogenes*-mediated root transformation (Figure 5.2, C). The nuclear protein *Mt*DMI3 (Messinese et al., 2007) fused to N-terminus YFP was used as negative control (Figure 5.2, C). Plants were inoculated with *Sinorhizobium meliloti* for 48 hours before protein extraction. AUK-HA proteins were purified from total protein samples using an anti-HA affinity column (Figure 5.2, C, right panel). Gβ-nYFP co-immunoprecipitated with AUK-HA in contrast to DMI3-nYFP (Figure 5.2, C, right panel), demonstrating that *Mt*Gβ and *Mt*AUK physically interact in *Medicago* roots. Besides, a Gβ-binding site was identified in the closest putative homolog of *Mt*AUK in Arabidopsis (*At*AUK) (Yu et al., 2016). Although the binding site is not conserved in *Mt*AUK (Figure 5.2, B), it is possible that the changed sequence still modulates protein-protein interaction with *Mt*Gβ. Thus, a truncated protein of *Mt*AUK with 15-amino-acid deletion (AUKΔGβ) was co-expressed with Gβ-nYFP in *M. truncatula* transformed roots (Figure 5.2, B-C). Gβ-nYFP co-immunoprecipitated with AUKΔGβ-HA (Figure 5.2, C), demonstrating that *Mt*Gβ and truncated *Mt*AUKΔGβ can still interact. However, the densitometry units of co-immunoprecipitated products normalised to the amounts of total protein was twice lower (Figure 5.2, D), suggesting that the 15-amino-acid-long site supports the interaction but is not essential. Altogether, the results demonstrate that *Mt*Gβ interacts with *Mt*AUK and suggests that Gβ-AUK interaction mediates nuclear Ca^{2+} signalling.

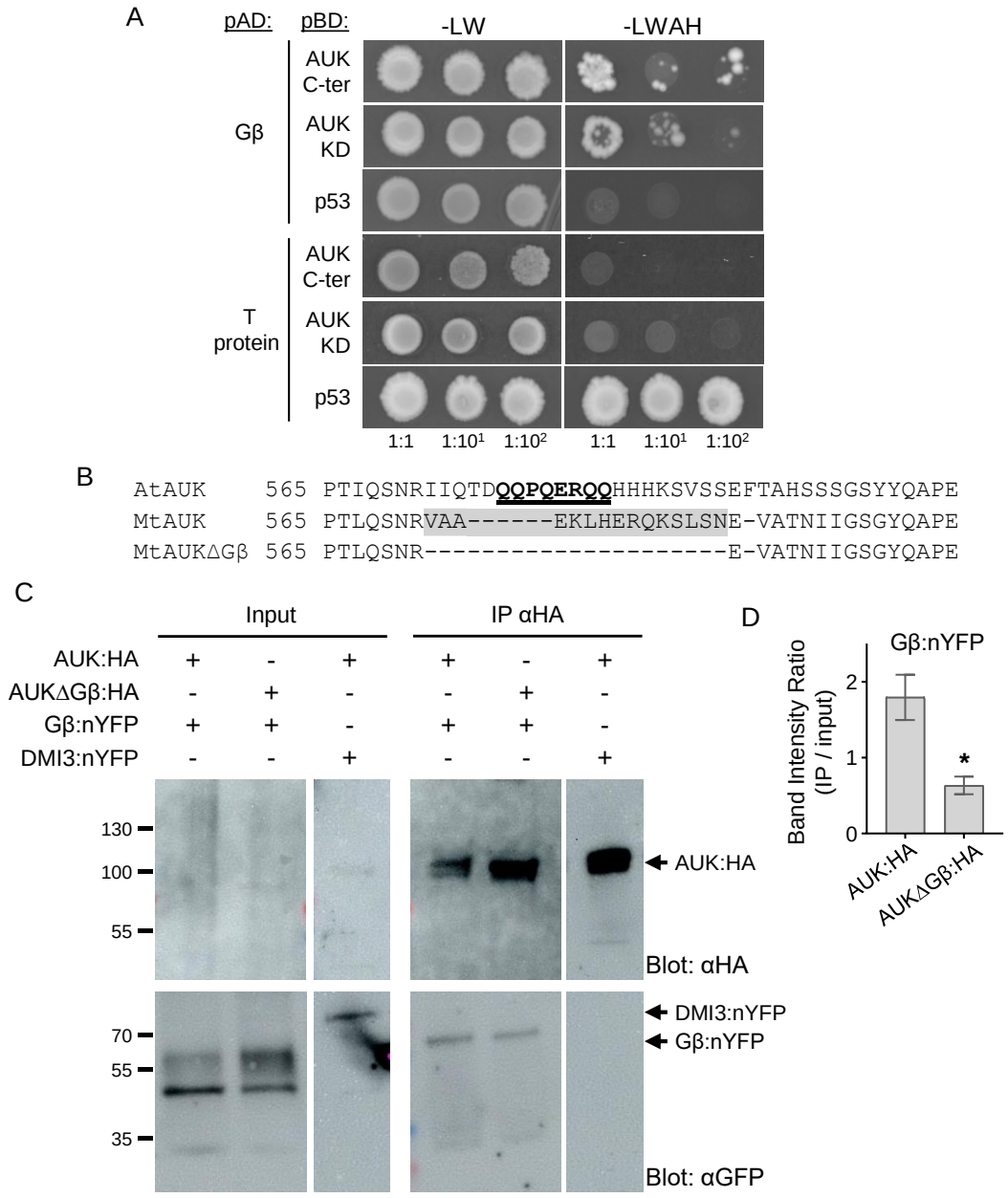

Figure 5.2 | Gβ interacts with AUK in *M. truncatula* roots.
(**A**) Pairwise GAL4-based yeast two-hybrid assay to assess pairwise interactions between *Mt*Gβ fused to GAL4 activator domain (AD) and the C-terminus (C-ter) or kinase domain (KD) of *Mt*AUK fused to the GAL4 binding domain (BD). Yeast growth was monitored after 7 days on synthetic dextrose minimal (SD) media lacking Leucine and Tryptophan (-LW) to assess co-transformation and on SD media lacking Alanine, Histidine, Leucine and Tryptophan (-LWAH) to assess pairwise interaction. Yeast cultures were diluted as indicated (bottom panel). The mouse p53 protein and its known interacting partner SV40 large T-antigen (T) were used as negative and positive controls. Pictures are representative of three replicates. (**B**) Protein sequence alignment of *Arabidopsis thaliana* (At) AUK, *Medicago truncatula* (Mt) AUK and the truncated *Mt*AUK (AUKΔGβ) used in **C**. The Gβ-binding site predicted in *At*AUK is bolded and underlined. (**C**) HA-tagged *Mt*AUK (AUK:HA) was immunoprecipitated with anti-HA antibody from *M. truncatula* root cells co-expressing Gβ:nYFP or DMI3:nYFP. HA-tagged *Mt*AUKΔGβ (AUKΔGβ:HA) was immunoprecipitated similarly from *M. truncatula* root cells co-expressing Gβ:nYFP to assess the function of the putative Gβ-binding domain identified in *At*AUK. Before immunoprecipitation, the *M. truncatula* transformed roots were inoculated with *Sinorhizobium meliloti* for 48h. Immunoblots were immunostained with αHA (top panel) or $\alpha GFP^{N\text{-}ter}$ (bottom panel) antibodies. Input: total protein lysate. Gβ:nYFP was detected in the immunoprecipitate from roots co-expressing AUK:HA or AUKΔGβ:HA, indicating Gβ-AUK interaction. The nuclear localised calcium and calmodulin dependent kinase, DMI3:nYFP, was used

as negative control. Data are representative of two biological replicates. Expected sizes: AUK:HA, 89 kDa; Gβ:nYFP, 61 kDa; DMI3:nYFP, 80 kDa. (**D**) Band intensity ratio (IP over input) of Gβ:nYFP immuno-bands in the indicated conditions were calculated from two biological replicates and from two immunoblots at two or three exposure levels (between 10 and 90 min of exposure time). Bars represent mean ± s.e.m.. * p-value < 0.05 (two-tailed t-test with a prior F-test for homoscedasticity).

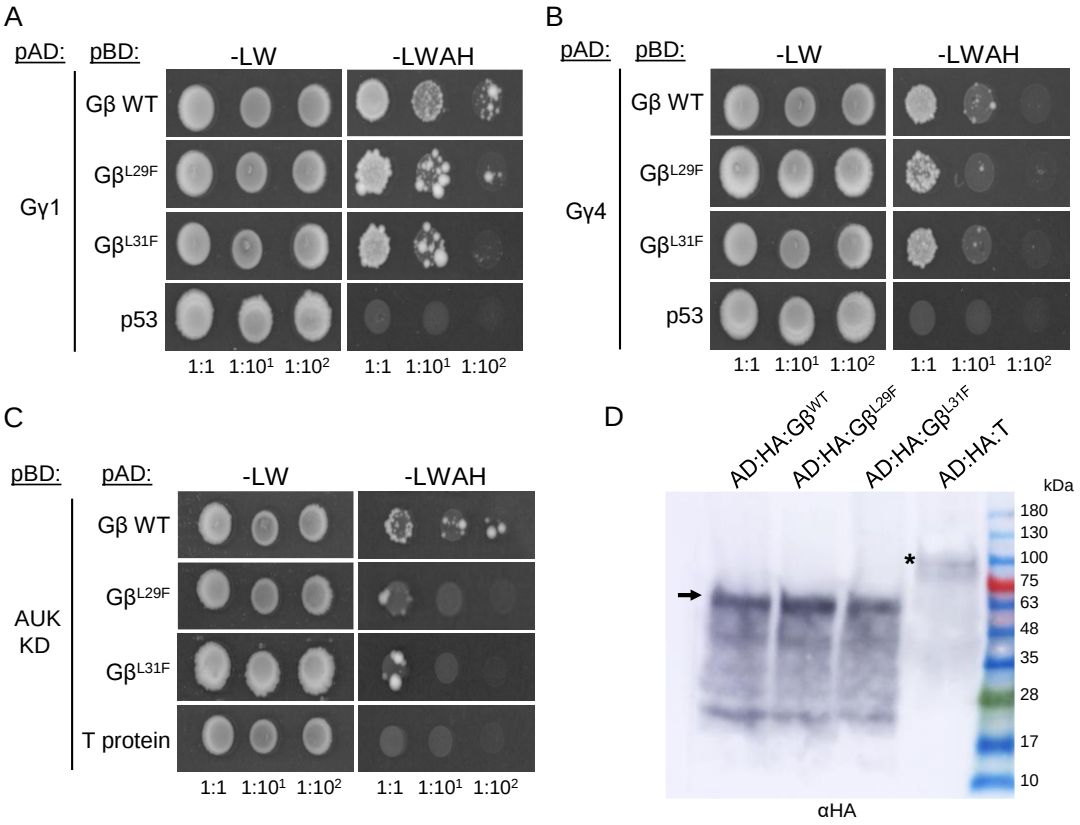

Figure 5.3 | Effects of L29F and L31F mutations on protein-protein interaction.
(**A**-**C**) Pairwise GAL4-based yeast two hybrid analysis of *Mt*Gβ wild-type (Gβ WT), *Mt*Gβ^{L29F} and *Mt*Gβ^{L31F} with *Mt*Gγ1 (**A**), *Mt*Gγ4 (**B**) and *Mt*AUK kinase domain (AUK KD) (**C**). The coding sequences (CDS) were cloned in frame with the GAL4 activator domain (AD) or binding domain (BD) as indicated. Yeast growth was monitored after 7 days on synthetic dextrose minimal (SD) media lacking Leucine and Tryptophan (-LW) to assess co-transformation and on SD media lacking Alanine, Histidine, Leucine and Tryptophan (-LWAH) to assess pairwise interaction. Yeast cultures were diluted as indicated (bottom of the panel). The mouse p53 protein and its known interacting partner SV40 large T-antigen (T) were used as negative controls. Pictures are representative of three replicates. (**D**) Detection by immunoblot of AD:HA:Gβs and AD:HA:T using anti-HA antibody. Proteins were extracted from co-transformants shown in **C.** Expected sizes: AD:HA:Gβs, 62 kDa (black arrow); AD:HA:T, 102 kDa (black asterisk).

5.2.3 Gβ^{L29F} and Gβ^{L31F} show impaired protein-protein interaction with *Mt*AUK in heterologous system.

Given the altered symbiosis phenotype observed in *Gβ^{L29F}* and *Gβ^{L31F}* mutants (Chapter 3, Figure 3.5), the effects of L29F and L31F mutations on *Mt*Gβ protein-protein interactions were tested. Gβ requires a Gγ subunit for correct localization at plasma membrane (Marrari et al., 2007; Wang et al., 2008). Thus, impairment in the formation of

Gβγ dimer would inhibit Gβ function in transducing signals. Protein-protein interactions between *Mt*Gβ, *Mt*Gβ^{L29F}, *Mt*Gβ^{L31F} and *Mt*Gγ1,4 were assessed using the GAL4-based yeast-two-hybrid system (Figure 5.3, A-B). Co-transformants expressing *Mt*Gβ wild-type, *Mt*Gβ^{L29F} or *Mt*Gβ^{L31F} with *Mt*Gγ1 or *Mt*Gγ4 showed all complementation of yeast auxotrophy (Figure 5.3, A-B), demonstrating that *Mt*Gγ1 and *Mt*Gγ4 are Gγ subunits *per se* capable of interacting with *Mt*Gβ. It furthermore indicates that L29F and L31F mutations do not abolish the interaction. One may argue that yeast growth in the presence of *Mt*Gβ^{L29F} and *Mt*Gβ^{L31F} is slightly reduced but additional experiments are required to determine the binding affinities and test whether L29F and L31F mutations negatively affect Gβγ dimer formation. On the other hand, impact of L29F and L31F mutations on the interaction with *Mt*AUK kinase domain was also assessed (Figure 5.3, C). Co-expression of *Mt*AUK kinase domain with *Mt*Gβ^{L29F} or *Mt*Gβ^{L31F} nearly abolished yeast growth on selective medium (Figure 5.3, C), suggesting that L29F and L31F mutations prevent *Mt*Gβ from interacting with *Mt*AUK. Future experiments will enable to confirm this observation. Overall, this suggests that *Mt*Gβ transduces the symbiotic signal by interacting with *Mt*AUK, and that impairment of this interaction resulting from amino acid substitution on *Mt*Gβ N-terminus ultimately impedes nuclear Ca^{2+} signalling activation.

To examine further the impact of L29F and L31F mutations on *Mt*Gβ function, subcellular localization of *Mt*Gβ^{L29F} and *Mt*Gβ^{L31F} in root hairs was analysed via fluorescent confocal laser scanning microscopy using a GFP (Green Fluorescence Protein) tag fused to their carboxyl-terminus (Figure 5.4). Roots were additionally treated with Nod-factors to test whether Gβ^{L29F}-GFP and Gβ^{L31F}-GFP relocalize. Surprisingly, in the absence of Nod-factors GFP fluorescence was observed in the cytoplasm and somewhat in the nucleoplasm (Figure 5.4). In the presence of Nod-factor, less fluorescence in the cytoplasm is observed in contrast to the nucleoplasm, suggesting that a pool of both Gβ^{L29F}-GFP and Gβ^{L31F}-GFP can relocate to the nucleus. However, these results are preliminary and leave open the possibility that the L29F and L31F mutations could alter the plasma membrane association, stability and/or partly the translocation to the nucleus. Additional experiments will be required to assess whether the *Mt*Gβ^{L29F} and *Mt*Gβ^{L31F} proteins correctly localize and remain stable at the plasma membrane as their wild-type counterpart. To this aim, additional confocal laser scanning microscopy will be required as well as subcellular protein fractionation. The latest could be informative to determine whether *Mt*Gβ^{L29F} and *Mt*Gβ^{L31F} associate with plasma membrane.

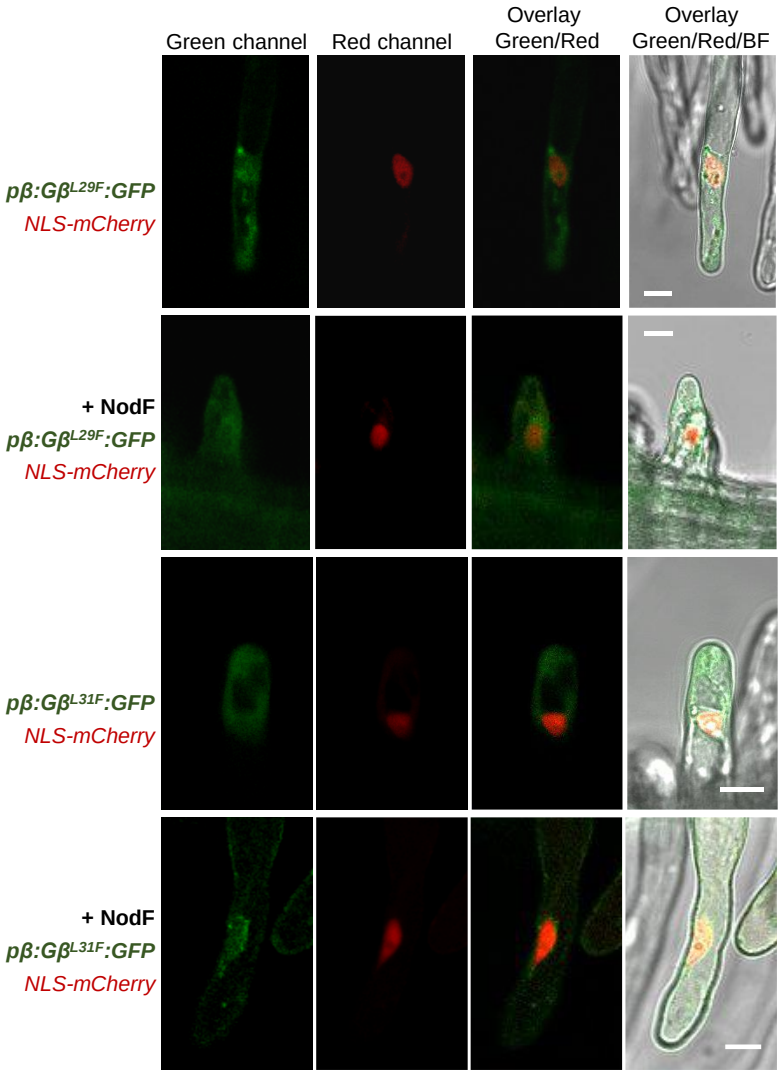

Figure 5.4 | Confocal imaging of GFP-tagged Gβ^{L29F} and Gβ^{L31F} proteins.
Laser scanning confocal microscopy pictures of *M. truncatula* wild-type root hairs co-expressing the transformation marker *NLS-mCherry* with C-terminally GFP-tagged *Gβ^{L29F}:GFP* or *Gβ^{L31F}:GFP* driven by *Gβ* native promoter (*pβ:Gβ^{L29F}:GFP*, *pβ:Gβ^{L31F}:GFP*) in the absence or presence of Nod-factor (+NodF). Mock and Nod-factor treatment lasted 30 minutes before imaging. Scale bars represent 10 µm. BF, brightfield.

5.2.4 Protein purification of Gβs in heterologous system.

To determine the precise binding affinities of *Mt*Gβ wild-type and mutants with *Mt*AUK, two protein purification protocols were tested to isolate the different proteins. Interaction of *Arabidopsis* Gβ with protein interactors has previously been tested via pull down assays in *Escherichia coli* Rosetta strain (Peng et al., 2018; Zhang et al., 2018) and plant Gα subunits were successfully purified in this strain (Urano et al., 2012b). Thus, *E. coli* Rosetta strain was used to expressed and purify *Mt*Gβ wild-type, *Mt*Gβ^{L29F} and *Mt*Gβ^{L31F} proteins (Figure 5.5). Coding sequences were cloned in-frame with a 6xHis (hexa-histidine) tag and an MBP (Maltose-binding protein) tag both at the N-terminus of each protein. The

resulting vectors were transformed into *E. coli* Rosetta strain and bacteria were grown overnight after induction of protein expression with isopropyl β-D-1-thiogalactopyranoside (IPTG). After solubilization, proteins were purified using a specific affinity column for poly-Histidine-tagged proteins. Samples were further purified via gel filtration chromatography. This process separates proteins by their molecular size in several elution fractions, which can be analysed via SDS-PAGE (Figure 5.5, A-B). Expected size of 6xHis:MBP:Gβs is 84 kDa. Accordingly, the eluted fractions that contained the proteins in this molecular size range were combined and further concentrated as shown in Figure 5.5, C. Analysis via SDS-PAGE of the concentrated fractions demonstrated that each recombinant Gβ were present in a small amount (Figure 5.5, C, black arrow). However, each fraction included a large amount of protein contaminants. To confirm that the thin bands observed around 84 kDa correspond to the proteins of interest, the concentrated samples were treated with 3C protease to cleave the 6xHis:MBP tag (Figure 5.5, D). The absence of the thin band in 3C-protease-treated samples confirmed the presence of 6xHis:MBP:Gβ (Figure 5.5, D). However, due to the large amount of contaminants and the small proportion of 6xHis:MBP:Gβs produced, another protocol was developed.

Gβ proteins from various species were successfully purified from insect cell culture using the *Spodoptera frugiperda* Sf9 isolate (Iñiguez-Lluhi et al., 1992; Jones et al., 2011b). In this system, cells are infected with genetically modified baculoviruses (Schneider and Seifert, 2010). The highly-expressed viral protein polyhedrin gene is replaced by a gene of interest, resulting in high-level expression of the corresponding protein. Thus, the coding sequences of *MtGβ* wild-type and $MtG\beta^{L29F}$ and $MtG\beta^{L31F}$ mutants were cloned in-frame with an MBP (Maltose-binding protein) tag at their N-terminus and recombinant sequences were inserted into the baculovirus genome. Insect cells were infected for three days before protein extraction and purification. Proteins were purified using an MBP-specific affinity column (Figure 5.6). Analysis via western-blot and SDS-page showed a large proportion of proteins of interest after protein purification, validating the use of this protocol for *Mt*Gβ purification. Accordingly, purified *Mt*Gβ wild-type, $MtG\beta^{L29F}$ and $MtG\beta^{L31F}$ proteins will be tested with *Mt*AUK via biolayer interferometry to determine their binding affinities and assess the effect of L29F and L31F mutations on *Mt*Gβ binding to *Mt*AUK.

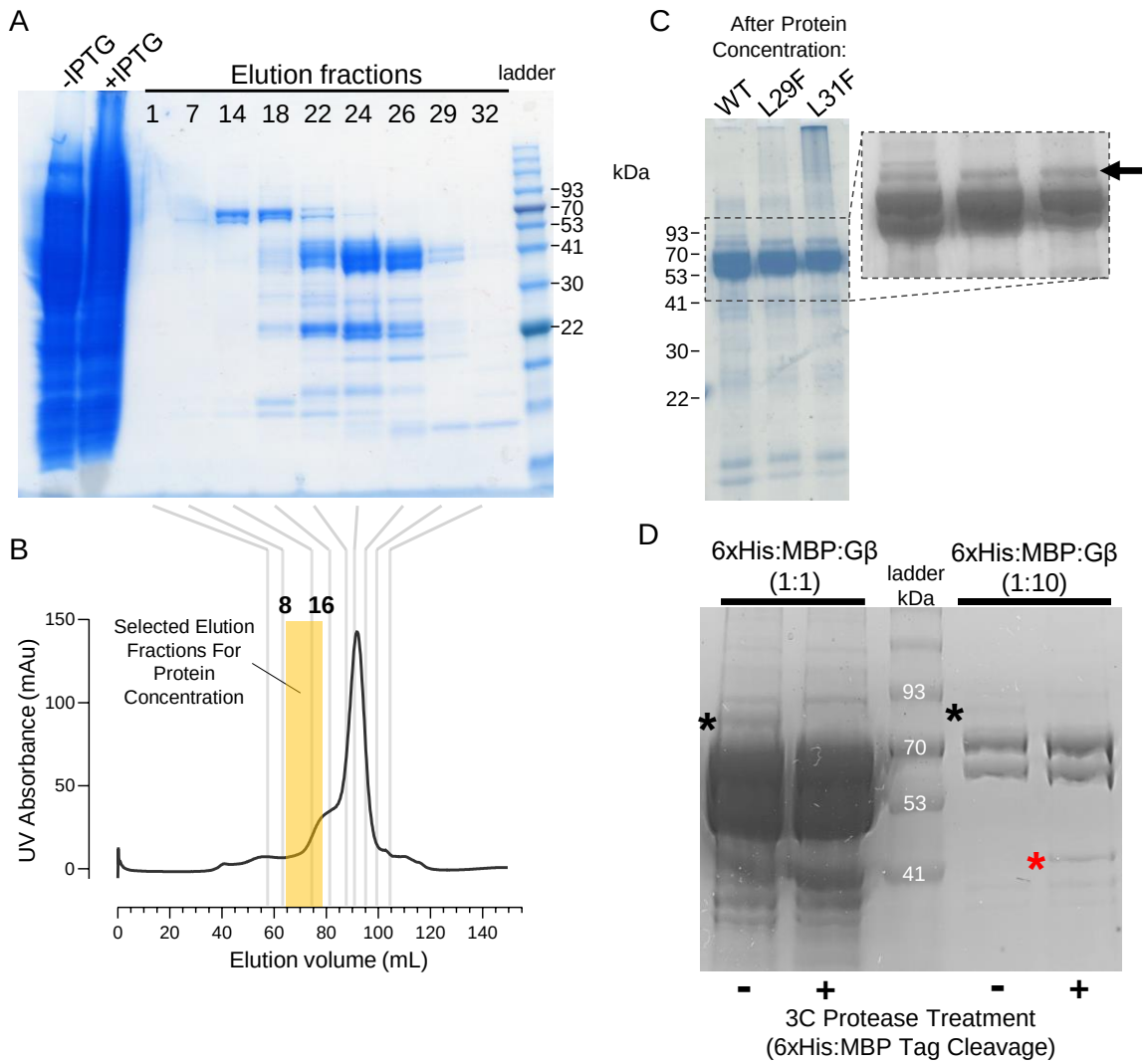

Figure 5.5 | Gβ protein purification in *Escherichia coli* conserves high amount of protein contaminants.

Escherichia coli strain Rosetta DE3 expressing recombinant *Mt*Gβ protein fused to 6xHis (hexa-histidine) and MBP (maltose-binding protein) tags at the N-terminus (6xHis:MBP:Gβ) was grown 14 hours in 8-litre culture in the presence of IPTG to induce expression of the protein of interest. Proteins were purified through Ni-NTA column (specific affinity for polyHis-tagged protein) and fractionated in several elution fractions via gel filtration chromatography. (**A**) Elution fractions were separated via SDS-PAGE and revealed by Coomassie blue staining to determine in which elution fractions the protein of interest is present. Expected size of 6xHis:MBP:Gβ, 84 kDa. Crude protein fractions before (-IPTG) and after (+IPTG) induction are shown. (**B**) Corresponding elution profile of the eluted fractions shown in **A** after gel filtration chromatography. Protein amount is determined via ultraviolet (UV) absorbance. The elution fractions selected for protein concentration of 6xHis:MBP:Gβ are highlighted in yellow (elution fractions 8 to 16). (**C**) The eluted fractions were collected and concentrated (~90-fold). The same method was used to purify and concentrate 6xHis:MBP:Gβ (WT), 6xHis:MBP:Gβ^{L29F} (L29F) and 6xHis:MBP:Gβ^{L31F} (L31F). Concentrated proteins for each Gβ recombinant were separated via SDS-PAGE and stained with Coomassie blue as shown in **C**. Black arrow on right panel points to the upper single bands corresponding to the 6xHis:MBP:Gβ$^{WT/L29F/L31F}$ proteins. The gel displays high amount of contaminants in the three concentrated fractions. (**D**) Purified and concentrated 6xHis:MBP:Gβ from **C** was treated with 3C Protease to cleave the 6xHis:MBP tag. Proteins were separated via SDS-PAGE before (-) and after (+) 3C protease treatment. Proteins were loaded at their initial concentration (1:1, left panel) or diluted 10 times (1:10, right panel). Black asterisks show 6xHis:MBP:Gβ bands in untreated (-) condition. The band is not present in treated (+) condition. Red asterisk shows 6xHis:MBP band. Expected sizes: 6xHis:MBP:Gβ, 84 kDa; 6xHis:MBP, 43 kDa; Gβ, 41 kDa.

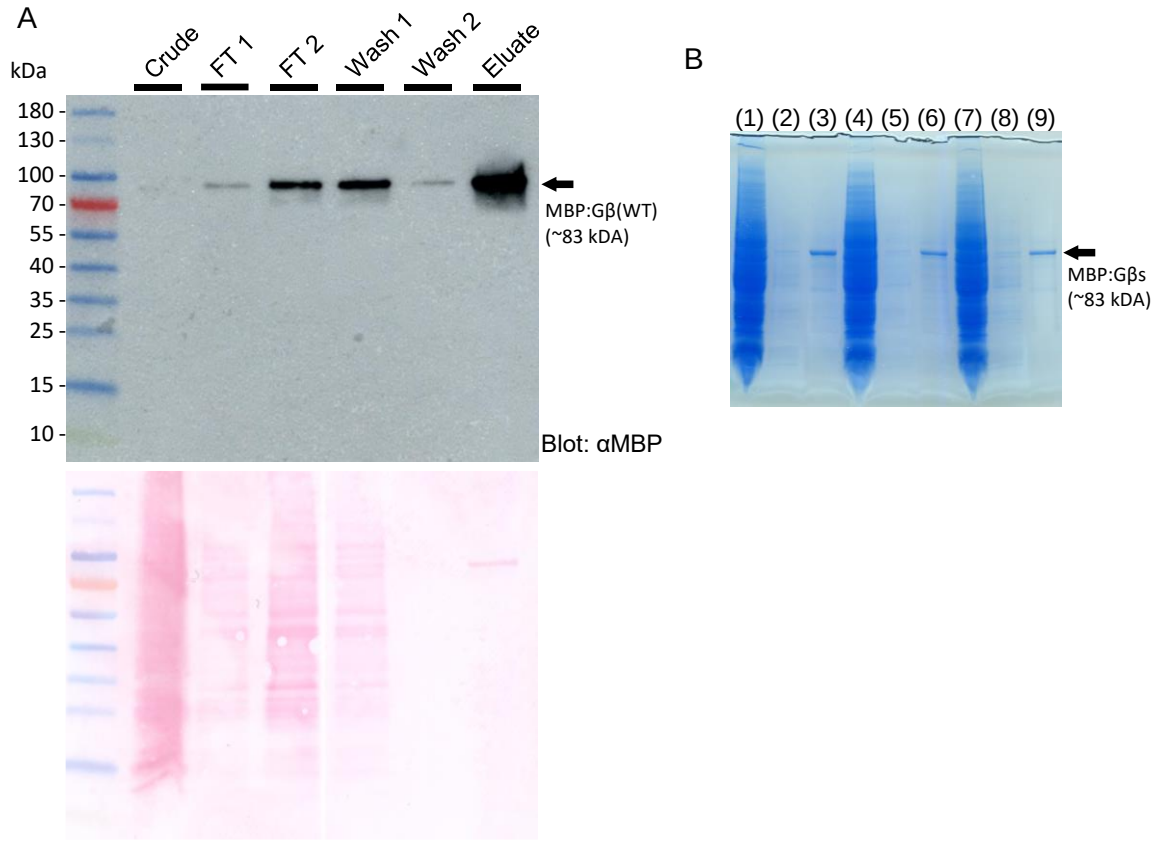

Figure 5.6 | Protein purification of MBP-tagged *Mt*Gβ in insect cells.
Sf9 insect cells expressing recombinant *Mt*Gβ protein fused to MBP (maltose-binding protein) tag at the N-terminus (MBP:Gβ) was grown 72 hours in 1-litre culture. Proteins were trapped in MBP-specific affinity column and eluted afterwards. (**A**) Detection by immunoblot of MBP:Gβ at different steps of the protein purification procedure. Crude, protein sample before purification; FT, flowthrough of proteins unbound to MBP-trap column; Wash, proteins washed from MBP-trap column after 1st and 2nd rinses with washing buffer; Eluate, MBP-tagged proteins eluted from the column. Immunostaining was done using αMBP antibody. Expected size of MBP:Gβ, 83 kDa (black arrow). Upper panel: immunoblot. Lower panel: ponceau staining. (**B**) Following the same method, MBP:Gβ (1)(2)(3), MBP:Gβ^{L29F} (4)(5)(6) and MBP:Gβ^{L31F} (7)(8)(9) proteins were purified and separated via SDS-PAGE. The gel was stained with blue Coomassie. (1)(4)(7), flowthrough of proteins unbound to MBP-trap columns; (2)(5)(8), washed proteins from the column after washing; (3)(6)(9), eluted proteins from the column with elution buffer. Black arrow points to the MBP:Gβs (83 kDa).

5.3 Discussion

In this chapter, the results demonstrate that *Mt*Gβ physically interacts with *Mt*AUK (Figure 5.2), which is involved in root endosymbiosis (Grubb et al., in preparation). *Mt*AUK localizes at the nuclear envelope and interacts with *Mt*DMI1 to regulate nuclear Ca^{2+} release. It is likely that *Mt*Gβ interacts with *Mt*AUK through several binding sites as truncated *Mt*AUKΔGβ showed reduced but not abolished physical interaction with *Mt*Gβ (Figure 5.2, B-C). This interaction is also consistent with the observed translocation of a pool of *Mt*Gβ upon application of a symbiotic elicitor (Chapter 4, Figure 4.4), and suggests that *Mt*Gβ transduces the symbiotic signal via *Mt*AUK to initiate nuclear Ca^{2+} oscillations. However,

the underlying mechanism is yet to be determined. It is possible that *Mt*Gβ influences *Mt*AUK kinase activity as it binds to *Mt*AUK kinase domain (Figure 5.2, A). Data also demonstrate that L29F and L31F mutations negatively influence this interaction as observed in yeast-two-hybrid (Figure 5.3, C). This will be confirmed *in vitro* via biolayer interferometry in future. To this aim, a protein purification protocol for *Mt*Gβ proteins has been developed (Figure 5.6). In mammals, amino acid substitution in the exact same region as L29 and L31 residues has similarly been shown to negatively influence Gβ binding to various interactors (Bonacci et al., 2005; Yuan et al., 2007; Brand et al., 2015). However, it remains to be confirmed whether $G\beta^{L29F}$ and $G\beta^{L31F}$ proteins are stably attached to the plasma membrane in native conditions and undergo correct trafficking from plasma membrane to the nucleus upon treatment with a symbiotic elicitor (Figure 5.4).

Production of Gβ proteins from insect cells was shown more suitable as the latter organism expresses endogenous heterotrimeric G proteins and can therefore perform most of the post-translational modifications (Schneider and Seifert, 2010). *Arabidopsis* Gβ purified from insect cells have been previously used for *in vitro* assays (Jones et al., 2011b). By contrast, bacteria do not possess endogenous heterotrimeric G proteins, even though plant Gα subunits can be successfully purified from *E. coli* cells (Urano et al., 2012b). But results showed that the latter system is rather unsuitable in regard to *Mt*Gβ (Figure 5.5).

Chapter VI

General Discussion

6.1 Heterotrimeric G protein β subunit: a new member of the common symbiosis pathway

The aim of this study was to characterize further the role of the heterotrimeric G protein β subunit (Gβ) in root endosymbiosis as it has been identified as a positive regulator of root nodule development in several legumes (Choudhury and Pandey, 2013; Bovin et al., 2022). In chapter 3, generation of *Gβ* knock-outs in *Agrobacterium*-mediated transformed roots using the CRISPR-CAS9 technology confirmed the role of *MtGβ* as a positive regulator of root nodule symbiosis and demonstrated further that *MtGβ* is essential for root nodule organogenesis. Besides, characterization of several TILLING mutants revealed a dual function of *MtGβ* in both arbuscular mycorrhizal (AM) and root nodule symbioses. AM and rhizobial entry are regulated by a common set of genes, referred to as the common symbiosis pathway (Parniske, 2008). The pathway is activated when symbiont-derived symbiotic elicitors are perceived and ultimately results in activation of nuclear calcium (Ca^{2+}) signalling essential to induce the expression of symbiosis genes. In chapter 4, *MtGβ* was shown to mediate nuclear Ca^{2+} signalling activation and be required for transcriptional reprograming of early endosymbiosis genes (*NIN* and *ENOD11*). Constitutive expression of different heterotrimeric G protein genes subtly induced root organogenesis in the same vein as other symbiosis genes (Schiessl et al., 2019; Soyano et al., 2019). Furthermore, *Mt*Gβ underwent nuclear relocalization after treatment with rhizobial-derived elicitors (Nod factors). This is in line with the identification in chapter 5 of a nuclear interactor, namely *Mt*AUK, which has also been characterised as essential for both AM and root nodule symbioses (Grubb et al., in preparation). Altogether, the results demonstrate that *Mt*Gβ is part of the common symbiosis pathway and constitutes the missing link between plasma membrane perception and ion channel activation at nuclear envelope. Future studies will help decipher the molecular mechanisms required for Gβ nuclear translocation on one hand, and those required for nuclear ion channel opening in concert with AUK on the other hand. Particularly, the development of a *Mt*Gβ native antibody would contribute in further characterizing the $G\beta^{L29F}$ and $G\beta^{L31F}$

mutants and assessing the effects of their mutation. Additionally, it would facilitate the study of the dynamics and subcellular accumulation of wild-type *Mt*Gβ before and after elicitation with a symbiotic elicitor.

6.2 The heterotrimeric G proteins constitute a hub for signal transduction

Heterotrimeric G proteins (hereafter referred to as G proteins) are key signal transducers of eukaryotic cells. This is exemplified in mammalian systems for which more than a third of human pharmaceutical drugs target G-protein-dependant signalling pathways (Hauser et al., 2018). In plants, G proteins are similarly involved in numerous signalling pathways, including developmental signalling such as seed germination, growth and cell division (reviewed in Perfus-Barbeoch et al., 2004), phytohormone response (reviewed in Jose and Roy Choudhury, 2020), ion channel opening (Wang et al., 2001; Fan et al., 2008; Jeon et al., 2019), light response (see references in Urano et al., 2012a), abiotic stress response (reviewed in Zhang et al., 2021), and plant innate immunity (reviewed in Zhong et al., 2019 and Zhang et al., 2021). The Gβ subunit actively participates in some of these pathways by direct binding to interactors (see table of some identified Gβ interactors listed in Pandey, 2019). It first raises the question of how a single protein can interact with so many interactors. This was questioned for example by Smrcka and Fisher (2019) in the mammalian system as its Gβ counterpart similarly binds to a large number of targets without a clear conservation of binding sequence among the interactors. Two key features of Gβs were highlighted. Firstly, Gβs are WD40 repeat proteins that form a seven-bladed β-propeller structure with a funnel-like shape. This structure enables them to bind to a wide range of protein targets. Secondly, Gβs are unique because they form a constitutive dimer with Gγ subunits through an amino-terminal α helix tail. This helical N-terminal tail is not present in other WD40 repeat proteins. Gγs are considerably more diverse than the Gβs, including in plants, and it is therefore commonly assumed that the Gγs allow for signal specificity in all eukaryotes even though the underlying mechanisms are not well understood. Crystal structures of the mammalian Gβγ complex, in association with various interactors, have revealed multiple binding sites on the Gβ structure. These sites can be found in different regions, ranging from the top of the funnel-like shape, which is conventionally considered the narrower part, to the side of the structure (see illustrations in Smrcka and Fisher, 2019). Besides, the N-terminal tail of Gβ has also

been identified via mutagenesis analysis as an integrant interacting domain of Gβ, essential for its binding activity to protein targets either in mammals (Bonacci et al., 2005; Yuan et al., 2007; Brand et al., 2015), yeast (Leeuw et al., 1998), or plants (Xu et al., 2017). The impairment of *Mt*Gβ-*Mt*AUK protein-protein interaction by L29F and L31F substitutions, as observed via yeast-two-hybrid in chapter 5, corroborates the role of Gβ N-terminus in mediating interaction with protein targets.

Given the wide range of G-protein-dependant signalling in plants, several regulatory mechanisms are necessary to fine-tune the signal outputs. These have been shown to involve receptor-like kinases, phosphorylation of G protein subunits, and RGS (regulator of G protein signalling) proteins. Differential translocation rates of Gβγ dimer were also shown to mediate the signal outcomes in the animal field. I would like to discuss here these elements and their putative function in regulating G protein signalling in the context of root endosymbiosis.

6.3 Regulating G proteins signal specificity

Plant G proteins comprise the canonical and non-canonical Gα, Gβ, and Gγ subunits. Gβγ dimer can form a heterotrimer complex with either the canonical or the non-canonical Gα (Temple and Jones, 2007; Chakravorty et al., 2015). Canonical Gα can bind to guanosine diphosphate (GDP) or guanosine triphosphate (GTP), and both GDP and GTP-bound forms exhibit specific physiological functions (Johnston et al., 2007; Jones et al., 2011b; Maruta et al., 2019). Non-canonical Gα, also referred to as extra-large G proteins (XLGs) in scientific publications, can bind GTP and function both redundantly and independently of canonical Gα proteins (Lee and Assmann, 1999; Heo et al., 2012; Pandey, 2019; Roy Choudhury et al., 2020). All G protein subunits participate in the different signalling pathways listed above at different degrees. However only the canonical Gα was shown to be involved in root nodule symbiosis (Choudhury and Pandey, 2013). The text below will therefore be mainly descriptive of the G protein heterocomplex comprising the canonical Gα (hereafter referred to as Gα). For clarity, the non-canonical Gα will not be mentioned unless specified otherwise.

6.3.1 Receptor-like kinases to discriminate the signals

It has been proposed that interaction with receptor-like kinases (RLKs) constitutes the primary activation mechanism of G protein signalling in plants (Pandey, 2020). RLKs

comprise over 600 members in *Arabidopsis* and 1000 in rice and regulate a myriad of biological responses (Gish and Clark, 2011). They harbour various extracellular domains allowing for detection of a wide range of signal ligands. Numerous RLK-dependant signalling have been linked to G protein signalling with evidence of direct interaction between G proteins and RLKs (see references in Pandey, 2019). In regard to Gβ, most studies were conducted in *Arabidopsis*. *At*Gβ was shown to interact with several RLKs including the brassinosteroid receptor BRI1 (brassinosteroid insensitive 1; Peng et al., 2018), the brassinosteroid and immunity co-receptor BAK1 (BRI1-associated receptor kinase 1; Peng et al., 2018), the negative regulator of immunity BIR1 (BAK1-interacting receptor-like kinase1; Tunc-Ozdemir and Jones, 2017), the receptor FER (FERONIA; Yu et al., 2018), and the CLAVATA receptor RPK2 (receptor-like protein kinase 2; Ishida et al., 2014). In some cases, the RLK-activated signals are partially or fully dependent on *AtGβ* which interacts with downstream effector proteins. This is exemplified in BRI1/BAK1 and FER-activated responses, in which their respective downstream effectors BES1 and OST1 were shown to interact with *At*Gβ (Yu et al., 2018; Zhang et al., 2018). However, the latter studies provided no direct evidence that these interactions were dependant on RLK activation, though this is greatly suggested. Therefore, there is no existing model of a signal transduction in plants where activated RLKs trigger Gβ binding to downstream effectors. That being said, it would be interesting to test whether the *Mt*Gβ-*Mt*AUK interaction reported in chapter 5 is dependent on *MtDMI2*.

On the other hand, the role of *At*Gβ in immunity RLK complexes rather aims at passively maintaining the canonical and non-canonical *At*Gα subunits in steady state as the latter are required to transduce immunity responses upon perception of plant defence elicitors in a RLK-dependent manner (Liang et al., 2016b; Liang et al., 2018; Xu et al., 2019). This is in contrast to root nodule symbiosis in legumes where Gα subunit is maintained deactivated (Choudhury and Pandey, 2015; Roy Choudhury and Pandey, 2022) while Gβ transduces the symbiosis signal as suggested in this work. In soybean, G proteins are regulated by two symbiosis RLKs: the Nod-factor receptor *Gm*NFR1α (ortholog of *Mt*LYK3/*Lj*NFR1) and the symbiosis co-receptor *Gm*SymRKα (ortholog of *Mt*DMI2/*Lj*SymRK) (Choudhury and Pandey, 2015; Roy Choudhury and Pandey, 2022). Of note, those two RLKs form a symbiosis complex with the Nod-factor receptor *Gm*NFR5α/*Mt*NFP/*Lj*NFR5 (Ried et al., 2014). *Gm*NFR1α and *Gm*SymRKα promote root nodule development via phosphorylation of *Gm*RGS2 and *Gm*Gα, respectively, resulting in deactivation of *Gm*Gα and release of free

*Gm*Gβγ (Choudhury and Pandey, 2015; Roy Choudhury and Pandey, 2022). Considering the function of *Mt*Gβ depicted in this work, it is likely that the *Medicago* symbiosis-related plasma membrane RLK complex functions similarly to its soybean counterpart in regulating G proteins during root nodule symbiosis. Nonetheless, one remaining question is how this scenario applies to AM symbiosis. Both AM and root nodule symbioses depend on the symbiosis co-receptor *Mt*DMI2/*Lj*SymRK (Endre et al., 2002; Stracke et al., 2002). Thus, G proteins could be similarly regulated during AM symbiosis through *Mt*DMI2/*Lj*SymRK (i.e., deactivation of Gα and release of Gβγ). Moreover, the *Medicago* and rice receptors *Mt*CERK1/*Os*CERK1 and *Mt*LYR4/*Os*MYR1 regulate (amongst other receptors) perception and colonization of AM in their respective species (Zhang et al., 2007; Bozsoki et al., 2017; Feng et al., 2019; Zhang et al., 2021a). Interestingly, rice transgenic plants co-expressing chimeric receptors consisting of *Mt*LYK3 and *Mt*NFP extracellular domains fused to *Os*CERK1 and *Os*MYR1 transmembrane and intracellular kinase domains, respectively, are capable to produce nuclear Ca^{2+} oscillations in response to rhizobia-derived Nod-factors (He et al., 2019). This has immense biological significance as rice species are unable to form endosymbiotic association with rhizobia nor to respond to Nod-factors in normal condition. Likewise, *Mtlyk3* and *Mtnfp* mutants in *Medicago*, which are unable to perform root nodule symbiosis due to the lack of Nod-factor receptor, can be fully complemented with the *Mt*LYK3-*Os*CERK1 and *Mt*NFP-*Os*MYR1 chimeric receptors, respectively (He et al., 2019). Taken together, these results demonstrate that the kinase domains of *Os*CERK1 and *Os*MYR1 have strictly identical function than those of Nod-factor receptors. Thus, it implies that the symbiosis RLKs regulating AM association could control G protein activity similarly to Nod-factor receptors, thereby leading to Gβ activation for transduction of symbiosis signal.

6.3.2 Phosphorylation of heterotrimeric G proteins

The limited number of G protein components (one Gα, one Gβ, and three and six Gγs in *Arabidopsis* and *Medicago*, respectively) does not correlate with the multiplicity of G-protein-mediated signalling events (Urano and Jones, 2014). Propagated signals from plant G proteins rely on different activator receptors as described above, but can also depend on various post-translational modifications of the G protein subunits such as phosphorylation. Plant Gαs, Gβs, and Gγs all harbour phosphorylation sites with diverse biological functions (reviewed in Oliveira et al., 2022). Fifteen phosphorylation sites have been identified on

Arabidopsis Gβ, both on its N-terminus and WD40 structure (Peng et al., 2018; Mergner et al., 2020). The brassinosteroid receptor BRI1 regulating sugar response was shown to phosphorylate *At*Gβ (Zhang et al., 2018). The BRI1-mediated phosphorylation is biologically relevant as phospho-dead and phospho-mimic *AtGβ* partially and fully complement the sugar response defect in *Atgβ* mutant, respectively. Interestingly, dissociation of *At*Gβ from *At*Gα during sugar response is dependent on *BRI1*, suggesting that *At*Gβ-*At*Gα dissociation is promoted through BRI1-mediated *At*Gβ phosphorylation. Given that Gβγ dimer is released from Gα during endosymbiosis (Roy Choudhury and Pandey, 2022), it is possible that Gβ and/or Gγs undergo post-translational modifications such as phosphorylation to fine-tune the signal output. Thus, it would be interesting to investigate if *Mt*Gβ integrates symbiosis-activated phosphorylation. This also applies to *Mt*Gγs as the latter can modulate Gβ activity. The interaction between Gβ/Gγs with symbiosis receptors have not been addressed to date. Other kinase proteins may also be involved. The *Lotus japonicus* NFR5-interacting cytoplasmic kinase 4 (*Lj*NiCK4) interestingly undergoes nuclear translocation 90 min after Nod-factor treatment similarly to *Mt*Gβ (Wong et al., 2019; chapter 4).

6.3.3 RGS proteins

Plant RGS (regulators of G protein signalling) are plasma membrane proteins with a predicted seven-transmembrane domain and a cytoplasmic C-terminal tail (Chen et al., 2003; Urano et al., 2012b). The tail harbours a GTPase-accelerating protein (GAP) domain that stimulates the GTP hydrolysis of Gα subunits and therefore promotes GDP-bound form of Gα (Chen et al., 2003; Jones et al., 2011b; Urano et al., 2012b). The characterization of RGS proteins provided a real breakthrough in the plant G protein signalling field as the latter exhibits major inconsistencies to the animal paradigm. Animal Gαs have a slow rate of nucleotide exchange (GDP release) and their activation rely on cell-surface receptors that promote GTP binding to Gα leading to dissociation of the heterotrimer (i.e., GTP-Gα dissociates from Gβγ dimer due to conformational change) (Sprang, 1997). The intrinsic GTP hydrolysis of Gα resets the system. For all metazoan and yeast Gα proteins, GDP-release is slower than GTP-hydrolysis, and thus the G protein is predominantly GDP-bound in its resting state. In contrast, plant Gαs rapidly release GDP without any stimulus, and the rate of GTP hydrolysis is in comparison >100-fold slower (Jones et al., 2011b; Urano et al., 2012b; Choudhury and Pandey, 2017). This implies that plant Gαs would be almost entirely GTP-

bound in a cell where GTP is in excess over GDP. Thus, GTP hydrolysis is the rate-limiting step in plant G proteins (Johnston et al., 2007; Urano et al., 2012b). The GAP activity of RGS proteins presumably maintains the G protein heterotrimer into a dynamic and self-repeating cycle, in which a Gα spontaneously associates with GTP and a RGS protein promotes its hydrolysis (Urano et al., 2012b; Urano et al., 2012c; Fu et al., 2014). Gβγ interaction with canonical and non-canonical Gαs is compromised in the absence of RGS (Liang et al., 2018), demonstrating it is essential for the maintenance of a heterotrimeric complex. Although Gβγ dimer cannot bind to Gα subunit in its GTP-bound conformation *in vitro* (Jones et al., 2011b), it was reported *in planta* to stay in close proximity of GTP-Gα in the absence of external stimuli (Adjobo-Hermans et al., 2006; Wang et al., 2008). GTP hydrolysis is nonetheless essential to maintain the formation of a heterotrimer. Indeed, when a constitutively active form of rice Gα (i.e., incapable of GTP hydrolysis) is expressed in a Gα-null background, it is predominately found in a free monomeric form (Kato et al., 2004). Accordingly, RGS-mediated self-repeating cycle of G proteins can be depicted as follows; Gβγ dimer binds to GDP-Gα, forming together an heterocomplex, or remains in close proximity of GTP-Gα until it switches back to its GDP-bound form through the RGS protein GAP activity. This dynamic equilibrium is presumably sustained as long as no stimuli are perceived. Additionally, it is worth noting that a relative proportion of Gα has been reported to remain in a free monomeric form in membrane fractions (Kato et al., 2004; Wang et al., 2008), suggesting that not all subunits are stabilised in their heterotrimeric conformation and/or spontaneous heterotrimeric dissociation frequently occurs .

Phosphorylation of the RGS C-terminal tail is a key modulator mechanism in G-protein-mediated signalling (Fu et al., 2014; Tunc-Ozdemir et al., 2017; Oliveira et al., 2022). Various phosphorylation patterns can be produced depending on the stimulus and the activated protein kinase, thereby modulating the signal specificity. In innate immunity response, three different RLKs have been shown to phosphorylate independently the RGS C-terminal with two distinct identified phosphorylation patterns leading to RGS endocytosis and/or dissociation from the heterotrimeric complex (Tunc-Ozdemir et al., 2016; Tunc-Ozdemir and Jones, 2017; Liang et al., 2018). In sugar response, three Ser/Thr kinases catalyse another phosphorylation pattern distinct from the two cited above that leads to RGS endocytosis (Urano et al., 2012c; Fu et al., 2014). A fourth RLK-mediated phosphorylation motif has been identified but the biological function has not yet been characterised (Tunc-Ozdemir et al., 2017). About 70% of the phosphorylated residues are highly conserved in

plant RGS (Oliveira et al., 2022), suggesting the different phosphorylation motifs are preserved between species.

The Nod-factor receptor *Gm*NFR1α phosphorylates *in vitro* *Gm*RGS2 (Choudhury and Pandey, 2015). A total of six phosphorylation sites were identified of which one is common to the innate immunity and sugar responses, namely the threonine residue 430 (*Medicago* numbering) that corresponds to the serine residue 428 in *Arabidopsis* (Tunc-Ozdemir et al., 2017; Liang et al., 2018), but the five other phosphorylation sites differ from those cited above. *Gm*NFR1α-mediated phosphorylation of *Gm*RGS2 does not lead to its endocytosis, nor to its dissociation from *Gm*Gα (Choudhury and Pandey, 2015; Pandey, 2020). Instead, phosphorylated *Gm*RGS2 has significantly greater GAP activity towards *Gm*Gαs, thereby accelerating the cycles of dissociation/association between *Gm*Gαs and *Gm*Gβγs (Choudhury and Pandey, 2015). Interestingly, constitutive expression of wild-type and phosphomimic *GmRGS2* in a *GmNFR1α*-null mutant background, leads to partial restoration of root nodule development, with phosphomimic *GmRGS2* displaying a greater efficiency (Choudhury and Pandey, 2015). Because the Nod-factor receptor NFR1 is required for symbiosis-activated nuclear Ca^{2+} signalling, it suggests that phosphomimic RGS in soybean promotes nuclear Ca^{2+} oscillation. *Medicago* RGS protein has conserved five of the six phosphorylation sites, namely the Thr-269, Ser-279, Ser-407, Thr-430, and Ser-439 residues (chapter 4). Replacement of those with aspartic acids resulted in spontaneous nuclear Ca^{2+} oscillations in *Medicago* root hairs (chapter 4). Because the present work suggests that Gβ transduces the symbiosis signal via nuclear translocation, this raises the question of how phosphomimic RGS protein would promote Gβγ dissociation and translocation to nuclei in root hairs.

Characterization of Gα, Gβ and Gγ subunits *in planta* on native gels demonstrated that the subunits are in large membrane-bound complexes ranging from 400 to 700 kDa, suggesting they are engaged amongst others with different membrane receptor complexes at basal level (Kato et al., 2004; Wang et al., 2008). Similarly, characterization of RGS protein endocytosis in sugar and immune responses indicated that two distinct pools of RGS proteins are natively engaged with their respective sugar and immune receptors at basal level (Watkins et al., 2021). Taken together, it is likely that RGS proteins and Gαβγ are in close proximity of the symbiosis receptors prior to ligand recognition. For clarity, *Mt*LYK3/*Lj*NFR1/*Gm*NFR1, *Mt*NFP/*Lj*NFR5/*Gm*NFR5 and *Mt*DMI2/*Lj*SymRK/

*Gm*SymRK will be in the next paragraph referred to as NFR1, NFR5 and SymRK, respectively.

In the absence of symbiotic elicitors, I speculate two scenarios (Figure 6.1, A-B): (i) the symbiosis RLK receptors and RGS/Gαβγ proteins form together a single membrane-bound complex which dismantles upon Gα nucleotide exchange (i.e., GDP-to-GTP switch) and a new pool is formed afterwards, or (ii) the whole complex is somewhat stable and RGS protein mediates a self-repeating cycle as depicted above, but Gα nucleotide exchange sets the G proteins in motion preventing their activation by the symbiosis RLK receptors. In both scenarios, recognition of symbiotic elicitor would activate the Nod-factor receptor NFR1 by an unknown mechanism, resulting in the phosphorylation of RGS protein. Phosphorylated RGS stabilizes Gα in GDP-bound form enabling its phosphorylation by the co-receptor SymRK. Gβγ dimer is consequently released and is shuttled to the nucleus either spontaneously or via an unknown mechanism. Hence, phosphomimic RGS would mimic activation by NFR1 and spontaneously promotes Gα phosphorylation by SymRK, leading to spontaneous activation of Gβγ. However, these scenarios assume that the different RLK receptors are in close proximity at basal level, but it should be considered that recognition of symbiotic elicitors is required for the formation of the symbiosis RLK complex. It has been reported that *Lj*SymRK and *Lj*NFR5 have strong binding affinity *in planta* (Antolín-Llovera et al., 2014). Besides, *Gm*NFR1α interacts *in planta* with *Gm*RGS1/2 and *Gm*Gα (Choudhury and Pandey, 2013; Choudhury and Pandey, 2015). One may speculate that two plasma membrane pools are formed comprising RGS/Gαβγ/NFR1 on one hand, NFR5/SymRK on the other (Figure 6.1, C). NFR1 constitutively phosphorylates RGS protein and promotes higher stabilization of the complex, but the absence of symbiotic elicitor prevents the recruitment of NFR5/SymRK. Extracellular symbiotic ligand promotes the formation of an RGS/Gαβγ/NFR1/NFR5/SymRK complex and allows for SymRK-mediated activation of the G proteins. In this scenario, phosphomimic RGS constitutively stabilizes the heterotrimeric complex at plasma membrane, independently of NFR1, allowing for spontaneous G protein activation whenever a SymRK protein is in the vicinity. In any case, it should be tested whether *SymRK* (*MtDMI2*) is required for *Mt*RGS^{PentaD}-activated spontaneous Ca^{2+} oscillations to assess if any of the above scenario is correct.

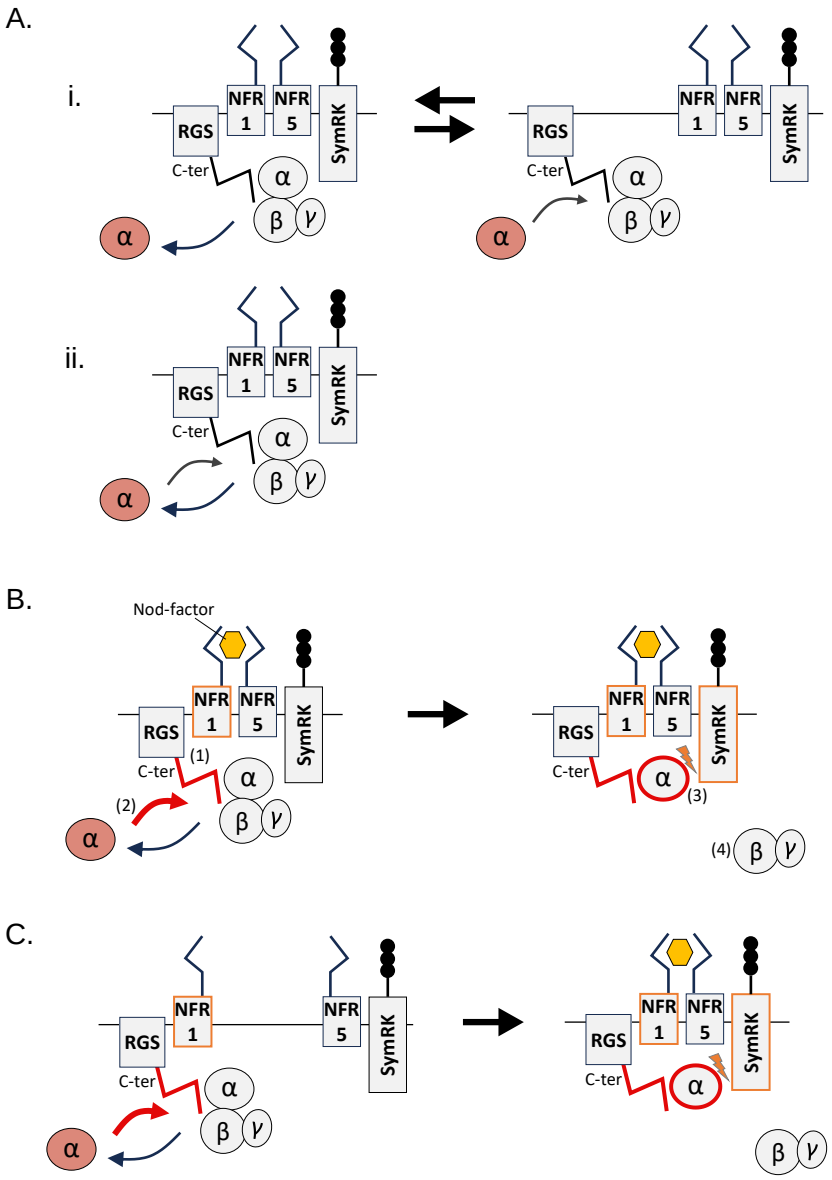

Figure 6.1 | Schematic models illustrating the proposed hypotheses of G protein signalling activation during endosymbiosis.

(**A**) The symbiosis RLK receptors NFR1, NFR5 and SymRK along with the G protein signalling complex comprising the GDP-Gα (in grey), Gβ, Gγ subunits and the RGS protein, together form a unique complex at the plasma membrane. In the absence of symbiotic elicitors, Gα nucleotide exchange (GTP-Gα in red) disrupts the complex. The GTPase-accelerating activity of the RGS C-terminal tail (C-ter) is too weak to maintain the current complex resulting in the formation of a new complex (i), or maintains a dissociation/association cycle of Gα to stabilize the complex but it is insufficient for Gα to be phosphorylated by SymRK (ii). (**B**) Upon recognition of Nod-factor, NFR1 phosphorylates the RGS C-terminal (red tail) (1), increasing the GTPase-accelerating activity of the RGS protein (2). This, in turn, enables SymRK to phosphorylate the Gα subunit (red outline) (3), and promotes the dissociation of the Gβγ dimer to transduce the symbiotic signal (4). (**C**) In this scenario, two complexes at the plasma membrane are present comprising RGS/Gαβγ/NFR1 on one hand, NFR5/SymRK on the other. NFR1 constitutively phosphorylates the RGS protein but the absence of symbiotic elicitor prevents the recruitment of NFR5/SymRK (left panel). Presence of extracellular Nod-factor promotes the formation of a unique complex (right panel), allowing for SymRK-mediated phosphorylation of Gα and release of the Gβγ dimer.

6.3.4 Different Gγs, different translocation kinetics

Mammalian Gβγ dimers can target downstream effectors at plasma membrane as well as at intracellular locations (Khan et al., 2016). Upon ligand perception at plasma membrane, Gβγ dimers can undergo plasma membrane dissociation and translocation to inner membranes at different kinetics depending on the Gγ subunit (Ajith Karunarathne et al., 2012; O'Neill et al., 2012). The twelve mammalian Gγ can be grouped into fast- (∼10 s), intermediate- (∼50 s), and slow (∼130 s)-translocating subunits. It was therefore suggested that the ability of Gβγ dimers to translocate at varying kinetics into intracellular regions following heterotrimer activation, may have important effects on downstream responses (O'Neill et al., 2012). Plasma-membrane-to-nucleus translocation of Gβ in a ligand-dependent manner has been evidenced in mammalian system (Bhatnagar et al., 2013), and it is likely that the different Gγ subunits affect differentially this response due to varying translocation kinetics amongst other regulatory mechanisms (i.e., differential binding affinity). Mammalian Gγ subunits are prenylated at their C-terminal with either a 15-carbon farnesyl or a 20-carbon geranylgeranyl depending on the C-terminal end motif (Wedegaertner et al., 1995). It has been evidenced that plasma membrane affinity of geranylgeranylated Gβγ subunits correlates with the translocation kinetics (O'Neill et al., 2012). Hydrophobic and positively charged residues next to the prenylation motif influence positively plasma membrane attachment, and therefore reduce translocation ability upon G protein activation.

Plant Gγ of group A are preferentially prenylated with a geranylgeranyl group, whereas group B and group C lack prenylation motifs but are predicted to be anchored at plasma membrane through an amphipathic α-helix (Adjobo-Hermans et al., 2006; Zeng et al., 2007; Trusov et al., 2012). To the best of my knowledge, plasma membrane affinities amongst plant Gγ subunits and groups have not been studied. But it is possible that this trait may coordinate G-protein-dependent responses in plants. In root nodule symbiosis, *Gm*Gγ group A and group B positively influence root nodule development, while group A is significantly more effective in that regard (Choudhury and Pandey, 2013). Thus, if group A and group B have different plasma membrane affinities it would shed light on the prerequisites for G-protein-mediated root endosymbiosis. If strong plasma membrane affinity is preferentially required, it would suggest that G proteins in steady state conformation is the rate-limiting step. Whereas low plasma membrane affinity would suggest that fast translocation is required for optimal transduction of the signal. Soybean and *Medicago* Gγs belonging to group A,

have only few hydrophobic and positively charged residues next to the prenylation motif, similarly to mammalian fast-translocating Gγs (data not shown). Nevertheless, it is difficult to speculate on their membrane binding affinity and/or translocation kinetics. Indeed, one Gγ in *Arabidopsis* from group A was shown to be S-acylated on a cysteine residue next to the prenylation motif, whereas the second *Arabidopsis* group A Gγ showed no S-acylation (Zeng et al., 2007). S-acylation would certainly increase membrane affinity. This cysteine residue is conserved in plant group A Gγs (Trusov et al., 2012), including in soybean and *Medicago*. It was postulated that S-acylation of this conserved cysteine residue may occur on some Gγs of group A (Trusov et al., 2012). Interestingly, the non-acylated *At*Gγ was localised in both plasma membrane and internal membranes in contrast to its acylated counterpart (Zeng et al., 2007), suggesting that S-acylation may coordinate differential cellular localization to optimize the location of the different pools of Gβγ. Furthermore, one may expect that some *Medicago* Gγ subunits translocate to the nucleus after Nod-factor application similarly to *Mt*Gβ (chapter 4). It would be interesting to test whether a particular group of Gγ translocates faster and whether it correlates to a greater positive effect. The latter experiment would inform whether translocation kinetic variation is a regulatory mechanism that has been conserved between plant and mammalian systems.

6.4 The role of mevalonate in root endosymbiosis

The *Medicago* 3-hydroxy-3-methyl-glutaryl-coenzyme A reductase1 (*Mt*HMGR1) has been identified via yeast-two-hybrid as a protein partner of *Mt*DMI2 (ortholog of *Lj*SymRK/*Gm*SymRKs) (Kevei et al., 2007). *Mt*HMGR1 is a key enzyme in the mevalonate biosynthetic pathway leading to the production of a diverse array of isoprenoid compounds. Interestingly, the use of the HMGR inhibitor lovastatin, that blocks the production of MVA and downstream compounds, significantly decreased number of root nodules and delayed nodulation (Kevei et al., 2007). The secondary metabolites derived from the mevalonate pathway comprise the geranylgeranyl- and farnesyl-pyrophosphate, which are the substrate for Gγ prenylation (Tennakoon et al., 2019). The use of lovastatin has been similarly used on mammalian cells to study the influence of mevalonate pathway inhibitors on Gβγ subcellular distribution (Tennakoon et al., 2019). Lovastatin impedes Gγ membrane anchoring through inhibition of Gγ prenylation. Likewise, Gβγ translocation to inner membranes following G protein activation was significantly impaired when cells were treated with a mevalonate

pathway inhibitor. Accordingly, pharmacological inhibition of nodulation with lovastatin corroborates the role of G proteins in root nodule symbiosis. Mevalonate has also been suggested to be a secondary messenger in the symbiosis pathway, as treatment with mevalonate is sufficient to induce Ca^{2+} oscillation dependently of the nuclear ion channel *Mt*DMI1 (Venkateshwaran et al., 2015). Interestingly, *Medicago*, *Lotus* and carrot but not *Arabidopsis* did respond to mevalonate, suggesting that the molecular machinery required for mevalonate-induced Ca^{2+} oscillations is only present in species capable of root endosymbiosis. I would like to emphasize here that the kinase domain of *AtSymRK* is not capable of supporting root nodulation in *Ljsymrk*-null mutant, in contrast to those of *LjSymRK*, *MtDMI2* and *OsSymRK* (Li et al., 2018). How mevalonate triggers cellular Ca^{2+} response in the absence of other stimuli remains however elusive. One possibility is that treatment with mevalonate leads to high accumulation of G proteins at plasma membrane in a sufficient proportion to be activated by DMI2/SymRK, as mevalonate was suggested to positively regulate the amount of G proteins at plasma membrane in mammalian cells (Chiloeches et al., 1997).

6.5 Future prospects

In conclusion, this work demonstrates the role of G proteins in the common signalling pathway controlling both AM and root nodule symbioses, and reveals the role of Gβ as the missing link between the Nod and Myc-factors receptors and the activation of nuclear Ca^{2+} oscillation. G proteins interact and are regulated by the Nod-factor receptor LYK3/NFR1 and co-receptor DMI2/SymRK (Choudhury and Pandey, 2015; Roy Choudhury and Pandey, 2022) and presumably by AM receptor in a similar fashion. I further discussed putative regulatory mechanisms that would result in Gβ nuclear translocation and transduction of the symbiosis signal. G protein signalling is also involved in plant innate immunity via RLK-dependent activation (reviewed in Zhong et al., 2019 and Zhang et al., 2021) and future analyses may shed light on how symbiosis and pathogen responses may affect each other in a G-protein-dependent manner. G proteins have been conserved in plants during evolution but some variations have occurred (Urano et al., 2012b). Understanding how G-protein-dependent endosymbioses are regulated in distant species including basal land plant would give some insights into the primary molecular mechanisms required for root endosymbiosis.

7. References

Adjobo-Hermans MJW, Goedhart J, Gadella TWJ (2006) Plant G protein heterotrimers require dual lipidation motifs of Gα and Gγ and do not dissociate upon activation. J Cell Sci **119**: 5087–5097

Ajith Karunarathne WK, O'Neill PR, Martinez-Espinosa PL, Kalyanaraman V, Gautam N (2012) All G protein βγ complexes are capable of translocation on receptor activation. Biochem Biophys Res Commun **421**: 605–611

Akiyama K, Matsuzaki K, Hayashi H (2005) Plant sesquiterpenes induce hyphal branching in arbuscular mycorrhizal fungi. Nature **435**: 824–827

Akiyama K, Ogasawara S, Ito S, Hayashi H (2010) Structural requirements of strigolactones for hyphal branching in AM fungi. Plant Cell Physiol **51**: 1104–1117

Andersen SU, Cvitanich C, Hougaard BK, Roussis A, Grønlund M, Jensen DB, Frøkjær LA, Jensen EØ (2003) The glucocorticoid-inducible GVG system causes severe growth defects in both root and shoot of the model legume Lotus japonicus. Mol Plant Microbe Interact **16**: 1069–1076

Anderson DJ, Botella JR (2007) Expression analysis and subcellular localization of the Arabidopsis thaliana G-protein β-subunit AGB1. Plant Cell Rep **26**: 1469–1480

Ané JM, Kiss GB, Riely BK, Penmetsa RV, Oldroyd GED, Ayax C, Lévy J, Debellé F, Baek JM, Kalo P, et al (2004) Medicago truncatula DMI1 Required for Bacterial and Fungal Symbioses in Legumes. Science (80-) **303**: 1364–1367

Antolín-Llovera M, Ried MK, Parniske M (2014) Cleavage of the SYMBIOSIS RECEPTOR-LIKE KINASE Ectodomain Promotes Complex Formation with Nod Factor Receptor 5. Curr Biol **24**: 422–427

Aoyama T, Chua NH (1997) A glucocorticoid-mediated transcriptional induction system in transgenic plants. Plant J **11**: 605–612

Ardourel M, Demont N, Debellé F, Maillet F, de Billy F, Promé JC, Dénarié J, Truchet G (1994) Rhizobium meliloti lipooligosaccharide nodulation factors: different structural requirements for bacterial entry into target root hair cells and induction of plant symbiotic developmental responses. Plant Cell **6**: 1357–1374

Arrighi J, Barre A, Ben Amor B, Bersoult A, Soriano L, Mirabella R, de Carvalho-Niebel F, Journet E, Ghérardi M, Huguet T, et al (2006) The Medicago truncatula Lysine Motif-Receptor-Like Kinase Gene Family Includes NFP and New Nodule-Expressed Genes. Plant Physiol **142**: 265–279

Bae S, Kweon J, Kim HS, Kim JS (2014) Microhomology-based choice of Cas9 nuclease target sites. Nat Methods 2014 117 **11**: 705–706

Barker DG, Bianchi S, Blondon F, Dattée Y, Duc G, Essad S, Flament P, Gallusci P, Génier G, Guy P, et al (1990) Medicago truncatula, a model plant for studying the molecular genetics of the Rhizobium-legume symbiosis. Plant Mol Biol Report **8**: 40–49

Behrendt M, Gruss F, Enzeroth R, Dembla S, Zhao S, Crassous PA, Mohr F, Nys M, Louros N, Gallardo R, et al (2020) The structural basis for an on-off switch controlling Gβγ-mediated inhibition of TRPM3 channels. Proc Natl Acad Sci U S A **117**: 29090–29100

Benedito VA, Torres-Jerez I, Murray JD, Andriankaja A, Allen S, Kakar K, Wandrey M, Verdier J, Zuber H, Ott T, et al (2008) A gene expression atlas of the model legume Medicago truncatula. Plant J **55**: 504–513

Berruti A, Lumini E, Balestrini R, Bianciotto V (2016) Arbuscular mycorrhizal fungi as natural biofertilizers: Let's benefit from past successes. Front Microbiol **6**: 1–13

Bhatnagar A, Unal H, Jagannathan R, Kaveti S, Duan ZH, Yong S, Vasanji A, Kinter M, Desnoyer R, Karnik SS (2013) Interaction of G-Protein βγ Complex with Chromatin Modulates GPCR-Dependent Gene Regulation. PLoS One **8**: e52689

Bhuvaneswari T V, Bhagwat2 AA, Bauer3 WD, Kettering CF, Evans WR, Kettering CF (1981) Transient Susceptibility of Root Cells in Four Common Legumes to Nodulation by Rhizobia. Plant Physiol **68**: 1144

Bidartondo MI, Read DJ, Trappe JM, Merckx V, Ligrone R, Duckett G, Supplement D, Duckett JG (2011) The dawn of symbiosis between plants and fungi. Biol Lett **7**: 574–577

Bonacci TM, Ghosh M, Malik S, Smrcka A V. (2005) Regulatory Interactions between the

Amino Terminus of G-protein βγ Subunits and the Catalytic Domain of Phospholipase Cβ2. J Biol Chem **280**: 10174–10181

Bovin AD, Pavlova OA, Dolgikh A V., Leppyanen I V., Dolgikh EA (2022) The Role of Heterotrimeric G-Protein Beta Subunits During Nodulation in Medicago truncatula Gaertn and Pisum sativum L. Front Plant Sci. doi: 10.3389/FPLS.2021.808573/FULL

Bozsoki Z, Cheng J, Feng F, Gysel K, Vinther M, Andersen KR, Oldroyd G, Blaise M, Radutoiu S, Stougaard J (2017) Receptor-mediated chitin perception in legume roots is functionally separable from Nod factor perception. Proc Natl Acad Sci U S A **114**: E8118–E8127

Brand CS, Sadana R, Malik S, Smrcka A V., Dessauer CW (2015) Adenylyl Cyclase 5 Regulation by Gβγ Involves Isoform-Specific Use of Multiple Interaction Sites. Mol Pharmacol **88**: 758–767

Breakspear A, Liu C, Roy S, Stacey N, Rogers C, Trick M, Morieri G, Mysore KS, Wen J, Oldroyd GED, et al (2015) The Root Hair "Infectome" of Medicago truncatula Uncovers Changes in Cell Cycle Genes and Reveals a Requirement for Auxin Signaling in Rhizobial Infection. Plant Cell **26**: 4680–4701

Broghammer A, Krusell L, Blaise M, Sauer J, Sullivan JT, Maolanon N, Vinther M, Lorentzen A, Madsen EB, Jensen KJ, et al (2012) Legume receptors perceive the rhizobial lipochitin oligosaccharide signal molecules by direct binding. Proc Natl Acad Sci U S A **109**: 13859–13864

van Brussel AAN, Bakhuizen R, Spronsen PC Van, Spaink HP, Tak T, Lugtenberg BJJ, Kijne JW (1992) Induction of Pre-Infection Thread Structures in the Leguminous Host Plant by Mitogenic Lipo-Oligosachharides of Rhizobium. Science (80-) **257**: 3–5

Buist G, Steen A, Kok J, Kuipers OP (2008) LysM, a widely distributed protein motif for binding to (peptido)glycans. Mol Microbiol **68**: 838–847

Capoen W, Sun J, Wysham D, Otegui MS, Venkateshwaran M, Hirsch S, Miwa H, Downie JA, Morris RJ, Ane J-M, et al (2011) Nuclear membranes control symbiotic calcium signaling of legumes. Proc Natl Acad Sci **108**: 14348–14353

Castel B, Tomlinson L, Locci F, Yang Y, Jones JDG (2019) Optimization of T-DNA architecture for Cas9-mediated mutagenesis in Arabidopsis. PLoS One **14**: e0204778

Catoira R, Galera C, De Billy F, Penmetsa R V., Journet EP, Maillet F, Rosenberg C, Cook D, Gough C, Denarie J (2000) Four genes of Medicago truncatula controlling components of a nod factor transduction pathway. Plant Cell **12**: 1647–1665

del Cerro P, Cook NM, Huisman R, Dangeville P, Grubb LE, Marchal C, Lam AHC, Charpentier M (2022) Engineered CaM2 modulates nuclear calcium oscillation and enhances legume root nodule symbiosis. Proc Natl Acad Sci U S A. doi: 10.1073/pnas.2200099119

Chakravorty D, Assmann SM (2018) G protein subunit phosphorylation as a regulatory mechanism in heterotrimeric G protein signaling in mammals, yeast, and plants. Biochem J **475**: 3331–3357

Chakravorty D, Gookin TE, Milner MJ, Yu Y, Assmann SM (2015) Extra-Large G Proteins Expand the Repertoire of Subunits in Arabidopsis Heterotrimeric G Protein Signaling. Plant Physiol **169**: 512–529

Charpentier M, Bredemeier R, Wanner G, Takeda N, Schleiff E, Parniske M (2008) Lotus japonicus CASTOR and POLLUX Are Ion Channels Essential for Perinuclear Calcium Spiking in Legume Root Endosymbiosis. Plant Cell Online **20**: 3467–3479

Charpentier M, Martins TV, Granqvist E, Oldroyd GED, Morris RJ (2013) The role of DMI1 in establishing Ca2+ oscillations in legume symbioses. Plant Signal Behav **8**: 2–5

Charpentier M, Sun J, Martins TV, Radhakrishnan G V, Findlay K, Soumpourou E, Thouin J, Véry A, Sanders D, Morris RJ, et al (2016) Nuclear-localized cyclic nucleotide–gated channels mediate symbiotic calcium oscillations. Science (80-) **352**: 1102–5

Charron D, Pingret JL, Chabaud M, Journet EP, Barker DG (2004) Pharmacological evidence that multiple phospholipid signaling pathways link rhizobium nodulation factor perception in Medicago truncatula root hairs to intracellular responses, including Ca2+ spiking and specific ENOD gene expression. Plant Physiol **136**: 3582–3593

Chen JG, Willard FS, Huang J, Liang J, Chasse SA, Jones AM, Siderovski DP (2003) A seven-transmembrane RGS protein that modulates plant cell proliferation. Science (80-) **301**: 1728–1731

Chen Y, Wang S, Du W, Wang Y, Wu Y, Li W, Ding Y, Wang Y (2022) G-protein couples MAPK cascade through maize heterotrimeric Gβ subunit. Plant Cell Rep **41**: 1763–1774

Chiloeches A, Usera F, Lasa M, Ropero S, Montes A, Toro MJ (1997) Effect of mevalonate availability on the association of G-protein α-subunits with the plasma membrane in GH4C1 cells. FEBS Lett **401**: 68–72

Chisari M, Saini DK, Cho JH, Kalyanaraman V, Gautam N (2009) G Protein Subunit Dissociation and Translocation Regulate Cellular Response to Receptor Stimulation. PLoS One **4**: e7797

Choi J, Summers W, Paszkowski U (2018) Mechanisms Underlying Establishment of Arbuscular Mycorrhizal Symbioses. Annu Rev Phytopathol Annu Rev Phytopathol **8**: 135–160

Choudhury SR, Bisht NC, Thompson R, Todorov O, Pandey S (2011) Conventional and novel gγ protein families constitute the heterotrimeric g-protein signaling network in soybean. PLoS One. doi: 10.1371/journal.pone.0023361

Choudhury SR, Pandey S (2013) Specific Subunits of Heterotrimeric G Proteins Play Important Roles during Nodulation in Soybean. Plant Physiol **162**: 522–533

Choudhury SR, Pandey S (2015) Phosphorylation-dependent regulation of G-protein Cycle during nodule formation in Soybean. Plant Cell **27**: 3260–3276

Choudhury SR, Pandey S (2017) Recently duplicated plant heterotrimeric Gα proteins with subtle biochemical differences influence specific outcomes of signal-response coupling. J Biol Chem **292**: 16188–16198

Choudhury SR, Westfall CS, Laborde JP, Bisht NC, Jez JM, Pandey S (2012) Two chimeric regulators of G-protein signaling (RGS) proteins differentially modulate soybean heterotrimeric G-protein cycle. J Biol Chem **287**: 17870–17881

Clarke VC, Loughlin PC, Day DA, Smith PMC (2014) Transport processes of the legume symbiosome membrane. **5**: 1–9

Cole GM, Reed SI (1991) Pheromone-induced phosphorylation of a G protein β subunit in S. cerevisiae is associated with an adaptive response to mating pheromone. Cell **64**: 703–716

Cordier C, Pozo MJ, Barea JM, Gianinazzi S, Gianinazzi-Pearson V (1998) Cell Defense Responses Associated with Localized and Systemic Resistance to Phytophthora parasitica Induced in Tomato by an Arbuscular Mycorrhizal Fungus. Mol Plant-Microbe Interact **11**: 1017–1028

Dascal N, Kahanovitch U (2015) The Roles of Gβγ and Gα in Gating and Regulation of GIRK Channels. Int Rev Neurobiol **123**: 27–85

Dazzo FB, Alfayate MC (2001) Novel infection process in the indeterminate root nodule symbiosis between Chamaecytisus proliferus (tagasaste) and Bradyrhizobium sp . New Phytol **150**: 707–721

Dénarié J, Debellé F, Promé J-C (1996) Rhizobium Lipo-Chitooligosaccharide Nodulation Factors: Signaling Molecules Mediating Recognition and Morphogenesis. Annu Rev Biochem **65**: 503–535

Ding L, Pandey S, Assmann SM (2008) Arabidopsis extra-large G proteins (XLGs) regulate root morphogenesis. Plant J **53**: 248–263

Ehrhardt DW, Wais R, Long SR (1996) Calcium spiking in plant root hairs responding to Rhizobium nodulation signals. Cell **85**: 673–681

Endre G, Kereszt A, Kevei Z, Mihacea S, Kaló P, Kiss G (2002) A receptor kinase gene regulating symbiotic nodule development. Nature **417**: 962–966

Engler C, Gruetzner R, Kandzia R, Marillonnet S (2009) Golden Gate Shuffling: A One-Pot DNA Shuffling Method Based on Type IIs Restriction Enzymes. PLoS One **4**: e5553

Engler C, Kandzia R, Marillonnet S (2008) A one pot, one step, precision cloning method with high throughput capability. PLoS One. doi: 10.1371/JOURNAL.PONE.0003647

Esseling JJ, Lhuissier FGP, Emons AMC (2003) Nod Factor-Induced Root Hair Curling : Continuous Polar Growth towards the Point of Nod Factor Application. Plant Physiol **132**: 1982–1988

Fan LM, Zhang W, Chen JG, Taylor JP, Jones AM, Assmann SM (2008) Abscisic acid regulation of guard-cell K+ and anion channels in Gβ- and RGS-deficient Arabidopsis lines. Proc Natl Acad Sci U S A **105**: 8476–8481

Feng F, Sun J, Radhakrishnan G V., Lee T, Bozsóki Z, Fort S, Gavrin A, Gysel K, Thygesen MB, Andersen KR, et al (2019) A combination of chitooligosaccharide and lipochitooligosaccharide recognition promotes arbuscular mycorrhizal associations in Medicago truncatula. Nat Commun 2019 101 **10**: 1–12

Fields S, Sternglanz R (1994) The two-hybrid system: an assay for protein-protein interactions. Trends Genet **10**: 286–292

Fu Y, Lim S, Urano D, Tunc-Ozdemir M, Phan NG, Elston TC, Jones AM (2014) Reciprocal encoding of signal intensity and duration in a glucose-sensing circuit. Cell **156**: 1084–1095

Gage DJ (2004) Infection and Invasion of Roots by Symbiotic , Nitrogen-Fixing Rhizobia during Nodulation of Temperate Legumes. Microbiol Mol Biol Rev **68**: 280–300

Genre A, Chabaud M, Balzergue C, Puech-pag V, Novero M, Rey T, Rochange S, Guillaume B, Bonfante P, Barker DG (2013) Short-chain chitin oligomers from arbuscular mycorrhizal fungi trigger nuclear Ca 2 + spiking in Medicago truncatula roots and their production is enhanced by strigolactone. 179–189

Genre A, Chabaud M, Faccio A, Barker DG, Bonfante P (2008) Prepenetration Apparatus Assembly Precedes and Predicts the Colonization Patterns of Arbuscular Mycorrhizal Fungi within the Root Cortex of Both Medicago truncatula and Daucus carota. Plant Cell Online **20**: 1407–1420

Genre A, Chabaud M, Timmers T, Bonfante P, Barker DG (2005) Arbuscular mycorrhizal fungi elicit a novel intracellular apparatus in Medicago truncatula root epidermal cells before infection. Plant Cell **17**: 3489–99

Genre A, Ivanov S, Fendrych M, Faccio A, Žárský V, Bisseling T, Bonfante P (2012) Multiple exocytotic markers accumulate at the sites of perifungal membrane biogenesis in arbuscular mycorrhizas. Plant Cell Physiol **53**: 244–255

Geurts R, Fedorova E, Bisseling T (2005) Nod factor signaling genes and their function in the early stages of Rhizobium infection. Curr Opin Plant Biol **8**: 346–352

Gietz RD, Woods RA (2002) Transformation of yeast by lithium acetate/single-stranded carrier DNA/polyethylene glycol method. Methods Enzymol **350**: 87–96

Giovannetti M, Mosse B (1980) an Evaluation of Techniques for Measuring Vesicular Arbuscular Mycorrhizal Infection in Roots. New Phytol **84**: 489–500

Gish LA, Clark SE (2011) The RLK/Pelle family of kinases. Plant J **66**: 117–127

Gomez-Roldan V, Fermas S, Brewer PB, Puech-Pagès V, Dun EA, Pillot JP, Letisse F, Matusova R, Danoun S, Portais JC, et al (2008) Strigolactone inhibition of shoot branching. Nature **455**: 189–194

Gomez SK, Javot H, Deewatthanawong P, Torres-Jerez I, Tang Y, Blancaflor EB, Udvardi MK, Harrison MJ (2009) Medicago truncatula and Glomus intraradices gene expression in cortical cells harboring arbuscules in the arbuscular mycorrhizal symbiosis. BMC Plant Biol. doi: 10.1186/1471-2229-9-10

González-Sama A, Lucas MM, De Felipe MR, Pueyo JJ (2004) An unusual infection mechanism and nodule morphogenesis in white lupin (Lupinus albus). New Phytol **163**: 371–380

Griesmann M, Chang Y, Liu X, Song Y, Haberer G, Crook MB, Billault-Penneteau B, Lauressergues D, Keller J, Imanishi L, et al (2018) Phylogenomics reveals multiple losses of nitrogen-fixing root nodule symbiosis. Science (80-). doi: 10.1126/science.aat1743

Groth M, Takeda N, Perry J, Uchida H, Draxl S, Brachmann A, Sato S, Tabata S, Kawaguchi M, Wang TL, et al (2010) NENA, a Lotus japonicus Homolog of Sec13, Is Required for Rhizodermal Infection by Arbuscular Mycorrhiza Fungi and Rhizobia but Dispensable for Cortical Endosymbiotic Development. Plant Cell **22**: 2509–2526

Gutjahr C&, Parniske M (2013) Cell and Developmental Biology of Arbuscular Mycorrhiza Symbiosis. Annu Rev Cell Dev Biol **29**: 593

Gutjahr C, Gobbato E, Choi J, Riemann M, Johnston MG, Summers W, Carbonnel S, Mansfield C, Yang SY, Nadal M, et al (2015) Rice perception of symbiotic arbuscular mycorrhizal fungi requires the karrikin receptor complex. Science (80-) **350**: 1521–1524

Harrison MJ (2002) A Phosphate Transporter from Medicago truncatula Involved in the Acquisition of Phosphate Released by Arbuscular Mycorrhizal Fungi. Plant Cell Online **14**: 2413–2429

Harrison MJ (1997) The Arbuscular Mycorrhizal Symbiosis. Plant-Microbe Interact 1–34

Hauser AS, Chavali S, Masuho I, Jahn LJ, Martemyanov KA, Gloriam DE, Babu MM (2018) Pharmacogenomics of GPCR Drug Targets. Cell **172**: 41-54.e19

He C, Holme J, Anthony J (2014) SNP genotyping: the KASP assay. Methods Mol Biol **1145**: 75–86

He J, Zhang C, Dai H, Liu H, Zhang X, Yang J, Chen X, Zhu Y, Wang D, Qi X, et al (2019) A LysM Receptor Heteromer Mediates Perception of Arbuscular Mycorrhizal Symbiotic Signal in Rice. Mol Plant **12**: 1561–1576

Heo JB, Sung S, Assmann SM (2012) Ca2+-dependent GTPase, Extra-large G Protein 2 (XLG2), Promotes Activation of DNA-binding Protein Related to Vernalization 1 (RTV1), Leading to Activation of Floral Integrator Genes and Early Flowering in Arabidopsis. J Biol Chem **287**: 8242–8253

Den Herder G, Yoshida S, Antolín-Llovera M, Ried MK, Parniske M (2012) Lotus japonicus E3 Ligase SEVEN IN ABSENTIA4 Destabilizes the Symbiosis Receptor-Like Kinase SYMRK and Negatively Regulates Rhizobial Infection . Plant Cell **24**: 1691–1707

Herrbach V, Remblière C, Gough C, Bensmihen S (2014) Lateral root formation and patterning in Medicago truncatula. J Plant Physiol **171**: 301–310

Indrasumunar A, Searle I, Lin MH, Kereszt A, Men A, Carroll BJ, Gresshoff PM (2011) Nodulation factor receptor kinase 1α controls nodule organ number in soybean (Glycine max L. Merr). Plant J **65**: 39–50

Ingraffia R, Amato G, Frenda AS, Giambalvo D (2019) Impacts of arbuscular mycorrhizal fungi on nutrient uptake, N 2 fixation, N transfer, and growth in a wheat/faba bean intercropping system. PLoS One **14**: 1–16

Iñiguez-Lluhi JA, Simon MI, Robishaw JD, Gilman AG (1992) G Protein βγ Subunits Synthesized in Sf9 cells. J Biol Chem. doi: 10.1016/S0021-9258(18)50106-X

Ishida T, Tabata R, Yamada M, Aida M, Mitsumasu K, Fujiwara M, Yamaguchi K, Shigenobu S, Higuchi M, Tsuji H, et al (2014) Heterotrimeric G proteins control stem cell proliferation through CLAVATA signaling in Arabidopsis. EMBO Rep **15**: 1202–1209

Javot H, Penmetsa R V., Terzaghi N, Cook DR, Harrison MJ (2007) A Medicago truncatula phosphate transporter indispensable for the arbuscular mycorrhizal symbiosis. Proc Natl Acad Sci **104**: 1720–1725

Jeon BW, Acharya BR, Assmann SM (2019) The Arabidopsis heterotrimeric G-protein β subunit, AGB1, is required for guard cell calcium sensing and calcium-induced calcium release. Plant J **99**: 231–244

Jin Y, Chen Z, Yang J, Mysore KS, Wen J, Huang J, Yu N, Wang E (2018a) IPD3 and IPD3L Function Redundantly in Rhizobial and Mycorrhizal Symbioses. Front Plant Sci. doi: 10.3389/fpls.2018.00267

Jin Y, Chen Z, Yang J, Mysore KS, Wen J, Huang J, Yu N, Wang E (2018b) IPD3 and IPD3L Function Redundantly in Rhizobial and Mycorrhizal Symbioses. Front Plant Sci **9**: 1–12

Johnston CA, Taylor JP, Gao Y, Kimple AJ, Grigston JC, Chen JG, Siderovski DP, Jones AM, Willard FS (2007) GTPase acceleration as the rate-limiting step in Arabidopsis G protein-coupled sugar signaling. Proc Natl Acad Sci U S A **104**: 17317–17322

Jones DT, Taylor WR, Thornton JM (1992) The rapid generation of mutation data matrices from protein sequences. Comput Appl Biosci **8**: 275–282

Jones JC, Duffy JW, Machius M, Temple BRS, Dohlman HG, Jones AM (2011a) The crystal structure of a self-activating g protein α subunit reveals its distinct mechanism of signal initiation. Sci Signal **4**: 1–8

Jones JC, Jones AM, Temple BRS, Dohlman HG (2012) Differences in intradomain and interdomain motion confer distinct activation properties to structurally similar Gα proteins. Proc Natl Acad Sci U S A **109**: 7275–7279

Jones JC, Temple BRS, Jones AM, Dohlman HG (2011b) Functional reconstitution of an atypical G protein heterotrimer and regulator of G protein signaling protein (RGS1) from arabidopsis thaliana. J Biol Chem **286**: 13143–13150

Jose J, Roy Choudhury S (2020) Heterotrimeric G-proteins mediated hormonal responses in plants. Cell Signal. doi: 10.1016/J.CELLSIG.2020.109799

Kanamori N, Madsen LH, Radutoiu S, Frantescu M, Quistgaard EMH, Miwa H, Downie JA, James EK, Felle HH, Haaning LL, et al (2006) A nucleoporin is required for induction of Ca2+ spiking in legume nodule development and essential for rhizobial and fungal symbiosis. Proc Natl Acad Sci **103**: 359–364

Kang HG, Fang Y, Singh KB (1999) A glucocorticoid-inducible transcription system causes severe growth defects in Arabidopsis and induces defense-related genes. Plant J **20**: 127–133

Kato C, Mizutani T, Tamaki H, Kumagai H, Kamiya T, Hirobe A, Fujisawa Y, Kato H, Iwasaki Y (2004) Characterization of heterotrimeric G protein complexes in rice plasma membrane. Plant J **38**: 320–331

Kelner A, Leitão N, Chabaud M, Charpentier M, de Carvalho-Niebel F (2018) Dual Color Sensors for Simultaneous Analysis of Calcium Signal Dynamics in the Nuclear and Cytoplasmic Compartments of Plant Cells. Front Plant Sci **9**: 1–14

Kevei Z, Lougnon G, Mergaert P, Horvath G V, Kereszt A, Jayaraman D, Zaman N, Marcel F, Regulski K, Kiss GB, et al (2007) 3-hydroxy-3-methylglutaryl coenzyme A reductase1 interacts with NORK and is crucial for nodulation in Medicago truncatula. Plant Cell **19**: 3974–3989

Khan SM, Sung JY, Hébert TE (2016) Gβγ subunits—Different spaces, different faces. Pharmacol Res **111**: 434–441

Khater M, Wei Z, Xu X, Huang W, Lokeshwar BL, Lambert NA, Wu G (2021) G protein βγ translocation to the Golgi apparatus activates MAPK via p110γ-p101 heterodimers. J Biol Chem **296**: 100325

Kim GB, Nam YW (2013) Isolation and Characterization of Medicago truncatula U6 Promoters for the Construction of Small Hairpin RNA-Mediated Gene Silencing Vectors. Plant Mol Biol Report **31**: 581–593

Kim S, Zeng W, Bernard S, Liao J, Venkateshwaran M, Ane JM, Jiang Y (2019) Ca2+-regulated Ca2+ channels with an RCK gating ring control plant symbiotic associations. Nat Commun 2019 101 **10**: 1–12

Kobayashi S, Tsugama D, Liu S, Takano T (2012) A U-Box E3 Ubiquitin Ligase, PUB20, Interacts with the Arabidopsis G-Protein β Subunit, AGB1. PLoS One **7**: e49207

Kosuta S, Hazledine S, Sun J, Miwa H, Morris RJ, Downie JA, Oldroyd GED (2008) Differential and chaotic calcium signatures in the symbiosis signaling pathway of legumes. Proc Natl Acad Sci U S A **105**: 9823–9828

Krebs M, Held K, Binder A, Hashimoto K, Den Herder G, Parniske M, Kudla J, Schumacher K (2012) FRET-based genetically encoded sensors allow high-resolution live cell imaging of Ca^{2+} dynamics. Plant J **69**: 181–192

Kretzschmar T, Kohlen W, Sasse J, Borghi L, Schlegel M, Bachelier JB, Reinhardt D, Bours R, Bouwmeester HJ, Martinoia E (2012) A petunia ABC protein controls strigolactone-dependent symbiotic signalling and branching. Nature **483**: 341–344

Labuhn M, Adams FF, Ng M, Knoess S, Schambach A, Charpentier EM, Schwarzer A, Mateo JL, Klusmann JH, Heckl D (2018) Refined sgRNA efficacy prediction improves large- and small-scale CRISPR-Cas9 applications. Nucleic Acids Res **46**: 1375–1385

Lambright DG, Sondek J, Bohm A, Skiba NP, Hamm HE, Sigler PB (1996) The 2.0 Å crystal structure of a heterotrimeric G protein. Nat 1996 3796563 **379**: 311–319

Lee E, Eo J, Ka K, Eom A (2013) Diversity of Arbuscular Mycorrhizal Fungi and Their Roles in Ecosystems. Mycobiology **41(3)**: 121–125

Lee YRJ, Assmann SM (1999) Arabidopsis thaliana 'extra-large GTP-binding protein' (AtXLG1): a new class of G-protein. Plant Mol Biol 1999 401 **40**: 55–64

Leeuw T, Wu C, Schrag JD, Whiteway M, Thomas DY, Leberer E (1998) Interaction of a G-protein β-subunit with a conserved sequence in Ste20/PAK family protein kinases. Nat 1998 3916663 **391**: 191–195

Lengger B, Jensen MK (2020) Engineering G protein-coupled receptor signalling in yeast for biotechnological and medical purposes. FEMS Yeast Res **20**: 87

Levy J, Bres C, Geurts R, Chalhoub B, Kulikova O, Journet E, Ane J-M, Lauber E,

Bisseling T, Denarie J, et al (2004) A Putative Ca2+ and Calmodulin-Dependent Protein Kinase Required for Bacterial and Fungal Symbioses. Science (80-) **303**: 1361–1364

Li H, Chen M, Duan L, Zhang T, Cao Y, Zhang Z (2018) Domain swap approach reveals the critical roles of different domains of symrk in root nodule symbiosis in lotus japonicus. Front Plant Sci **9**: 697

Liang G, Zhang H, Lou D, Yu D (2016a) Selection of highly efficient sgRNAs for CRISPR/Cas9-based plant genome editing. Sci Reports 2016 61 **6**: 1–8

Liang X, Ding P, Lian K, Wang J, Ma M, Li L, Li L, Li M, Zhang X, Chen S, et al (2016b) Arabidopsis heterotrimeric G proteins regulate immunity by directly coupling to the FLS2 receptor. Elife. doi: 10.7554/ELIFE.13568

Liang X, Ma M, Zhou Z, Wang J, Yang X, Rao S, Bi G, Li L, Zhang X, Chai J, et al (2018) Ligand-triggered de-repression of Arabidopsis heterotrimeric G proteins coupled to immune receptor kinases. Cell Res **28**: 529–543

Limpens E, Franken C, Smit P, Willemse J, Bisseling T, Geurts R (2003) LysM Domain Receptor Kinases Regulating Rhizobial Nod Factor-Induced Infection. Science (80-) **302**: 630–633

Liu H, Ding Y, Zhou Y, Jin W, Xie K, Chen LL (2017) CRISPR-P 2.0: An Improved CRISPR-Cas9 Tool for Genome Editing in Plants. Mol Plant **10**: 530–532

Liu H, Lin JS, Luo Z, Sun J, Huang X, Yang Y, Xu J, Wang YF, Zhang P, Oldroyd GED, et al (2022) Constitutive activation of a nuclear-localized calcium channel complex in Medicago truncatula. Proc Natl Acad Sci U S A. doi: 10.1073/pnas.2205920119

Liu Q, Han R, Wu K, Zhang J, Ye Y, Wang S, Chen J, Pan Y, Li Q, Xu X, et al (2018) G-protein βγ subunits determine grain size through interaction with MADS-domain transcription factors in rice. Nat Commun **9**: 1–12

Liu S, Yoder JI (2016) Chemical induction of hairpin RNAi molecules to silence vital genes in plant roots. Sci Rep **6**: 1–11

Lodwig E, Poole P (2003) Metabolism of Rhizobium bacteroids. CRC Crit Rev Plant Sci **22**: 37–78

Ma X, Zhang Q, Zhu Q, Liu W, Chen Y, Qiu R, Wang B, Yang Z, Li H, Lin Y, et al (2015) A Robust CRISPR/Cas9 System for Convenient, High-Efficiency Multiplex Genome Editing in Monocot and Dicot Plants. Mol Plant **8**: 1274–1284

Madsen EB, Antolín-Llovera M, Grossmann C, Ye J, Vieweg S, Broghammer A, Krusell L, Radutoiu S, Jensen ON, Stougaard J, et al (2011) Autophosphorylation is essential for the in vivo function of the Lotus japonicus Nod factor receptor 1 and receptor-mediated signalling in cooperation with Nod factor receptor 5. Plant J **65**: 404–417

Madsen EB, Madsen LH, Radutoiu S, Olbryt M, Rakwalska M, Szczyglowski K, Sato S, Kaneko T, Tabata S, Sandal N, et al (2003) A receptor kinase gene of the LysM type is involved in legume perception of rhizobial signals. Nature **425**: 637–640

Maillet F, Poinsot V, André O, Puech-Pagés V, Haouy A, Gueunier M, Cromer L, Giraudet D, Formey D, Niebel A, et al (2011) Fungal lipochitooligosaccharide symbiotic signals in arbuscular mycorrhiza. Nature **469**: 58–64

Malik S, De Rubio RG, Trembley M, Irannejad R, Wedegaertner PB, Smrcka A V. (2015) G protein βγ subunits regulate cardiomyocyte hypertrophy through a perinuclear Golgi phosphatidylinositol 4-phosphate hydrolysis pathway. Mol Biol Cell **26**: 1188–1198

Marrari Y, Crouthamel M, Irannejad R, Wedegaertner PB (2007) Assembly and trafficking of heterotrimeric G proteins. Biochemistry **46**: 7665–7677

Marsh JF, Rakocevic A, Mitra RM, Brocard L, Sun J, Eschstruth A, Long SR, Schultze M, Ratet P, Oldroyd GED (2007) Medicago truncatula NIN Is Essential for Rhizobial-Independent Nodule Organogenesis Induced by Autoactive Calcium/Calmodulin-Dependent Protein Kinase. Plant Physiol **144**: 324

Maruta N, Trusov Y, Chakravorty D, Urano D, Assmann SM, Botella JR (2019) Nucleotide exchange–dependent and nucleotide exchange–independent functions of plant heterotrimeric GTP-binding proteins. Sci Signal **12**: 9526

Matiolli CC, Melotto M (2018) A comprehensive arabidopsis yeast two-hybrid library for protein-protein interaction studies: A resource to the plant research community. Mol Plant-Microbe Interact **31**: 899–902

McCarty NS, Graham AE, Studená L, Ledesma-Amaro R (2020) Multiplexed CRISPR technologies for gene editing and transcriptional regulation. Nat Commun 2020 111 **11**: 1–13

McCudden CR, Hains MD, Kimple RJ, Siderovski DP, Willard FS (2005) G-protein signaling: Back to the future. Cell Mol Life Sci **62**: 551–577

Mergner J, Frejno M, List M, Papacek M, Chen X, Chaudhary A, Samaras P, Richter S, Shikata H, Messerer M, et al (2020) Mass-spectrometry-based draft of the Arabidopsis proteome. Nat 2020 5797799 **579**: 409–414

Messinese E, Mun J-H, Yeun LH, Jayaraman D, Rougé P, Barre A, Lougnon G, Schornack S, Bono J-J, Cook DR, et al (2007) A novel nuclear protein interacts with the symbiotic DMI3 calcium- and calmodulin-dependent protein kinase of Medicago truncatula. Mol Plant-Microbe Interact **20**: 912–21

Mitra RM, Gleason CA, Edwards A, Hadfield J, Downie JA, Oldroyd GED, Long SR (2004) A Ca2+/calmodulin-dependent protein kinase required for symbiotic nodule development: Gene identification by transcript-based cloning. Proc Natl Acad Sci **101**: 4701–4705

Miyahara A, Richens J, Starker C, Morieri G, Smith L, Long S, Downie JA, Oldroyd GED (2010) Conservation in Function of a SCAR / WAVE Component During Infection Thread and Root Hair Growth in Medicago truncatula. **23**: 1553–1562

Miyata K, Kozaki T, Kouzai Y, Ozawa K, Ishii K, Asamizu E, Okabe Y, Umehara Y, Miyamoto A, Kobae Y, et al (2014) The bifunctional plant receptor, OsCERK1, regulates both chitin-triggered immunity and arbuscular mycorrhizal symbiosis in rice. Plant Cell Physiol **55**: 1864–1872

Miyawaki A, Llopis J, Heim R, Michael McCaffery J, Adams JA, Ikura M, Tsien RY (1997) Fluorescent indicators for Ca2+based on green fluorescent proteins and calmodulin. Nat 1997 3886645 **388**: 882–887

Moling S, Pietraszewska-Bogiel A, Postma M, Fedorova E, Hink MA, Limpens E, Gadell TWJ, Bisseling T (2014) Nod Factor Receptors Form Heteromeric Complexes and Are Essential for Intracellular Infection in Medicago Nodules. Plant Cell **26**: 4188–4199

Morieri G, Martinez EA, Jarynowski A, Driguez H, Morris R, Oldroyd GED, Downie JA (2013) Host-specific Nod-factors associated with Medicago truncatula nodule infection differentially induce calcium influx and calcium spiking in root hairs. New Phytol **200**: 656–662

Mulder L, Lefebvre B, Cullimore J, Imberty A (2006) LysM domains of Medicago truncatula NFP protein involved in Nod factor perception. Glycosylation state, molecular modeling and docking of chitooligosaccharides and Nod factors. Glycobiology **16**: 801–809

Nagai T, Ibata K, Park ES, Kubota M, Mikoshiba K, Miyawaki A (2002) A variant of yellow fluorescent protein with fast and efficient maturation for cell-biological applications. Nat Biotechnol 2002 201 **20**: 87–90

Nagai T, Yamada S, Tominaga T, Ichikawa M, Miyawaki A (2004) Expanded dynamic range of fluorescent indicators for Ca2+ by circularly permuted yellow fluorescent proteins. Proc Natl Acad Sci U S A **101**: 10554–10559

Nakai J, Ohkura M, Imoto K (2001) A high signal-to-noise Ca(2+) probe composed of a single green fluorescent protein. Nat Biotechnol **19**: 137–141

Nakmee PS, Techapinyawat S, Ngamprasit S (2016) Comparative potentials of native arbuscular mycorrhizal fungi to improve nutrient uptake and biomass of Sorghum bicolor Linn. Agric Nat Resour **50**: 173–178

Newman-Griffis AH, del Cerro P, Charpentier M, Meier I (2019) Medicago LINC Complexes Function in Nuclear Morphology , Nuclear Movement , and Root Nodule Symbiosis. Plant Physiol **179**: 491–506

Nutman PS (1959) Some observations on root-hair infection by nodule bacteria. J Exp Bot **10**: 250–263

O'Neill PR, Karunarathne WKA, Kalyanaraman V, Silvius JR, Gautama N (2012) G-protein signaling leverages subunit-dependent membrane affinity to differentially control βγ translocation to intracellular membranes. Proc Natl Acad Sci U S A **109**: E3568–E3577

Offermanns S (2003) G-proteins as transducers in transmembrane signalling. Prog Biophys Mol Biol **83**: 101–130

Oldroyd GED (2013) Speak, friend, and enter: Signalling systems that promote beneficial symbiotic associations in plants. Nat Rev Microbiol **11**: 252–263

Oldroyd GED, Downie JA (2008) Coordinating Nodule Morphogenesis with Rhizobial Infection in Legumes. Annu Rev Plant Biol **59**: 519–546

Oldroyd GED, Murray JD, Poole PS, Downie JA (2011) The Rules of Engagement in the Legume-Rhizobial Symbiosis. Annu Rev Genet **45**: 119–144

Oliveira CC;, Jones AM;, Fontes EPB;, Reis PABD, Oliveira CC, Jones AM, Pacheco E, Fontes B, Braga Dos Reis PA (2022) G-Protein Phosphorylation: Aspects of Binding Specificity and Function in the Plant Kingdom. Int J Mol Sci 2022, Vol 23, Page 6544 **23**: 6544

Ott T, Van Dongen JT, Günther C, Krusell L, Desbrosses G, Vigeolas H, Bock V, Czechowski T, Geigenberger P, Udvardi MK (2005) Symbiotic leghemoglobins are crucial for nitrogen fixation in legume root nodules but not for general plant growth and development. Curr Biol **15**: 531–535

Ouwerkerk PB, De Kam RJ, Hoge HJ, Meijer AH (2001) Glucocorticoid-inducible gene expression in rice. Planta **213**: 370–378

Pandey S (2020) Plant receptor-like kinase signaling through heterotrimeric G-proteins. J Exp Bot **71**: 1742–1751

Pandey S (2019) Heterotrimeric G-Protein Signaling in Plants: Conserved and Novel Mechanisms. Annu Rev Plant Biol **70**: 213–238

Pandey S, Vijayakumar A (2018) Emerging themes in heterotrimeric G-protein signaling in plants. Plant Sci **270**: 292–300

Pandey S, Wang RS, Wilson L, Li S, Zhao Z, Gookin TE, Assmann SM, Albert R (2010) Boolean modeling of transcriptome data reveals novel modes of heterotrimeric G-protein action. Mol Syst Biol **6**: 1–17

Parniske M (2008) Arbuscular mycorrhiza: The mother of plant root endosymbioses. Nat Rev Microbiol **6**: 763–775

Peix A, Ramírez-Bahena MH, Velázquez E, Bedmar EJ (2015) Bacterial Associations with Legumes. CRC Crit Rev Plant Sci **34**: 17–42

Peng Y, Chen L, Li S, Zhang Y, Xu R, Liu Z, Liu W, Kong J, Huang X, Wang Y, et al (2018) BRI1 and BAK1 interact with G proteins and regulate sugar-responsive growth and development in Arabidopsis. Nat Commun 2018 91 **9**: 1–13

Penmetsa RV, Cook DR (1997) A Legume Ethylene-Insensitive Mutant Hyperinfected by Its Rhizobial Symbiont. Science **275**: 527–530

Perfus-Barbeoch L, Jones AM, Assmann SM (2004) Plant heterotrimeric G protein function: insights from Arabidopsis and rice mutants. Curr Opin Plant Biol **7**: 719–731

Peškan T, Oelmüller R (2000) Heterotrimeric G-protein β-subunit is localized in the plasma membrane and nuclei of tobacco leaves. Plant Mol Biol **42**: 915–922

Pfaffl MW (2001) A new mathematical model for relative quantification in real-time RT-PCR. Nucleic Acids Res **29**: E45

Pirozynski KA, Malloch DW (1975) The origin of land plants: A matter of mycotrophism. Biosystems **6**: 153–164

Radutoiu S, Madsen LH, Madsen EB, Felle HH, Umehara Y, GrÃ¸nlund M, Sato S, Nakamura Y, Tabata S, Sandal N, et al (2003) Plant recognition of symbiotic bacteria requires two LysM receptor-like kinases. Nature **425**: 585–592

Redecker D, Kodner R, Graham LE (2000) Glomalean Fungi from the Ordovician. **289**: 1920–1922

Remigi P, Zhu J, Young JPW, Masson-Boivin C (2016) Symbiosis within Symbiosis: Evolving Nitrogen-Fixing Legume Symbionts. Trends Microbiol **24**: 63–75

Remy W, Taylor TN, Hass H, & Kerp H (1994) Four hundred-million-year-old vesicular arbuscular mycorrhizae. Proc Natl Acad Sci U S A **91**: 11841–11843

Ren X, Yang Z, Xu J, Sun J, Mao D, Hu Y, Yang SJ, Qiao HH, Wang X, Hu Q, et al (2014) Enhanced specificity and efficiency of the CRISPR/Cas9 system with optimized sgRNA parameters in Drosophila. Cell Rep **9**: 1151–1162

Reynolds CR, Islam SA, Sternberg MJE (2018) EzMol: A Web Server Wizard for the Rapid Visualization and Image Production of Protein and Nucleic Acid Structures. J Mol Biol **430**:

2244–2248

Ridge RW, Rolfe BG (1985) Rhizobium Degradation of Legume Root Hair Cell Wall at the Site of Infection Thread Origin. Appl Environ Microbiol **50**: 717–720

Ried MK, Antolin-Llovera M, Parniske M (2014) Spontaneous symbiotic reprogramming of plant roots triggered by receptor-like kinases. Elife **3**: 1–17

Roche P, Debelle F, Maillet F, Lerouge P, Faucher C, Truchet G (1991) Molecular Basis of Symbiotic Host Specificity in Rhizobium meliloti : nodH and nodPQ Genes Encode the Sulfation of Lipo-Oligosaccharide Signals. Cell **67**: 1131–1143

Roy Choudhury S, Li M, Lee V, Nandety RS, Mysore KS, Pandey S (2020) Flexible functional interactions between G-protein subunits contribute to the specificity of plant responses. Plant J **102**: 207–221

Roy Choudhury S, Pandey S (2016) The role of PLDα1 in providing specificity to signal-response coupling by heterotrimeric G-protein components in Arabidopsis. Plant J **86**: 50–61

Roy Choudhury S, Pandey S (2022) SymRK-dependent phosphorylation of Gα protein and its role in signaling during soybean (Glycine max) nodulation. Plant J **110**: 277–291

Sagan M, Morandi D, Tarenghi E, Duc G (1995) Selection of nodulation and mycorrhizal mutants in the model plant Medicago truncatula (Gaertn.) after γ-ray mutagenesis. Plant Sci **111**: 63–71

Saha S, Dutta A, Bhattacharya A, DasGupta M (2014) Intracellular Catalytic Domain of Symbiosis Receptor Kinase Hyperactivates Spontaneous Nodulation in Absence of Rhizobia. Plant Physiol **166**: 1699–1708

Saito K, Yoshikawa M, Yano K, Miwa H, Uchida H, Asamizu E, Sato S, Tabata S, Imaizumi-Anraku H, Umehara Y, et al (2007) NUCLEOPORIN85 Is Required for Calcium Spiking, Fungal and Bacterial Symbioses, and Seed Production in Lotus japonicus. Plant Cell **19**: 610–624

Schiessl K, Lilley JLS, Lee T, Tamvakis I, Kohlen W, Bailey PC, Thomas A, Luptak J, Ramakrishnan K, Carpenter MD, et al (2019) NODULE INCEPTION Recruits the Lateral Root Developmental Program for Symbiotic Nodule Organogenesis in Medicago truncatula. Curr Biol **29**: 3657-3668.e5

Schneider EH, Seifert R (2010) Sf9 cells: A versatile model system to investigate the pharmacological properties of G protein-coupled receptors. Pharmacol Ther **128**: 387–418

Schwarzott D, Walker C (2001) A new fungal phylum , the Glomeromycota : phylogeny and evolution *. Mycol Res **105**: 1413–1421

Sieberer BJ, Chabaud M, Fournier J, Timmers ACJ, Barker DG (2012) A switch in Ca2+ spiking signature is concomitant with endosymbiotic microbe entry into cortical root cells of Medicago truncatula. Plant J **69**: 822–830

Le Signor C, Savois V, Aubert G, Verdier J, Nicolas M, Pagny G, Moussy F, Sanchez M, Baker D, Clarke J, et al (2009) Optimizing TILLING populations for reverse genetics in Medicago truncatula. Plant Biotechnol J **7**: 430–441

Simon MI, Strathmann MP, Gautam N (1991) Diversity of G proteins in signal transduction. Science **252**: 802–808

Singh S, Katzer K, Lambert J, Cerri M, Parniske M (2014) CYCLOPS, A DNA-binding transcriptional activator, orchestrates symbiotic root nodule development. Cell Host Microbe **15**: 139–152

Smrcka A V., Fisher I (2019) G-protein βγ subunits as multi-functional scaffolds and transducers in G-protein-coupled receptor signaling. Cell Mol Life Sci **76**: 4447–4459

Sondek J, Bohm A, Lambright DG, Hamm HE, Sigier PB (1996) Crystal structure of a G-protein beta gamma dimer at 2.1A resolution. Nature **379**: 369–374

Soyano T, Shimoda Y, Kawaguchi M, Hayashi M (2019) A shared gene drives lateral root development and root nodule symbiosis pathways in Lotus. Science (80-) **366**: 1021–1023

Sprang SR (1997) G protein mechanisms: Insights from structural analysis. Annu Rev Biochem **66**: 639–678

Stael S, Miller LP, Fernández-Fernández ÁD, Van Breusegem F (2022) Detection of Damage-Activated Metacaspase Activity by Western Blot in Plants. Methods Mol Biol **2447**: 127–137

Stougaard J, Abildsten D, Marcker KA (1987) The Agrobacterium rhizogenes pRi TL-DNA segment as a gene vector system for transformation of plants. MGG Mol Gen Genet **207**: 251–255

Stracke S, Kistner C, Yoshida S, Mulder L, Sato S, Kaneko T, Tabata S, Sandal N, Stougaard J, Szczyglowski K, et al (2002) A plant receptor-like kinase required for both bacterial and fungal symbiosis. Nature **417**: 959–962

Subramanian S, Stacey G, Yu O (2006) Endogenous isoflavones are essential for the establishment of symbiosis between soybean and Bradyrhizobium japonicum. Plant J **48**: 261–273

Sun J, Miller JB, Granqvist E, Wiley-Kalil A, Gobbato E, Maillet F, Cottaz S, Samain E, Venkateshwaran M, Fort S, et al (2015) Activation of Symbiosis Signaling by Arbuscular Mycorrhizal Fungi in Legumes and Rice. Plant Cell **27**: 823–838

Sun S, Wang L, Mao H, Shao L, Li X, Xiao J, Ouyang Y, Zhang Q (2018) A G-protein pathway determines grain size in rice. Nat Commun. doi: 10.1038/s41467-018-03141-y

Sytsma KJ, Morawetz J, Chris Pires J, Nepokroeff M, Conti E, Zjhra M, Hall JC, Chase MW (2002) Urticalean rosids: Circumscription, rosid ancestry, and phylogenetics based on rbcL, trnL-F, and ndhF sequences. Am J Bot **89**: 1531–1546

Temple BRS, Jones AM (2007) The Plant Heterotrimeric G-Protein Complex. https://doi.org/101146/annurev.arplant58032806103827 **58**: 249–266

Tennakoon M, Kankanamge D, Senarath K, Fasih Z, Karunarathne A (2019) Statins Perturb G βγ Signaling and Cell Behavior in a G γ Subtype Dependent Manner . Mol Pharmacol **95**: 361–375

Thung L, Trusov Y, Chakravorty D, Botella JR (2012) Gγ1+Gγ2+Gγ3=Gβ: The search for heterotrimeric G-protein γ subunits in Arabidopsis is over. J Plant Physiol **169**: 542–545

Timmers ACJ, Auriac MC, Truchet G (1999) Refined analysis of early symbiotic steps of the Rhizobium-Medicago interaction in relationship with microtubular cytoskeleton rearrangements. Development **126**: 3617–3628

Trusov Y, Chakravorty D, Botella JR (2012) Diversity of heterotrimeric G-protein subunits in plants. BMC Res Notes. doi: 10.1186/1756-0500-5-608

Tunc-Ozdemir M, Jones AM (2017) Ligand-induced dynamics of heterotrimeric G protein-coupled receptor-like kinase complexes. PLoS One **12**: e0171854

Tunc-Ozdemir M, Li B, Jaiswal DK, Urano D, Jones AM, Torres MP (2017) Predicted functional implications of phosphorylation of regulator of G protein signaling protein in plants. Front Plant Sci **8**: 1–14

Tunc-Ozdemir M, Urano D, KumarJaiswal D, Clouse SD, Jones AM (2016) Direct Modulation of Heterotrimeric G Protein-coupled Signaling by a Receptor Kinase Complex. J Biol Chem **291**: 13918–13925

Ullah H, Chen J-G, Temple B, Boyes DC, Alonso JM, Davis KR, Ecker JR, Jones AM (2003) The beta-Subunit of the Arabidopsis G Protein Negatively Regulates Auxin-Induced Cell Division and Affects Multiple Developmental Processes. Plant Cell Online **15**: 393–409

Urano D, Chen JG, Botella JR, Jones AM (2012a) Heterotrimeric G protein signalling in the plant kingdom. Open Biol. doi: 10.1098/RSOB.120186

Urano D, Jones AM (2014) Heterotrimeric G Protein–Coupled Signaling in Plants. Annu Rev Plant Biol **65**: 365–384

Urano D, Jones JC, Wang H, Matthews M, Bradford W, Bennetzen JL, Jones AM (2012b) G protein activation without a GEF in the plant kingdom. PLoS Genet. doi: 10.1371/journal.pgen.1002756

Urano D, Maruta N, Trusov Y, Stoian R, Wu Q, Liang Y, Jaiswal DK, Thung L, Jackson D, Botella JR, et al (2016a) Saltational evolution of the heterotrimeric G protein signaling mechanisms in the plant kingdom. Sci Signal. doi: 10.1126/SCISIGNAL.AAF9558

Urano D, Miura K, Wu Q, Iwasaki Y, Jackson D, Jones AM (2016b) Plant Morphology of Heterotrimeric G Protein Mutants. Plant Cell Physiol **57**: 437–445

Urano D, Phan N, Jones JC, Yang J, Huang J, Grigston J, Philip Taylor J, Jones AM (2012c) Endocytosis of the seven-transmembrane RGS1 protein activates G-protein-coupled signalling in Arabidopsis. Nat Cell Biol **14**: 1079–1088

van Velzen R, Doyle JJ, Geurts R (2019) A Resurrected Scenario: Single Gain and Massive

Loss of Nitrogen-Fixing Nodulation. Trends Plant Sci **24**: 49–57

van Velzen R, Holmer R, Bu F, Rutten L, van Zeijl A, Liu W, Santuari L, Cao Q, Sharma T, Shen D, et al (2018) Comparative genomics of the nonlegume Parasponia reveals insights into evolution of nitrogen-fixing rhizobium symbioses. Proc Natl Acad Sci U S A **115**: E4700–E4709

Venkateshwaran M, Cosme A, Han L, Banba M, Satyshur KA, Schleiff E, Parniske M, Imaizumi-Anraku H, Ané J-M (2012) The Recent Evolution of a Symbiotic Ion Channel in the Legume Family Altered Ion Conductance and Improved Functionality in Calcium Signaling. Plant Cell **24**: 2528–2545

Venkateshwaran M, Jayaraman D, Chabaud M, Genre A, Balloon AJ, Maeda J, Forshey K, Den Os D, Kwiecien NW, Coon JJ, et al (2015) A role for the mevalonate pathway in early plant symbiotic signaling. Proc Natl Acad Sci U S A **112**: 9781–9786

Vernié T, Camut S, Camps C, Rembliere C, de Carvalho-Niebel F, Mbengue M, Timmers T, Gasciolli V, Thompson R, le Signor C, et al (2016) PUB1 Interacts with the Receptor Kinase DMI2 and Negatively Regulates Rhizobial and Arbuscular Mycorrhizal Symbioses through Its Ubiquitination Activity in Medicago truncatula . Plant Physiol **170**: 2312–2324

Wais RJ, Galera C, Oldroyd G, Catoira R, Penmetsa RV, Cook D, Gough C, Dénarié J, Long SR (2000) Genetic analysis of calcium spiking responses in nodulation mutants of Medicago truncatula. Proc Natl Acad Sci **97**: 13407–13412 PLANT

Wall MA, Coleman DE, Lee E, Iñiguez-Lluhi JA, Posner BA, Gilman AG, Sprang SR (1995) The structure of the G protein heterotrimer Giα1β1γ2. Cell **83**: 1047–1058

Wang E, Schornack S, Marsh JF, Gobbato E, Schwessinger B, Eastmond P, Schultze M, Kamoun S, Oldroyd GED (2012) A common signaling process that promotes mycorrhizal and oomycete colonization of plants. Curr Biol **22**: 2242–2246

Wang S, Assmann SM, Fedoroff N V. (2008) Characterization of the Arabidopsis heterotrimeric G protein. J Biol Chem **283**: 13913–13922

Wang S, Narendra S, Fedoroff N (2007) Heterotrimeric G protein signaling in the Arabidopsis unfolded protein response. Proc Natl Acad Sci **104**: 3817–3822

Wang XQ, Ullah H, Jones AM, Assmann SM (2001) G protein regulation of ion channels and abscisic acid signaling in Arabidopsis guard cells. Science (80-) **292**: 2070–2072

Watkins JM, Ross-Elliott TJ, Shan X, Lou F, Dreyer B, Tunc-Ozdemir M, Jia H, Yang J, Oliveira CC, Wu L, et al (2021) Differential regulation of G protein signaling in Arabidopsis through two distinct pathways that internalize AtRGS1. Sci Signal **14**: 4090

Weber E, Engler C, Gruetzner R, Werner S, Marillonnet S (2011) A Modular Cloning System for Standardized Assembly of Multigene Constructs. PLoS One **6**: e16765

Wedegaertner PB, Wilson PT, Bourne HR (1995) Lipid modifications of trimeric G proteins. J Biol Chem **270**: 503–506

Wettschureck N, Offermanns S (2005) Mammalian G proteins and their cell type specific functions. Physiol Rev **85**: 1159–1204

Wong JEMM, Nadzieja M, Madsen LH, Bücherl CA, Dam S, Sandal NN, Couto D, Derbyshire P, Uldum-Berentsen M, Schroeder S, et al (2019) A Lotus japonicus cytoplasmic kinase connects Nod factor perception by the NFR5 LysM receptor to nodulation. Proc Natl Acad Sci U S A **116**: 14339–14348

Wu Q, Xu F, Liu L, Char SN, Ding Y, Je B Il, Schmelz E, Yang B, Jackson D (2020) The maize heterotrimeric G protein β subunit controls shoot meristem development and immune responses. Proc Natl Acad Sci U S A **117**: 1799–1805

Xiao TT, Schilderink S, Moling S, Deinum EE, Kondorosi E, Franssen H, Kulikova O, Niebel A, Bisseling T (2014) Fate map of Medicago truncatula root nodules. Dev **141**: 3517–3528

Xu D bei, Gao S qing, Ma Y nan, Wang X ting, Feng L, Li L cheng, Xu Z shi, Chen Y feng, Chen M, Ma Y zhi (2017) The G-Protein β Subunit AGB1 Promotes Hypocotyl Elongation through Inhibiting Transcription Activation Function of BBX21 in Arabidopsis. Mol Plant **10**: 1206–1223

Xu L, Yao X, Zhang N, Gong BQ, Li JF (2019) Dynamic G protein alpha signaling in Arabidopsis innate immunity. Biochem Biophys Res Commun **516**: 1039–1045

Xu Q, Zhao M, Wu K, Fu X, Liu Q (2016) Emerging insights into heterotrimeric G protein

signaling in plants. J Genet Genomics **43**: 495–502

Yadav DK, Shukla D, Tuteja N (2014) Isolation, in silico characterization, localization and expression analysis of abiotic stressresponsive rice G-protein β subunit (RGB1). Plant Signal Behav **9**: 1–12

Yang S-Y, Grønlund M, Jakobsen I, Grotemeyer MS, Rentsch D, Miyao A, Hirochika H, Kumar CS, Sundaresan V, Salamin N, et al (2012) Nonredundant Regulation of Rice Arbuscular Mycorrhizal Symbiosis by Two Members of the *PHOSPHATE TRANSPORTER1* Gene Family. Plant Cell **24**: 4236–4251

Yano K, Yoshida S, Muller J, Singh S, Banba M, Vickers K, Markmann K, White C, Schuller B, Sato S, et al (2008) CYCLOPS, a mediator of symbiotic intracellular accommodation. Proc Natl Acad Sci **105**: 20540–20545

Yu TY, Shi DQ, Jia PF, Tang J, Li HJ, Liu J, Yang WC (2016) The Arabidopsis Receptor Kinase ZAR1 Is Required for Zygote Asymmetric Division and Its Daughter Cell Fate. PLoS Genet **12**: 1005933

Yu Y, Chakravorty D, Assmann SM (2018) The G Protein β -Subunit, AGB1, Interacts with FERONIA in RALF1-Regulated Stomatal Movement . Plant Physiol **176**: 2426–2440

Yuan C, Sato M, Lanier SM, Smrcka A V. (2007) Signaling by a Non-dissociated Complex of G Protein βγ and α Subunits Stimulated by a Receptor-independent Activator of G Protein Signaling, AGS8. J Biol Chem **282**: 19938–19947

Yuan S, Zhu H, Gou H, Fu W, Liu L, Chen T, Ke D, Kang H, Xie Q, Hong Z, et al (2012) A Ubiquitin Ligase of Symbiosis Receptor Kinase Involved in Nodule Organogenesis. Plant Physiol **160**: 106–117

Zamponi GW, Currie KPM (2013) Regulation of CaV2 calcium channels by G protein coupled receptors. Biochim Biophys Acta - Biomembr **1828**: 1629–1643

Zeng Q, Wang X, Running MP (2007) Dual Lipid Modification of Arabidopsis Gγ-Subunits Is Required for Efficient Plasma Membrane Targeting. Plant Physiol **143**: 1119–1131

Zhang C, He J, Dai H, Wang G, Zhang X, Wang C, Shi J, Chen X, Wang D, Wang E (2021a) Discriminating symbiosis and immunity signals by receptor competition in rice. Proc Natl Acad Sci U S A **118**: e2023738118

Zhang H, Xie P, Xu X, Xie Q, Yu F (2021b) Heterotrimeric G protein signalling in plant biotic and abiotic stress response. Plant Biol **23**: 20–30

Zhang T, Xu P, Wang W, Wang S, Caruana JC, Yang HQ, Lian H (2018) Arabidopsis G-protein β subunit AGB1 interacts with BES1 to regulate brassinosteroid signaling and cell elongation. Front Plant Sci **8**: 2225

Zhang XC, Wu X, Findley S, Wan J, Libault M, Nguyen HT, Cannon SB, Stacey G (2007) Molecular evolution of lysin motif-type receptor-like kinases in plants. Plant Physiol **144**: 623–636

Zhao J, Wang X (2004) Arabidopsis Phospholipase Dα1 Interacts with the Heterotrimeric G-protein α-Subunit through a Motif Analogous to the DRY Motif in G-protein-coupled Receptors. J Biol Chem **279**: 1794–1800

Zhao Y, Araki S, Wu J, Teramoto T, Chang YF, Nakano M, Abdelfattah AS, Fujiwara M, Ishihara T, Nagai T, et al (2011) An expanded palette of genetically encoded Ca2+ indicators. Science (80-) **333**: 1888–1891

Zhong CL, Zhang C, Liu JZ (2019) Heterotrimeric G protein signaling in plant immunity. J Exp Bot **70**: 1109–1118

List of Publications

During the course of this thesis, I contributed to the following manuscripts based on data aside from those presented in this work.

E. Tipper, N. Leitão, P. Dangeville, D. M. Lawson, M. Charpentier. **A novel mutant allele of AtCNGC15 reveals a dual function of nuclear calcium release in the root meristem**. Journal of Experimental Botany. 2023. 10.1093/jxb/erad041.

P. Del Cerro ⌘, R. Huisman ⌘, N. Cook, P. Dangeville, L. Grubb, C. Marchal, A. Ho Ching Lam, M. Charpentier. **Engineered CaM2 modulates nuclear calcium oscillation and enhances legume root nodule symbiosis**. PNAS. 2022. 10.1073/pnas.2200099119

N. Leitão, P. Dangeville, R. Carter, M. Charpentier. **Nuclear calcium signatures are associated with root development**. Nature Communication. 2019. 10.1038/s41467-019-12845-8